

Investigating the Prognostic and Diagnostic Value of Anesthetic-Induced Changes in Functional Brain Network Topologies for Patients with Coma and Disorders of Consciousness

Kira Dolhan



Integrated Program in Neuroscience

McGill University

Montréal, Québec, Canada

August 2024

A thesis submitted to McGill University in partial fulfillment of the requirements of the degree of
Master of Science in Neuroscience

© Kira Dolhan 2024

Table of Contents

List of Figures	III
List of Tables	VII
List of Acronyms	VIII
Abstract	1
Agrégé.....	3
Acknowledgements.....	5
Contribution of Authors.....	7
Introduction.....	8
Chapter 1: Investigating the Prognostic and Diagnostic Value of Anesthetic-Induced Brain Network Motif Reconfiguration in Coma and Disorders of Consciousness.....	13
Introduction.....	13
Methods	19
Results	34
Discussion.....	53
Conclusion	59
Chapter 2: Using Anesthetic-Induced Brain Network Reconfiguration to Prognosticate Recovery from Coma After Cardiac Arrest	60

	ii
Introduction.....	60
Methods	63
Results	67
Discussion.....	81
Conclusion	86
Discussion	87
Consciousness and its Many Definitions.....	88
Modeling Cognition at Different Spatiotemporal Scales	90
Limitations of this Thesis	91
Strengths of this Thesis	93
Conclusion	96
Bibliography	97
Appendix	117
Supplementary Material for Chapter 1	117

List of Figures

Chapter 1

<i>Figure 1.1.</i> A visual representation of all possible connection patterns between 3-nodes in a network.	16
<i>Figure 1.2.</i> Anesthetic protocols used.	21
<i>Figure 1.3.</i> Topological plots between prognostic groups for motif 1 frequency, distance, source, and target properties during anesthesia withdrawal.	37
<i>Figure 1.4.</i> Topological plots between prognostic groups for motif 7 frequency and distance properties during anesthesia withdrawal.	38
<i>Figure 1.5.</i> Individual cosine similarity values for motif 1 frequency (A), distance (B), source (C), and target (D) properties during propofol withdrawal.	39
<i>Figure 1.6.</i> Individual cosine similarity values for motif 7 frequency (A) and distance (B) properties during propofol withdrawal.	40
<i>Figure 1.7.</i> Topological plots between prognostic groups for motif 1 frequency, distance, source, and target properties during anesthesia administration.	41
<i>Figure 1.8.</i> Individual cosine similarity values for motif 1 frequency (A), distance (B), source (C), and target (D) properties during propofol administration.	42
<i>Figure 1.9.</i> Topological plots between prognostic groups for motif 1 frequency, distance, source, and target properties during baseline states.	44
<i>Figure 1.10.</i> Topological plots between prognostic groups for motif 7 frequency and distance properties during baseline states.	45
<i>Figure 1.11.</i> Individual cosine similarity values for motif 1 frequency (A), distance (B), source (C), and target (D) properties during baseline states.	46

<i>Figure 1.12.</i> Individual cosine similarity values for motif 7 frequency (A) and distance (B) properties during baseline states.	47
<i>Figure 1.13.</i> Non-topological scalar counts of motif 1 frequency during anesthesia withdrawal.	48
<i>Figure 1.14.</i> Whole-network small-worldness (A), clustering coefficient (B), global efficiency (C), and modularity (D) between prognostic groups during anesthesia withdrawal.	50
<i>Figure 1.15.</i> Topological plots between prognostic groups for alpha power during anesthesia withdrawal.	51
<i>Figure 1.16.</i> Topological plots between prognostic groups for network hubs during anesthesia withdrawal.	52

Chapter 2

<i>Figure 2.1.</i> Box plots depicting the degree of topological hub (node degree) reconfiguration between sedation on and off states for coma patients who did not recover consciousness (orange) and for patients who recovered consciousness (blue).	67
<i>Figure 2.2.</i> Box plots depicting the degree of reconfiguration in the directed phase-lag index (dPLI) between sedation on and off states for coma patients who did not recover consciousness (orange) and for patients who recovered consciousness (blue).	68
<i>Figure 2.3.</i> The receiver operating characteristic (ROC) curve for the logistic regression (log reg) model categorizing recovered versus non-recovered post-cardiac arrest comatose patients.	70
<i>Figure 2.4.</i> Confusion matrix for the logistic regression model categorizing recovered versus non-recovered post-cardiac arrest comatose patients.	71
<i>Figure 2.5.</i> The logistic regression decision boundary (indicated by the dotted black line) plotted in the feature space of the Adaptive Reconfiguration Index.	72

<i>Figure 2.6.</i> Weighted phase-lag index (wPLI), directed phase-lag index (dPLI), and normalized hubs for recovered patient 5.	74
<i>Figure 2.7.</i> Weighted phase-lag index (wPLI), directed phase-lag index (dPLI), and normalized hubs for recovered patient 20.	75
<i>Figure 2.8.</i> Weighted phase-lag index (wPLI), directed phase-lag index (dPLI), and normalized hubs for non-recovered patient 2.	77
<i>Figure 2.9.</i> Weighted phase-lag index (wPLI), directed phase-lag index (dPLI), and normalized hubs for non-recovered patient 16.	78
<i>Figure 2.10.</i> Weighted phase-lag index (wPLI), directed phase-lag index (dPLI), and normalized hubs for recovered patient 9 – an outlier in our dataset.	80

Appendix

<i>Supplementary Figure 1.</i> Correlations between patient Glasgow Coma Scale (GCS) scores when off sedation and motif frequency cosine similarity during sedation withdrawal.	117
<i>Supplementary Figure 2.</i> Topological plots between diagnostic groups for motif 1 frequency, distance, source, and target properties during anesthesia withdrawal.	118
<i>Supplementary Figure 3.</i> Topological plots between diagnostic groups for motif 7 frequency and distance properties during anesthesia withdrawal.	119
<i>Supplementary Figure 4.</i> Individual cosine similarity values for motif 1 frequency (A), distance (B), source (C), and target (D) properties during propofol withdrawal.	120
<i>Supplementary Figure 5.</i> Individual cosine similarity values for motif 7 frequency (A) and distance (B) properties during propofol withdrawal.	121
<i>Supplementary Figure 6.</i> Topological plots between diagnostic groups for motif 1 frequency, distance, source, and target properties during anesthesia administration.	122

<i>Supplementary Figure 7.</i> Individual cosine similarity values for motif 1 frequency (A), distance (B), source (C), and target (D) properties during propofol administration.	123
<i>Supplementary Figure 8.</i> Topological plots between diagnostic groups for motif 1 frequency, distance, source, and target properties during baseline states.	124
<i>Supplementary Figure 9.</i> Topological plots between diagnostic groups for motif 7 frequency and distance properties during baseline states.	125
<i>Supplementary Figure 10.</i> Individual cosine similarity values for motif 1 frequency (A), distance (B), source (C), and target (D) properties during baseline states.	126
<i>Supplementary Figure 11.</i> Individual cosine similarity values for motif 7 frequency (A) and distance (B) properties during baseline states.	127
<i>Supplementary Figure 12.</i> Non-topological scalar counts of motif 1 frequency during anesthesia withdrawal.	128

List of Tables

Chapter 1

Table 1.1. Mean and standard deviation (SD) of motif scalar counts for prognostic groups during anesthesia withdrawal. 36

Appendix

Supplementary Table 1. Mean and standard deviation (SD) of motif scalar counts for diagnostic groups during anesthesia withdrawal. 129

List of Acronyms

ARI	Adaptive Reconfiguration Index
BCT	Brain Connectivity Toolbox
CPC	Cerebral Performance Category
CRS-R	Coma Recover Scale-Revised
DOC	Disorder of Consciousness
dPLI	Directed Phase-Lag Index
EEG	Electroencephalography
FC	Functional Connectivity
FOOOF	Fitting Oscillations and One Over f
GCS	Glasgow Coma Scale
hd	High-Density
ICU	Intensive Care Unit
M1	Motif 1
M7	Motif 7
MCS	Minimally Conscious State
ROC	Receiver Operating Characteristic
UWS	Unresponsive Wakefulness Syndrome
WOLST	Withdrawal of Life-Sustaining Treatment
wPLI	Weighted Phase-Lag Index

Abstract

Coma and disorders of consciousness (DOCs) are states of chronically impaired arousal and/or awareness caused by severe brain injury. Little is known about how to accurately diagnose and prognosticate these disorders, as the current “gold standard” of behavioural examination has a misdiagnosis rate of around 40%, cannot identify patients with cognitive-motor dissociation, and performs poorly in predicting long-term patient outcome (Edlow et al., 2021; Owen et al., 2006; Schnakers, 2020). Thus, there is a strong clinical need to combine behavioral assessments of responsiveness with electrophysiological and neuroimaging modalities. Electroencephalography (EEG) is a promising candidate due to its ease of use and cost-effectiveness in the intensive care unit (Duclos et al., 2022; Estraneo & Trojano, 2018). Furthermore, using EEG to quantify the brain’s response to external perturbations has shown great promise as a tool to measure consciousness in coma and DOC patients (Casali et al., 2013). Combining these approaches, we quantified EEG signatures as coma/DOC patients underwent propofol anesthetic perturbations and investigated whether anesthetic-induced changes in these signatures could be leverage in the clinic – particularly for patient diagnosis and/or prognostication.

In the first study, we measured propofol-induced topological changes in 3-node network motifs derived from high-density EEG in the alpha (8-13 Hz) frequency band. Two motifs, one comprised of long-range chain-like connections and another of short-range loop-like connections, were found to recur at significant frequencies in coma/DOC patients ($n = 56$) and topologically reconfigure between sedation states. Despite being able to replicate the descriptive

properties of these motifs in accordance with past literature, they were found to have neither prognostic nor diagnostic value for our patient cohort. In the second study, we investigated topological differences in directed connectivity and network hubs as post-cardiac arrest comatose patients ($n = 16$) were on versus off propofol sedation. These two metrics, derived from clinical-grade 19-channel EEG in the alpha band, were combined to generate scores for the previously developed Adaptive Reconfiguration Index (Duclos et al., 2022), which were then used as input for a logistic regression model. This model achieved an area under the receiver operating characteristic curve of 0.76, accuracy score of 0.75, sensitivity of 0.67, and specificity of 0.86.

Taken together, these studies converge on the idea that patient diagnosis and prognostication should not be treated as a “one-size-fits-all” matter. Factors such as etiology, age, and sex should be taken into consideration when trying to develop and apply novel clinical tools – as a given tool may not be appropriate for all patients. In the future, more personalized approaches to the treatment of patient subpopulations should be explored.

Agrégé

Le coma et les troubles de la conscience (DOCs) sont des états d'altération chronique de l'éveil et/ou de la conscience provoqués par des lésions cérébrales graves. On comprend encore peu comment diagnostiquer et pronostiquer ces troubles avec précision, car l'examen comportemental actuellement considéré l'"étalon-or", présente environ 40% de diagnostic erroné. Cet examen ne permet pas d'identifier les patients présentant une dissociation cognitivo-motrice, et ne prédit guère l'évolution à long terme des patients (Edlow et al., 2021; Owen et al., 2006; Schnakers, 2020). Il existe donc un besoin clinique important de combiner les évaluations comportementales de la réactivité avec des modalités électrophysiologiques et de neuro-imagerie. L'électroencéphalographie (EEG) est un candidat prometteur grâce à sa facilité d'utilisation et à sa rentabilité dans l'unité de soins intensifs (Duclos et al., 2022; Estraneo & Trojano, 2018). En outre, l'utilisation de l'EEG pour quantifier la réponse du cerveau aux perturbations externes s'est révélée très prometteuse en tant qu'outil de mesure de la conscience chez les patients dans le coma et le DOC (Casali et al., 2013). En combinant ces approches, nous avons quantifié les signatures EEG pendant que les patients dans le coma ou en état de choc subissaient des perturbations anesthésiques dues au propofol. Nous avons cherché à déterminer si les changements induits par l'anesthésie dans ces signatures pouvaient être utilisés en clinique, notamment pour le diagnostic et/ou le pronostic des patients.

Dans la première étude, nous avons mesuré les changements topologiques induits par le propofol dans les motifs de réseaux à trois nœuds dérivés de l'EEG à haute densité dans la bande de fréquence alpha (8-13 Hz). Deux motifs, l'un composé de connexions de type chaîne à longue

portée et l'autre de connexions de type boucle à courte portée, se sont révélés récurrents à des fréquences significatives chez les patients coma/DOC ($n = 56$) et se reconfigurent topologiquement entre les états de sédation. Bien que nous ayons pu reproduire les propriétés descriptives de ces motifs conformément à la littérature antérieure, il s'est avéré qu'ils n'avaient aucune valeur pronostique ou diagnostique pour notre cohorte de patients. Dans la seconde étude, nous avons examiné les différences topologiques dans la connectivité dirigée et les nœuds du réseau lorsque les patients comateux après un arrêt cardiaque ($n = 16$) étaient sous sédation au propofol et non sous sédation. Ces deux mesures, dérivées de l'EEG à 19 canaux de qualité clinique dans la bande alpha, ont été combinées pour générer des scores pour l'indice de reconfiguration adaptative développé précédemment (Duclos et al., 2022), qui ont ensuite été utilisés comme données d'entrée pour un modèle de régression logistique. Ce modèle a permis d'obtenir une aire sous la courbe caractéristique d'exploitation du récepteur de 0,76, un score de précision de 0,75, une sensibilité de 0,67 et une spécificité de 0,86.

Dans l'ensemble, ces études convergent vers l'idée que le diagnostic et le pronostic des patients ne doivent pas être traités comme une question de "taille unique". Des facteurs tels que l'étiologie, l'âge et le sexe doivent être pris en considération lors de l'élaboration et de l'application de nouveaux outils cliniques, car un outil donné ne convient pas nécessairement à tous les patients. À l'avenir, il faudra explorer des approches plus personnalisées du traitement des sous-populations de patients.

Acknowledgements

First, I would like to thank my supervisor Dr. Stefanie Blain-Moraes for her continued support and mentorship throughout my master's degree. You have been a wonderful role model – particularly with respect to effective and healthy leadership, and navigating being a woman in STEM. Thank you for all the opportunities that you afforded me, for fostering an encouraging work environment, and for supporting me as I work towards my goals. I would also like to thank those who have been a part of the BIAPT Lab – my colleagues were a large motivating force in helping me to complete my master's. Each of you have made coming to work a very positive experience, and I hope that our friendships continue to grow. I would especially like to thank Charlotte Maschke and Miriam Han for training me in EEG collection in the intensive care unit, EEG preprocessing, and functional connectivity analyses. Furthermore, I would like to thank you both for accompanying me during many EEG preprocessing and data collection sessions – we formed a great and effective trio. Thank you, Raphaël Lavoie, for coordinating data collection with families and doctors. You were always a very organized and responsive lab manager.

This work would not exist without all of the patients and their families who courageously contributed to the science of coma and disorders of consciousness. I hope that one day the treatment and understanding of these conditions will progress far beyond its current state. I would also like to thank Dr. Adrian Owen, Dr. Catherine Duclos, and their teams for contributing to data collection. Similarly, thank you to Dr. Mypinder Sekhon and his team for providing the data used in the second chapter of this thesis. Thank you, Yacine Mahdid, Charlotte Maschke, and Miriam Han, for providing the backbone of the scripts which I used and modified to perform

my analyses. To Drs Catherine Duclos and George Mashour, thank you for the significant parts you played in developing the anesthetic paradigms used in Chapter 1. Thank you, Dr Catherine Duclos, for your part in developing the functional network metric tested in Chapter 2. To Drs. Justin Létourneau and Mohammed Badawy, thank you for inviting us into the intensive care unit for data collection and facilitating our anesthetic protocols. I want to thank my committee members, Drs. Adrian Owen and Karim Jerbi, for taking the time to provide helpful feedback on my master's projects as they evolved. To Drs. Lara Boyd and Stefanie Blain-Moraes, thank you for your thoughtful feedback and editorial contributions to this thesis.

Thank you to my family and friends who have provided invaluable moral support as I navigated these past two years – including moving across the country and back again. Finally, I would like to acknowledge the generous funding of my master's from the Canadian Institutes of Health Research, McGill University, McGill University Health Centre, and UNIQUE (Unifying Neuroscience and Artificial Intelligence in Quebec) Center.

Contribution of Authors

For the work in Chapter 1, Kira Dolhan^{1,2} had a significant role in collecting and preprocessing the data. She also analyzed the data and interpreted the results. Dr. Adrian Owen^{3,4,5} and his lab contributed to data collection. Dr. Stefanie Blain-Moraes^{2,6} developed the anesthetic paradigms, collected data, and interpreted results.

In Chapter 2, Kira Dolhan^{1,2} analyzed the data and interpreted the results. Dr. Mypinder Sekhon^{7,8} and his team provided the data. Dr. Stefanie Blain-Moraes^{2,6} facilitated data transfer from Vancouver General Hospital and interpreted results.

1. Integrated Program in Neuroscience, McGill University, Montreal, Canada
2. Montreal General Hospital, McGill University Health Centre, Montreal, Canada
3. Western Institute for Neuroscience, Western University, London, Ontario, Canada
4. Department of Physiology and Pharmacology, Western University, London, Ontario, Canada
5. Department of Psychology, Western University, London, Ontario, Canada
6. School of Physical and Occupational Therapy, McGill University, Montreal, Canada
7. Vancouver General Hospital, University of British Columbia, Vancouver, British Columbia, Canada
8. Vancouver Coastal Health Research Institute, University of British Columbia, Vancouver, British Columbia, Canada

Introduction

Coma and disorders of consciousness (DOCs) are characterized by chronic impairments in arousal and/or awareness resulting from severe brain injury (Giacino et al., 2018; Gosseries & Laureys, 2022; Schnakers & Laureys, 2018). In clinical contexts, arousal is often operationalized by spontaneous eye-opening and awareness by evidence for basic command-following (Benghanem et al., 2022; Edlow et al., 2021). DOC is an umbrella term which includes the minimally conscious states (MCS) and unresponsive wakefulness syndrome (UWS) or vegetative state (Gosseries et al., 2011; Gosseries & Laureys, 2022). In order of least to worst severity: MCS patients show signs of wakefulness and minimal, reproducible, but inconsistent sign of awareness; while UWS patients show signs of wakefulness, but not awareness; and coma patients do not show signs of wakefulness, nor awareness (Edlow et al., 2021; Schnakers & Laureys, 2018).

Clinicians treating these patients are trying to assess two broad questions: the first is determining their level of consciousness. This is primarily assessed through behavioural examinations, with the goal of correctly labeling patients with a coma, UWS, or MCS status (Edlow et al., 2021; Porcaro et al., 2022). However, these behavioural tests are known to perform poorly: DOC misdiagnosis rates have repeatedly been estimated at $\approx 40\%$ (Schnakers et al., 2007, 2009; J. Wang et al., 2020). Furthermore, it is estimated that 15 to 20% of coma/DOC patients have cognitive-motor dissociation – a condition in which patients can, despite their behavioural unresponsiveness, volitionally alter their neural activity in accordance with verbal commands (Claassen et al., 2019; Edlow et al., 2021; Owen et al., 2006). These misdiagnosis rates are

problematic, as proper diagnoses carry important prognostic information regarding the potential for patient recovery (Edlow et al., 2021; Gosseries & Laureys, 2022; B. Liu et al., 2021).

This leads into the second question facing clinicians: determining whether the patient will recover. Determining patient outcome, or their prognosis, is a particularly challenging but important question – as families want to know the likelihood of recovery when faced with decisions about medical treatment for their loved one (Giacino et al., 2018; Turner-Stokes et al., 2022). Unfortunately, there are a lack of prognostication techniques for coma and DOC patients – especially in intensive care unit (ICU) – yet decisions about withdrawal of life-sustaining treatment (WOLST) are often made within the first 1-2 weeks of hospital admission (Edlow et al., 2021; Kotchoubey & Pavlov, 2018; Sandroni et al., 2021).

Improving prognostication in the ICU using electroencephalography (EEG) is a highly relevant clinical problem, since EEG is a relatively inexpensive brain imaging technique which can be readily employed at the hospital bedside (Duclos et al., 2022; Estraneo & Trojano, 2018). For example, EEG is the most widely used tool by clinicians for assessing hypoxic-ischemic brain injury severity (Benghanem et al., 2022; Maciel et al., 2020).

Previous literature has shown that quantifying the brain's response to perturbations can be a promising technique to measure consciousness (Casali et al., 2013; Duclos et al., 2022; Perl et al., 2021). For example, the perturbational complexity index – which is arguably the most promising technique to measure consciousness in unresponsive patients developed to date – quantifies the brain's response to transcranial magnetic stimulation using EEG (Casali et al., 2013). However, inducing brain perturbations using techniques such as transcranial magnetic

stimulation (Casali et al., 2013) or electrical stimulation (Z. Liu et al., 2023) poses pragmatic issues: the required equipment is expensive, not readily available to clinicians, and require specialized training to use (Duclos et al., 2022).

Given the pragmatic and clinical importance of using EEG, paired with the promise of the perturbational complexity index, we investigated the clinical value of EEG signatures associated with changes in general anesthesia. Throughout this thesis, we utilize general anesthesia as a tool to perturbate the brain. More specifically, we quantified brain changes recorded from coma and DOC patients during the administration and withdrawal of propofol anesthesia, to investigate whether these brain dynamics have prognostic or diagnostic value. Thus, we leveraged brain perturbations which naturally occur in clinical practice to aid us in prognostication. Thereby avoiding the pragmatic limitations of the perturbational complexity index, whilst maintaining its core component of using EEG to measure the neural response to an external perturbation. Both chapters in this thesis are designed to test the general hypothesis that patients with favorable clinical outcomes, relative to those with unfavorable outcomes, will show greater neural changes in response to an external perturbation – as observed with the perturbational complexity index (Casali et al., 2013).

To test this hypothesis, we modeled functional connections between pairs of EEG electrodes. When referring to a large number of functional connections, these models are described as “brain networks” or “functional connectomes” – which are commonly used in coma/DOC research to describe how information is exchanged across regions of the cortex (e.g., Chennu et al., 2017; Demertzi et al., 2015; Di Gregorio et al., 2022; Norton et al., 2012). This

functional connectivity (FC) can also be analyzed at smaller spatial scales – as done with functional network motifs (Milo et al., 2002). Motifs are patterns of connectivity between a small group of EEG electrodes which reoccur at a frequency significantly greater than chance (Milo et al., 2002; Sporns & Kötter, 2004). In the context of this thesis, motifs refer to recurring connection patterns between three EEG electrodes and given the techniques we used to quantify phase-based connectivity between EEG electrodes, only unidirectional motifs were considered. Unidirectional motifs consist of one-way connectivity between all electrodes, in contrast to bidirectional or “two-way” connections (Nadin et al., 2020; Sporns & Kötter, 2004). Since these sub-connections keep recurring within the network, with a frequency that significantly exceeds chance, it is presumed that said connection patterns are important for the underlying function of the overall brain network (Milo et al., 2002; Sporns & Kötter, 2004). Thus, motifs are conceptualized as the “building blocks” of a network (Milo et al., 2002; Sporns & Kötter, 2004).

The primary advantage of motifs, compared to traditional large-scale brain networks, is that motifs are based on connections between a small number of electrodes – which offers advantages in terms of computational resources and clinical translatability. For example, motifs may be calculated using fewer EEG electrodes than traditional brain networks – which is particularly advantageous given that standard EEG systems used in the clinic are often comprised of a small number of electrodes (Acharya et al., 2016). However, rather than advocating for the replacement of large-scale brain networks with motifs, we recognize that the two spatial scales provide important complementary information about neural connectivity within the severely injured brain of coma and DOC patients (Betz et al., 2018; Duclos et al.,

2021; Nadin et al., 2020). Thus, this thesis contains a chapter dedicated to each approach to network quantification: Chapter 1 investigates the clinical utility of motifs, and Chapter 2 the clinical utility of large-scale brain network properties, for the prognostication and/or diagnosis of coma and DOC patients.

In the first chapter of this thesis, we investigated whether functional brain network motifs had 1) prognostic or 2) diagnostic potential for a cohort of coma and DOC patients of mixed etiologies. This study focused on changes in motif topologies (i.e., spatial distributions across the scalp) associated with propofol anesthetic perturbations, and whether motif reconfiguration can be used to distinguish patient prognostic and diagnostic groups. We hypothesized that anesthetic-induced changes in functional network motif topologies have prognostic and/or diagnostic value for brain-injured patients in the ICU diagnosed with coma or DOC.

In the second chapter, we tested the ability of a previously developed FC metric, called the Adaptive Reconfiguration Index (ARI), to retrospectively predict the outcomes of coma patients following cardiac arrest. This study leveraged topological changes in network hubs and directed FC associated with propofol anesthetic perturbations, examining their ability to categorize comatose patients who recovered versus did not recover consciousness 6-months after injury. We hypothesized that the ARI could serve as a prognostic tool when applied to clinical-grade EEG recorded from comatose patients in the ICU with hypoxic-ischemic brain injury after cardiac arrest.

Chapter 1: Investigating the Prognostic and Diagnostic Value of Anesthetic-Induced Brain Network Motif Reconfiguration in Coma and Disorders of Consciousness

Kira Dolhan^{1,2}, Adrian Owen^{3,4,5}, & Stefanie Blain-Moraes^{2,6}

1. Integrated Program in Neuroscience, McGill University, Montreal, Canada
2. Montreal General Hospital, McGill University Health Centre, Montreal, Canada
3. Western Institute for Neuroscience, Western University, London, Ontario, Canada
4. Department of Physiology and Pharmacology, Western University, London, Ontario, Canada
5. Department of Psychology, Western University, London, Ontario, Canada
6. School of Physical and Occupational Therapy, McGill University, Montreal, Canada

Introduction

Accurately performing diagnostic and prognostic assessments of patients in a coma or DOC is a very difficult clinical challenge. Diagnosis by clinical consensus is estimated to result in misdiagnosis for up to 40% of patients (Schnakers et al., 2007, 2009; J. Wang et al., 2020), and behavioural assessments of unresponsiveness are further complicated by conditions such as cognitive-motor dissociation – which is highly prevalent and estimated to afflict 15 to 20% of coma/DOC patients (Claassen et al., 2019; Edlow et al., 2021; Owen et al., 2006). Furthermore, there are a lack of tools available to clinicians for accurate patient prognostication – which is reflected in high-degrees of reported uncertainty when clinical professionals are asked to predict

patient outcome (Papadimitriou et al., 2022; Robertsen et al., 2019). Given these clinical shortcomings, there is a strong need for new clinical tools which can accurately assess coma and DOC patients in the ICU. Strategies targeting point-of-care assessments at the bedside are of particular relevance, as decisions regarding WOLST often occur within the first week or two of hospital admission (Edlow et al., 2021; Kotchoubey & Pavlov, 2018; Sandroni et al., 2021; Turgeon et al., 2011).

Fortunately, quantifying neuronal FC has shown promise in improving patient diagnosis and prognostication (Chennu et al., 2017; Demertzi et al., 2015; Di Gregorio et al., 2022; Norton et al., 2012). These networks can be quantified using various graph theoretical metrics – which can be characterized at macro-, meso-, or nodal scales (Betzel et al., 2018; Mursa et al., 2021). Macro-scale network properties describe the entire network, while the meso-scale focuses on network communities, and nodal metrics quantify the happenings at a single node in the network (Betzel et al., 2018; Mursa et al., 2021). Nodal metrics are limited in their ability to capture the dynamic interactions between brain regions, while macro-scale measures are at a disadvantage in terms of their computational resources and clinical translatability – with the meso-scale offering a balance between the two (Newman, 2006; Sporns & Betzel, 2016). One such meso-scale metric – called network motifs – will be the focus of this study.

Motifs describe subgraphs of the overall brain network: they are connection patterns within a network which reoccur significantly more frequently than in random networks (Milo et al., 2002; Sporns & Kötter, 2004). When networks are constructed from the functional connections between electrodes in an EEG, motifs represent the functional organization of the

underlying neural activity (Duclos et al., 2021; Sporns & Kötter, 2004). Motifs are valuable in that they provide unique meso-scale insight into the nature of information processing within a network (e.g., if a network is primarily comprised of feedforward or feedback loops), and thus are often described as the network “building blocks” (Betz et al., 2018; Milo et al., 2002).

Past studies have found that the topological reorganization of motifs derived from EEG show promise in tracking the loss and recovery of consciousness caused by general anesthesia (Duclos et al., 2021; Nadin et al., 2020; Shin et al., 2013). For example, Duclos et al. (2021) studied unidirectional 3-node motifs calculated from high-density (hd) EEG in the alpha frequency band (8-13 Hz). Motifs were calculated for healthy controls ($n = 9$) who underwent a 3-hour propofol and isoflurane anesthetic protocol. Duclos et al. (2021) found that motifs 1, 2, and 7 (Figure 1.1) recurred at significant frequencies in the healthy controls, but motif 2 failed to topologically reconfigure between anesthesia states. Motif 1 consisted of long-range chain-like connections, converging onto a single node, and was concentrated in central electrodes. In contrast, motif 7 was comprised of short-range loop-like connections and was concentrated in peripheral electrodes (Duclos et al., 2021; Figure 1.1). Notably, topologies for both motifs significantly changed from baseline as anesthesia was administered, and started to return to baseline patterns after anesthesia was withdrawn. Non-topological motif frequency (i.e., the number of times a given motif occurred – irrespective of spatial topology), however, did not significantly change over anesthesia states – suggesting that motif spatial reconfiguration was key to indexing consciousness (Duclos et al., 2021).

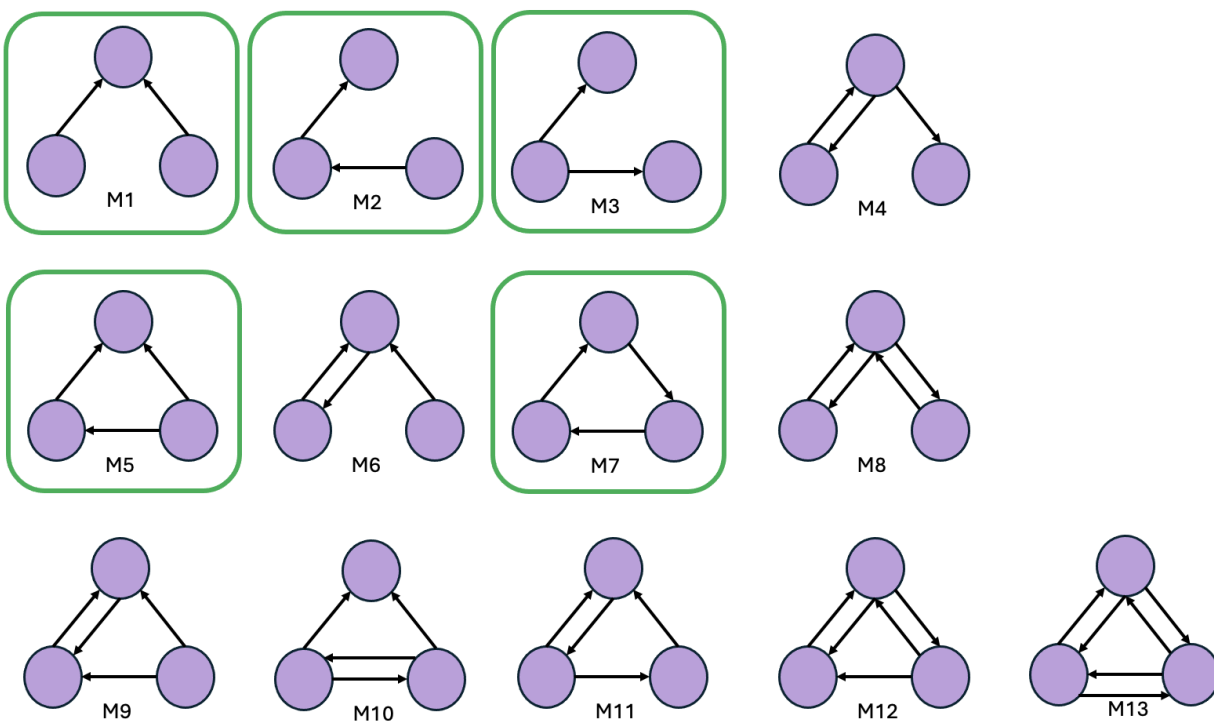


Figure 1.1. A visual representation of all possible connection patterns between 3-nodes in a network. Unidirectional motifs are highlighted by green squares.

Using similar methods, Nadin et al. (2020) conducted a case series on three patients with DOCs exposed to propofol anesthesia. Two of the patients had hd-EEG collected during propofol administration and withdrawal – one of whom was a 50-year-old female who suffered a stroke, but later recovered consciousness and emerged from her UWS status [Glasgow Coma Scale (GCS) = 15]. The second was a 24-year-old male who acquired an anoxic injury and had been in a chronic UWS state for over 8.5 years [Coma Recover Scale-Revised (CRS-R) = 5; Nadin et al., 2020]. Motifs 1 and 7 recurred with significant frequencies in these brain-injured patients and changed topology between anesthesia states (Nadin et al., 2020). In the case of the 24-year-old

chronic DOC patient who did not recover, the motifs changed from baseline topology during anesthesia administration, but failed to return to baseline patterns after anesthesia withdrawal. In contrast, the 50-year-old DOC patient who later recovered consciousness had their motifs topologically reconfigure under anesthesia, then return to baseline patterns after anesthesia withdrawal. The differences in these two case studies led Nadin et al. (2020) to suggest that 3-node network motif topologies from the alpha frequency band may have prognostic value for DOC patients.

As for the diagnostic value of functional brain network motifs, Guo et al. (2023) recently investigated 3-node unidirectional motifs in the resting-state networks of DOC patients using functional magnetic resonance imaging. Relative to healthy controls, patients showed abnormal motif frequencies at the whole-brain level, within resting state networks, and between resting state networks. Interestingly, in the default mode network, the degree to which patient motif frequencies deviated from that of healthy controls correlated with auditory, visual, motor, and oromotor subscales of the CRS-R (Guo et al., 2023).

Currently, there are no published studies on the clinical value of motifs for comatose patients, and only the two aforementioned studies of motifs in the context of DOCs (Guo et al., 2023; Nadin et al., 2020). However, given the established ability of motifs to differentiate states of consciousness in healthy controls (Duclos et al., 2021; Kafashan et al., 2016; Shin et al., 2013), in combination with the potential prognostic and diagnostic value of motifs for brain-injured patients as demonstrated by Nadin et al. (2020) and Guo et al. (2023), we aimed to further investigate the clinical utility of 3-node network motifs derived from hd-EEG.

Our general hypothesis was that functional network motifs have prognostic and/or diagnostic value for brain-injured patients in the ICU diagnosed with coma or DOC. To test this hypothesis, we examined anesthetic-induced motif reconfiguration and its ability to distinguish favourable versus unfavorable diagnoses and prognostic outcomes in patients. Coma and DOC patients had 128-channel EEG recorded during an anesthetic protocol. At baseline, patients were either receiving propofol or were off sedation, and subsequently underwent propofol withdrawal or administration (changing their level of anesthetic exposure), before returning to their baseline state. Weighted and directed FC in the alpha band was calculated for all anesthetic epochs, from which five 3-node motifs were calculated. Motif topologies were then analyzed for motifs which recurred at a significant frequency. For our prognostic analyses, patients were delegated into “recovered” or “not recovered” groups based on their recovery of command-following abilities within 1-year post-injury. This criterion was used to delegate prognostic groups since command-following – either through functional object use or accurate communication – is widely used to denote emergence from a DOC in clinical practice (Giacino et al., 2004). For diagnostic analyses, patients were delegated into “favorable” or “unfavorable” groups according to their GCS scores when off sedation. A GCS score of 8 was used as a threshold to delegate diagnostic groups, since a $GCS \leq 8$ indicates severe brain injury, while a $GCS > 8$ indicates moderate/mild injury (Teasdale & Jennett, 1974).

We specifically hypothesized that patients with favorable diagnoses and prognoses, relative to those with unfavorable measures, would: 1) show greater motif topological reconfiguration during anesthesia administration and withdraw, and 2) more effectively return to

baseline topological patterns after the anesthetic perturbation. Reconfiguration in motif topologies across the scalp, but not non-topological motif scalar values (e.g., a count of overall motif frequency), were hypothesized to be associated with clinical measures, as suggested by the findings of Duclos et al. (2021). Thus, motif scalar properties were examined as an experimental control. Furthermore, four graph theory properties served as whole-network control metrics to test whether meso-scale motifs were informative beyond that of macro-scale network properties (Betzel et al., 2018). Network hub and alpha power topologies served as topological controls, so that we could observe whether motifs were epiphenomenal to either metric.

Methods

Anesthetic Protocol

Coma and DOC patients ($n = 56$) with severe brain injury had 128-channel EEG recorded during an anesthetic protocol. Patients recruited under the “NETICU” study ($n = 37$) received propofol at baseline, had propofol withdrawn, then were subsequently re-administered propofol at their baseline infusion rate (Figure 1.2). The propofol infusion rate for this cohort was based on the clinical needs of the individual patients and ranged from 33 to 83 mcg/kg/min. Patients who had been previously weaned off sedation were recruited under the “WSAS” study ($n = 18$) and underwent the inverse protocol: At baseline patients were off sedation, then underwent propofol administration and subsequent propofol withdrawal back to their baseline state (Figure 1.2). All WSAS patients received a targeted effect site concentration of 2.0 $\mu\text{g/ml}$ according to the Marsh pharmacokinetic model (Marsh et al., 1991).

The NETICU and WSAS projects were multicenter studies, as data collection occurred across sites in Quebec and Ontario, Canada. Data collection in Montreal, Quebec occurred at Montréal General Hospital, Montréal Neurological Institute, and Hôpital du Sacré-Cœur-de-Montréal; while data collection in London, Ontario took place at Victoria Hospital and University Hospital. Patient data and EEG collection was conducted by our team and collaborators who later shared data with us. Procedures were consistent across sites, such that the same anesthetic manipulations and data collection protocols were followed. After obtaining the data, all EEG preprocessing and analyses were conducted by our team. Propofol was administered intravenously for both NETICU and WSAS datasets; however, since the WSAS protocol employed a targeted effect site concentration, an Alaris PK Carefusion target-controlled infusion pump (Carefusion, Switzerland) was used to administer propofol and model its pharmacokinetics. In contrast, during the NETICU protocol, propofol was administered by nurses according to standard of care and the patient's individual needs.

Upon preliminary analysis of the NETICU dataset, it was found that, of the 37 patients with significant motifs, only 2 of them failed to recover command-following abilities. Due to the skew between recovered and non-recovered patients, we combined NETICU and WSAS datasets. Indeed, this helped, as of the 18 WSAS patients with significant motifs, 10 of them did not recover. Data from the two inverse NETICU and WSAS protocols were merged by combining states in which propofol was withdrawn or administered (Figure 1.2 – indicated by green and pink stars, respectively). Additionally, baseline state comparisons (between the first and last states of each protocol) were grouped together.

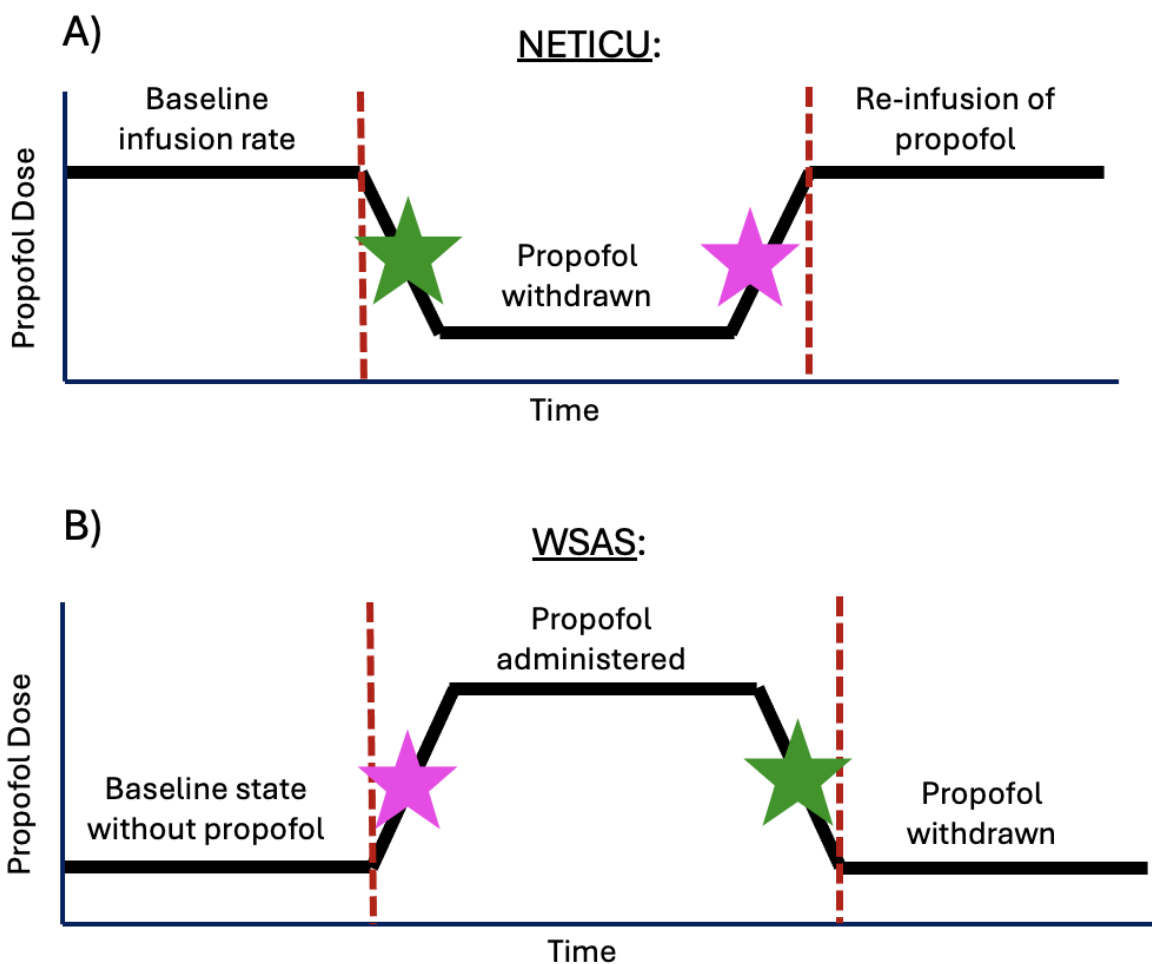


Figure 1.2. Anesthetic protocols used. The NETICU protocol is shown in (A) and the WSAS protocol in (B). For both protocols, transitions in which propofol was withdrawn are indicated by green stars, and transitions in which propofol was administered by pink stars.

Patient exclusion criteria was as follows: a GCS > 8 while on sedation, non-neurological cause of impaired consciousness, or EEG which was determined to be unusable due to excessive noise. Patients were excluded from prognostic analyses if they underwent WOLST and failed to

show command-following abilities before withdrawal of treatment – as this functional outcome was confounded and may not accurately reflect the brain’s capacity for recovery.

Furthermore, only patients who received a propofol infusion rate > 30 mcg/kg/min were included in this study. This additional exclusion criterion was derived from exploratory preliminary analyses of the NETICU data during propofol withdrawal, where we examined the effects of propofol dosage. Patients who received a propofol dose ≤ 30 mcg/kg/min showed positive correlations between their motif cosine similarity values and behavioural measures of diagnosis and prognosis. Conversely, patients who received a dose > 30 mcg/kg/min showed negative correlations between these measures. An example of dose-dependent inverse correlations between motif frequency cosine similarity and patient GCS during anesthesia withdrawal can be seen in Supplementary Figure 1.

Behavioural Assessments

GCS scores collected while patients were off sedation served as an index for patient diagnosis (Teasdale & Jennett, 1974). For the NETICU dataset, attending clinical staff assessed GCS scores. For patients recruited under the WSAS protocol, experimenters assessed patient CRS-R scores immediately prior to any anesthetic intervention. Given that the two datasets involved different measures of patient diagnoses, and the CRS-R is more thorough than the GCS (Giacino et al., 2004), we converted CRS-R scores from the WSAS dataset into GCS scores. A “good” diagnosis was defined as a GCS (off sedation) > 8 .

To index patient recovery, in both the NETICU and WSAS datasets, experimenters conducted phone interviews and assessed patients 3-, 6-, and 12-months after the EEG recording

session. Patients were classified as recovered if, at any point, they were able to consistently follow commands and/or verbally respond to speech in a context-appropriate manner. This criterion was selected since it signifies the presence of functional object use or accurate communication – denoting emergence from a DOC according to the CRS-R (Giacino et al., 2004).

EEG Recording and Preprocessing

Resting-state 128-channel EEG was recorded with the EGI Sensor Net using an Amps 400 amplifier (Electrical Geodesic, Inc., USA). Signals were recorded at 1,000 Hz and referenced to the vertex electrode (Cz). Prior to recording, electrode impedances were kept below 50 K Ω . Baseline, intervention, and post-intervention states were then isolated from the continuous EEG recordings. All states were approximately the same length within each patient. The length of these states ranged from 5 to 10 minutes – depending on data availability. EEG recordings were preprocessed by resampling to 250 Hz, bandpass filtering between 0.1 and 50 Hz, notch filtering at 60 Hz, manually identifying and removing noisy channels, segmenting into 10-second epochs, re-referencing to the average of all electrodes, discarding non-brain electrodes, then manually identifying and removing noisy epochs (the pipeline is available at https://github.com/BIAPT/NET_ICU). After preprocessing, epoched data was concatenated back into continuous EEG using the MATLAB (version R2020a) *eeg_epoch2continuous* function. Data was bandpass filtered at 8-13 Hz to isolate the alpha frequency band because motifs derived from the alpha band have shown the most promise in tracking consciousness in both healthy

controls (Duclos et al., 2021) and DOC patients (Nadin et al., 2020). EEG recording, preprocessing, and analyses were the same for NETICU and WSAS datasets.

Functional Network Construction

FC was quantified using the weighted phase-lag index (wPLI) (Vinck et al., 2011) and directed phase-lag index (dPLI) (Stam & van Straaten, 2012). wPLI models the weight (strength) of connections using the magnitude of the imaginary component of the cross-spectrum, making it robust against volume-conduction (Vinck et al., 2011). wPLI is calculated as follows:

$$wPLI_{ij} = \frac{|E\{\text{Im}\{C_{ij}\}\}|}{E\{|\text{Im}\{C_{ij}\}|\}} = \frac{|E\{|\text{Im}\{C_{ij}\}| \text{sgn}\{\text{Im}\{C_{ij}\}\}\}|}{E\{|\text{Im}\{C_{ij}\}|\}}$$

Where $\text{Im}\{C_{ij}\}$ denotes the imaginary part of the cross-spectrum between electrodes i and j , sgn denotes the signum function, and E denotes the expected value operator (Vinck et al., 2011). wPLI values range from 0 to 1: A wPLI score of 1 indicates a perfect phase-lock relationship between electrodes, while a score of 0 indicates no phase relationship.

The dPLI models connection directionality by determining which signal is phase-lead, and which is phase-lag (Stam & van Straaten, 2012). dPLI is calculated as follows:

$$dPLI_{ij} = \frac{1}{T} \sum_{t=1}^T H\{\Delta \phi_{ij}\}$$

Where T denotes the entire length of the time series, t a specific time point, H the Heaviside step function, and $\Delta \phi_{ij}$ the difference in phase between electrodes i and j (Stam & van Straaten, 2012). dPLI values range from 0 to 1. A dPLI between 0.5 and 1 indicates that electrode i is

phase-lead relative to j , a value between 0 and 0.5 indicates that electrode i is phase-lag relative to j , and a dPLI value of exactly 0.5 indicates no phase relationship.

Both wPLI and dPLI connectivity were calculated across 10-second non-overlapping windows, then averaged across windows to produce the mean FC for each anesthesia state (baseline, intervention, and post-intervention). The effects of spurious connectivity were further controlled for using wPLI and dPLI surrogate analyses – in which phase relationships are destroyed by randomizing the phase time series at electrode j , whilst keeping that at electrode i fixed. Connectivity values in the observed network were then compared to the distribution of 100 random surrogate networks using a Wilcoxon signed rank test. Connections which were significantly different ($p < 0.05$) from the surrogate distribution were kept, while non-significant connections were assigned a value of 0 (in the case of wPLI) or 0.5 (in the case of dPLI).

Motif Analyses

We focused our investigation to unidirectional 3-node motifs, since this facilitated cross-study comparisons and low computational costs. All existing work using EEG to study motifs and their relation to conscious states have used unidirectional motifs calculated from phase-based connectivity measures, and have quantified motif topological reconfiguration using cosine similarity (Duclos et al., 2021; Nadin et al., 2020; Shin et al., 2013). Thus, we replicated these methodological choices to facilitate comparisons between our results and previous literature. Furthermore, we decided to focus on 3-node motifs to maintain low computational costs: When analyzing 3-node motifs, there are only 13 possible (uni- and bi-directional) connection patterns

between nodes (Figure 1.1). However, in making the step to 4-node motifs, the number of possible connection patterns increases to 199 (Milo et al., 2002).

Identifying Motifs

Motifs were calculated from dPLI matrices using the Brain Connectivity Toolbox (BCT) (Rubinov & Sporns, 2010) and custom MATLAB scripts adapted from Duclos et al. (2021). To confirm the presence of a motif, a given connection pattern must have a significantly greater frequency in the observed network than in random networks (Milo et al., 2002). Motif frequency is defined as the number of times a node participates in a given motif with any other node in the network (Duclos et al., 2021; Sporns & Kötter, 2004). We tested whether connection patterns had a significant frequency by generating 100 surrogate networks. Surrogates were constructed by randomly shuffling connections whilst preserving the degree and weight of each node in the patient's observed network. The motif frequency at each node in the observed network was summed, and the total network frequency was compared to the frequency distribution of the 100 surrogates. Network Z-scores were calculated for each of the 5 possible unidirectional motifs, as follows:

$$Z_i = \frac{N_i^{observed} - N_i^{surrogates}}{std\{N_i^{surrogates}\}}$$

Where $N_i^{observed}$ indicates the frequency of connection pattern i summed across all nodes in the observed patient's network, and $N_i^{surrogates}$ indicates the frequency of connection pattern i summed across all nodes in the 100 surrogate networks (Duclos et al., 2021). Connection pattern i was deemed a motif if Z_i exceeded 1.96, while non-significant connection patterns were

assigned a motif frequency of 0 and were not further analyzed. Note that dPLI does not enable the quantification of bidirectional connections, which is why only unidirectional motifs were considered (Stam & van Straaten, 2012).

Calculating Motif Properties

After identifying motifs via their frequency values, we delved into the distance, source, and target properties of significant motifs (Duclos et al., 2021). Motif distance is defined as the Euclidean distance between a node and all nodes it is connected to within a given motif – normalized by the nodal motif frequency (Duclos et al., 2021). Motif source value is defined as the number of times a node was phase-lead within the context of a given motif. Conversely, motif target value is the number of times a node was phase-lag within a motif (Duclos et al., 2021). This enabled us to quantify how often a node was a source or target of information flow according to the dPLI matrices. All motif properties were calculated using BCT and MATLAB scripts adapted from Duclos et al. (2021).

Motif frequency, distance, source, and target properties can be quantified in terms of their topological distribution across the scalp, or by their non-topological scalar counts. For example, on a group level, we can take the topological distribution of nodal frequency averaged across all patients in a group. Conversely, we can sum the frequency for which all nodes participate in a motif, yielding a single number and thereby losing information on spatial topology. Both forms of group analyses were conducted in our study, as we compared motif properties across diagnostic and prognostic groups in terms of their topologies and scalar counts.

Motif Topological Analyses

For our topological analyses, motif frequency, distance, source, and target Z-scores were calculated for each node. This was done by normalizing the nodal motif frequency, distance, source, or target value to that of all other nodes within the network. Then, nodal Z-scores were plotted on a topographic map of our EEG electrode montage for visualization. All topologies were plotted using custom Python (version 3.9.17) scripts. Reconfiguration of motif topology between anesthesia states was quantified using cosine similarity. This metric is a single number, ranging from -1 to 1, which quantifies the degree of similarity between two topologies (Duclos et al., 2021; Nadin et al., 2020; Shin et al., 2013). It is generated by representing two topologies as vectors and calculating the cosine angle between the vectors, as follows:

$$S = \frac{V_i \cdot V_j}{\|V_i\| \|V_j\|}$$

Where V_i and V_j indicate vectors of a given motif property (frequency, distance, source, or target) for anesthesia states i and j (Duclos et al., 2021). A cosine similarity value of 1 signifies that the two vectors have an identical topological distribution, 0 signifies that the topological vectors are orthogonal, and -1 signifies that the vectors have opposite topologies. Cosine similarity values were calculated using custom MATLAB scripts adapted from Duclos et al. (2021).

For diagnostic and prognostic group comparisons, motif topologies for frequency, distance, source, and target properties were averaged across patients belonging to a given group (recovered, not recovered, good GCS, and bad GCS). Thus, electrodes which were not shared between all members of a given group were excluded from topological group comparisons. After

average topographic maps were constructed for favorable and unfavorable diagnostic/prognostic groups, cosine similarity values were calculated for all anesthesia state comparisons (pre- versus post-propofol administration, pre- versus post-propofol withdrawal, and baseline state 1 versus baseline state 2; Figure 1.2).

Statistical Group Comparisons

Cosine similarity values between patients with favorable versus unfavorable diagnoses and prognoses were contrasted using Mann-Whitney U tests. The Benjamini-Hochberg procedure was used to obtain p-values corrected for multiple comparisons. Differences between favorable and unfavorable groups were considered statistically significant at $p < 0.05$. Statistical tests and p-value corrections were conducted in SPSS (version 29.0.0.0).

Motif Scalar Analyses

Motif scalar properties were investigated as a control analyses, since we hypothesized that reconfiguration in motif topologies (and not scalar counts) would have clinical value – in accordance with the findings by Duclos et al. (2021). For diagnostic and prognostic group comparisons, motif frequency, distance, source, and target scalar counts were averaged across patients belonging to a given group (recovered, not recovered, good GCS, and bad GCS). This was done using custom Python scripts. Differences in motif scalar properties between diagnostic and prognostic groups were visually analyzed.

Whole-Network Control Analyses

Several graph theory metrics (clustering coefficient, small-worldness, global efficiency, and modularity) were calculated for all 3 anesthesia states (baseline, intervention, and post-intervention) and were contrasted between patients with favorable versus unfavorable diagnoses and prognoses. These metrics were non-topological: They consisted of a single number representing the average metric value over the entire network. Whole-network control analyses were conducted to test whether the spatial scale of motifs – being situated at the meso-scale between individual network nodes and the entire brain network – offered additional information beyond what can be achieved by studying the whole-network (i.e., the macro-scale; Betzel et al., 2018). Changes in graph theory properties across anesthesia states were visually analyzed and compared to the changes observed in motifs.

Graph Theory Properties

Graph theory metrics were calculated from wPLI matrices which were binarized at a 35% threshold. Meaning, if a given connection was in the top 35% of the strongest connections within the network, it was assigned a connectivity value of 1. Connections which failed to meet this threshold were assigned a connectivity value of 0. This yielded an adjacency matrix, from which graph theory properties were calculated using BCT and MATLAB scripts adapted from Duclos et al. (2021). Network properties were averaged across all nodes in the network and across 10-second non-overlapping windows to yield a single value for a given anesthesia state (baseline, intervention, or post-intervention). To control for spurious connections, 10 random surrogate networks were constructed by shuffling connections in the observed adjacency matrix, without

changing the network's degree distributions. Clustering coefficient and global efficiency were calculated for the surrogate networks, which were used to normalize the clustering coefficient and global efficiency scores in the observed patient network. Normalization was done by taking the observed network score and dividing it by the average score of the 10 surrogate networks.

Clustering coefficient is defined by the proportion of connections which exist between a node and its neighbours, relative to the number of all possible connections which could exist between them (Watts & Strogatz, 1998). Thus, it is a measure of local information integration and the degree to which connections have a tendency to cluster around individual nodes (Bullmore & Sporns, 2009; Rubinov & Sporns, 2010). Small-worldness measures the balance between network segregation and integration (Watts & Strogatz, 1998). It is defined as follows:

$$SWN = \frac{CC^{observed} / CC^{random}}{PL^{observed} / PL^{random}}$$

Where $CC^{observed} / CC^{random}$ indicates the clustering coefficient of the observed network over that measured in random networks, and $PL^{observed} / PL^{random}$ indicates the characteristic path length of the observed network over that measured in random networks (Watts & Strogatz, 1998). Characteristic path length refers to average shortest path length between all possible pairwise combinations of nodes within a network (Watts & Strogatz, 1998). Thus, small-worldness is calculated by taking the fraction of clustering within a network (local integration) over the smallest average path length separating two given nodes (global integration; Bullmore & Sporns, 2009; Rubinov & Sporns, 2010). Global efficiency is defined by the inverse of the characteristic path length ($1/PL$; Latora & Marchiori, 2001). Thus, global efficiency is a measure

of network-wide integration well suited for sparse networks (Bullmore & Sporns, 2009; Rubinov & Sporns, 2010). Finally, modularity measures the network's tendency to separate into distinct modules, which was calculated using the Louvain algorithm (Bullmore & Sporns, 2009; Rubinov & Sporns, 2010). In doing so, the strength of connections within a module were summed: High modularity is defined by strong within-module connections and weak between-module connections. Thus, modularity serves as an index of network segregation (Newman, 2006).

Topological Control Analyses

Alpha power and hub topologies were computed for all 3 anesthesia states (baseline, intervention, and post-intervention) and were contrasted between patients with favorable versus unfavorable diagnoses and prognoses. These control analyses were conducted to test whether motifs provided unique information beyond that of traditional network properties, or if they were simply epiphenomenal (e.g., to alpha power). Patterns in alpha power and hub topologies were visually analyzed and compared to motifs using topographic maps and cosine similarity values.

Alpha Power Topologies

Alpha power topology (dB) was calculated for all nodes across the full length of the anesthesia state. Nodal power was translated into Z-scores by normalizing by the mean and standard deviation of each node in the network. Nodal Z-score were plotted on a topographic map of our EEG electrode montage and plotting was done using custom Python scripts.

Network Hub Topologies

Network hubs were identified from binarized adjacency matrices (described previously in *Graph Theory Properties*) using BCT and MATLAB scripts adapted from Duclos et al. (2021). Network hubs are defined as nodes with a high degree (i.e., nodes with many connections to other nodes), thus node degree was calculated by counting the number of binary connections each node had to all other nodes in the network (Bullmore & Sporns, 2009; Rubinov & Sporns, 2010). Node degree was then translated into Z-scores by normalizing by the mean and standard deviation of each node in the network. These nodal Z-score were plotted on a topographic map of our EEG electrode montage for visualization and plotting was done using custom Python scripts.

Alpha Peak Identification

As a post hoc analysis, we quantified the number of patients who had a periodic alpha peak in their power spectra. Our rationale for this analysis was that the presence or absence of alpha peaks could influence the clinical utility of motifs: if patients do not show alpha oscillatory power, phase-based FC measures derived from alpha power (including motifs) are unlikely to be very informative. In contrast, if many patients display alpha peaks, motifs derived from alpha power may be a good approach to addressing questions surrounding patient diagnosis and prognosis.

The Welch method was used to calculate average band power for the anesthesia states (baseline, intervention, and post-intervention) of each patient. Then, power was separated into periodic and aperiodic components using Python's fitting oscillations and one over f (FOOOF) package (Donoghue et al., 2020). Periodic alpha peaks were modeled and plotted alongside the

aperiodic slope for frequencies between 1 and 20 Hz. Various *FOOOF* function parameters were tested, and parameters were adjusted to maximize visual agreeance between the *FOOOF* algorithm and a trained EEG analyst in identifying 8-13 Hz peaks. Maximal agreeance was found using the following parameters: aperiodic mode = knee, peak width limits = (0.3, 4), minimum peak height = 0.4. Using this model, the number of patients who had a peak with a central frequency between 8 and 13 Hz were counted for anesthesia withdrawal, administration, and baseline state transitions.

Results

Descriptive Analyses of Significant Motifs

Of the five unidirectional 3-node motifs tested (Figure 1.1), motifs 1 (M1) and 7 (M7) recurred significantly more often in patient networks than in random networks and changed topology between sedation states ($p < 0.05$). The proportion of patients with a significant M1 was $\approx 50\%$ (22/43) during anesthesia withdrawal, $\approx 67\%$ (18/27) during anesthesia administration, and $\approx 60\%$ (16/27) between baseline states. For M7, the proportions were $\approx 70\%$ (30/43) during anesthesia withdrawal, $\approx 85\%$ (23/27) during anesthesia administration, and $\approx 74\%$ (20/27) between baseline states.

Among the patients with significant motifs, there were no systematic imbalances in the number of patients with favorable versus unfavorable prognostic and diagnostic labels. For example, of the 22 patients with a significant M1 during anesthesia withdrawal, 10 were recovered and 7 were non-recovered patients (the remaining 7 patients lacked prognostic data

and could only be included in our diagnostic analyses), while 5 had a “good” GCS and 17 a “bad” GCS (this potential imbalance could be explained by the fact that, in total, only 7 patients belonged to the good GCS group and 23 belonged to the bad GCS group). Similar trends were observed for M7. Also of note, patients who displayed a significant M1 often also displayed a significant M7, and vice versa. Thus, there was a large overlap between the patients with an observable M1 and those with an observable M7. For example, of the 43 patients with data during anesthesia withdrawal, 2 had a significant M1 in the absence of an M7, 10 had a significant M7 in the absence of an M1, and the remaining 31 had both a significant M1 and M7.

M1 was comprised of long-range connections: across anesthesia states and group comparisons, M1 extended approximately five-fold further across the scalp than M7. A representative example of such, taken from prognostic comparisons during anesthesia withdrawal, can be observed in Table 1.1 (see *Mean Distance* columns). Furthermore, across anesthesia states and group comparisons, M1 occurred approximately two-fold more often than M7. A representative example of such can also be observed in Table 1.1 (see *Mean Frequency* columns). It is important to note that, for M7, source and target properties are not calculated in any of our analyses because all nodes in this motif are simultaneously a source and target of information flow (Figure 1.1).

Table 1.1. Mean and standard deviation (SD) of motif scalar counts for prognostic groups during anesthesia withdrawal. For significant motifs 1 and 7, scalar counts for motif frequency, distance, source, and target properties are shown during sedation on (pre-anesthesia withdrawal) and off (post-anesthesia withdrawal) states. Motif counts for patients who recovered consciousness are displayed in the top table and counts for patients who did not recover are displayed in the bottom table.

Group: Recovered										
Motif	State	Sample Size	Mean Frequency	SD Frequency	Mean Distance	SD Distance	Mean Source	SD Source	Mean Target	SD Target
1	Sedation On	14	2.78E+05	4.40E+04	5.53E+06	8.83E+05	1.85E+05	2.93E+04	1.85E+05	2.93E+04
1	Sedation Off	18	2.36E+05	4.87E+04	4.62E+06	9.59E+05	1.57E+05	3.25E+04	1.57E+05	3.25E+04
7	Sedation On	16	1.88E+05	5.32E+04	1.50E+06	4.33E+05	---	---	---	---
7	Sedation Off	19	1.79E+05	5.47E+04	1.46E+06	4.52E+05	---	---	---	---
Group: Not Recovered										
Motif	State	Sample Size	Mean Frequency	SD Frequency	Mean Distance	SD Distance	Mean Source	SD Source	Mean Target	SD Target
1	Sedation On	9	2.92E+05	5.96E+04	5.86E+06	1.28E+06	1.95E+05	3.97E+04	1.95E+05	3.97E+04
1	Sedation Off	8	2.65E+05	6.84E+04	5.28E+06	1.43E+06	1.77E+05	4.56E+04	1.77E+05	4.56E+04
7	Sedation On	11	1.89E+05	5.47E+04	1.56E+06	4.34E+05	---	---	---	---
7	Sedation Off	10	1.89E+05	6.08E+04	1.56E+06	4.79E+05	---	---	---	---

Motif Topological Reconfiguration During Propofol Withdrawal

Prognostic Analyses

During propofol withdrawal, neither M1 nor M7 showed a significant difference in topological reconfiguration for frequency (M1: $U = 16.0, p = .434$; M7: $U = 50.0, p = .600$), distance (M1: $U = 31.0, p = .888$; M7: $U = 54.0, p = .600$), source (M1: $U = 34.0, p = .962$), or target (M1: $U = 23.0, p = .506$) properties across prognostic categories [recovered (M1: $n = 10$, M7: $n = 14$); not recovered (M1: $n = 7$, M7: $n = 10$)]. The average topographic maps and cosine similarity values show that both prognostic groups underwent topological reconfiguration in their motif properties between anesthesia states (see Figure 1.3 for M1 and Figure 1.4 for M7).

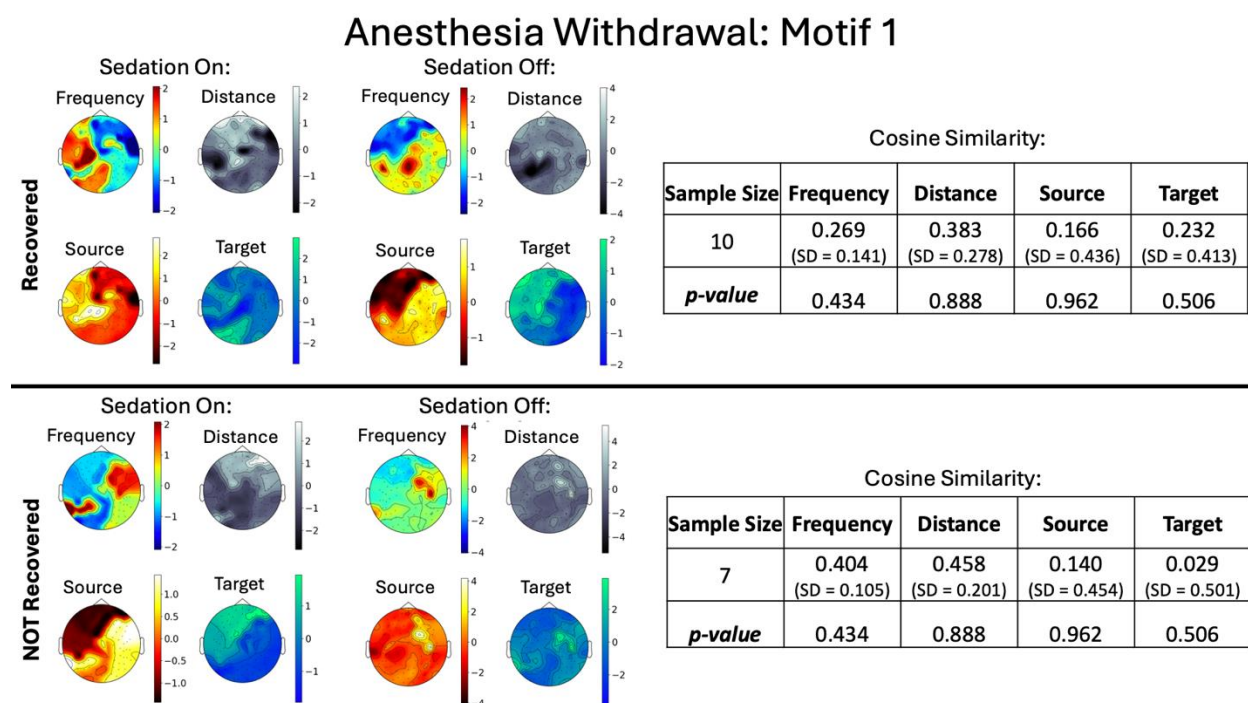


Figure 1.3. Topological plots between prognostic groups for motif 1 frequency, distance, source, and target properties during anesthesia withdrawal. Motif properties were plotted using nodal Z-scores during sedation on (pre-anesthesia withdrawal) and sedation off (post-anesthesia

withdrawal) states. Cosine similarity mean and standard deviation (SD) values between sedation on and off states are displayed in the tables. Group data for recovered patients are displayed on top and not recovered patients on the bottom.

Anesthesia Withdrawal: Motif 7

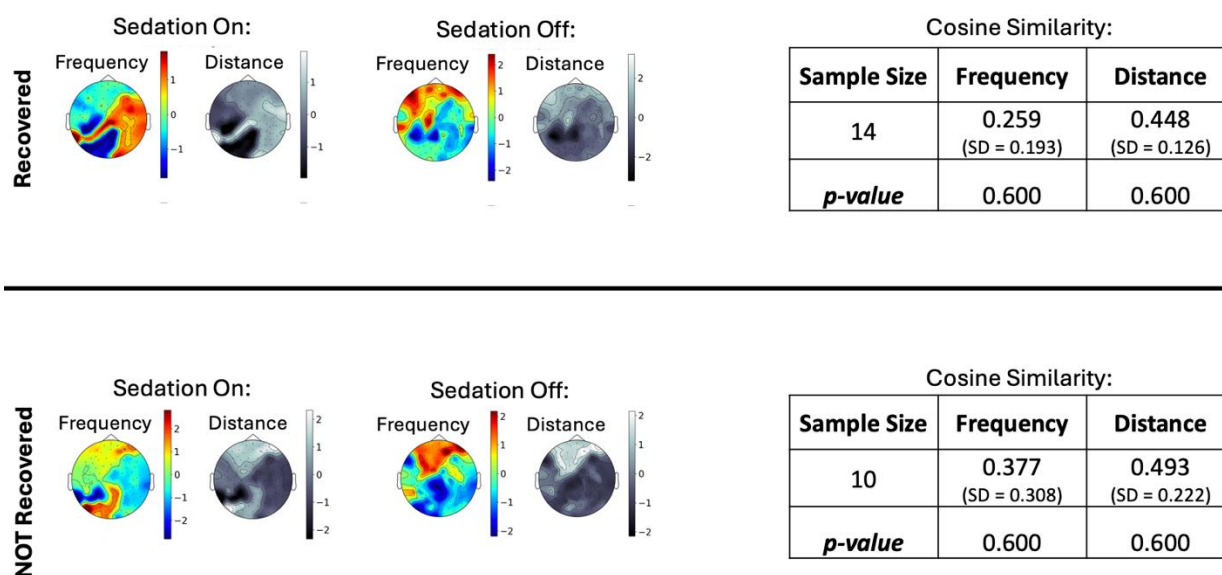


Figure 1.4. Topological plots between prognostic groups for motif 7 frequency and distance properties during anesthesia withdrawal. Motif properties were plotted using nodal Z-scores during sedation on (pre-anesthesia withdrawal) and sedation off (post-anesthesia withdrawal) states. Cosine similarity mean and standard deviation (SD) values between sedation on and off states are displayed in the tables. Group data for recovered patients are displayed on top and not recovered patients on the bottom.

Individual cosine similarity values for each patient were plotted to visually examine data for potential trends (e.g., if a potential separation between groups was starting to emerge, and we simply needed more data points to parcellate the groups). However, after visually inspecting the scatterplots, no emerging trends could be identified for M1 (Figure 1.5) nor M7 (Figure 1.6): The

recovered and not recovered groups completely overlapped in their cosine similarity values. This was true for motif frequency, distance, source, and target properties.

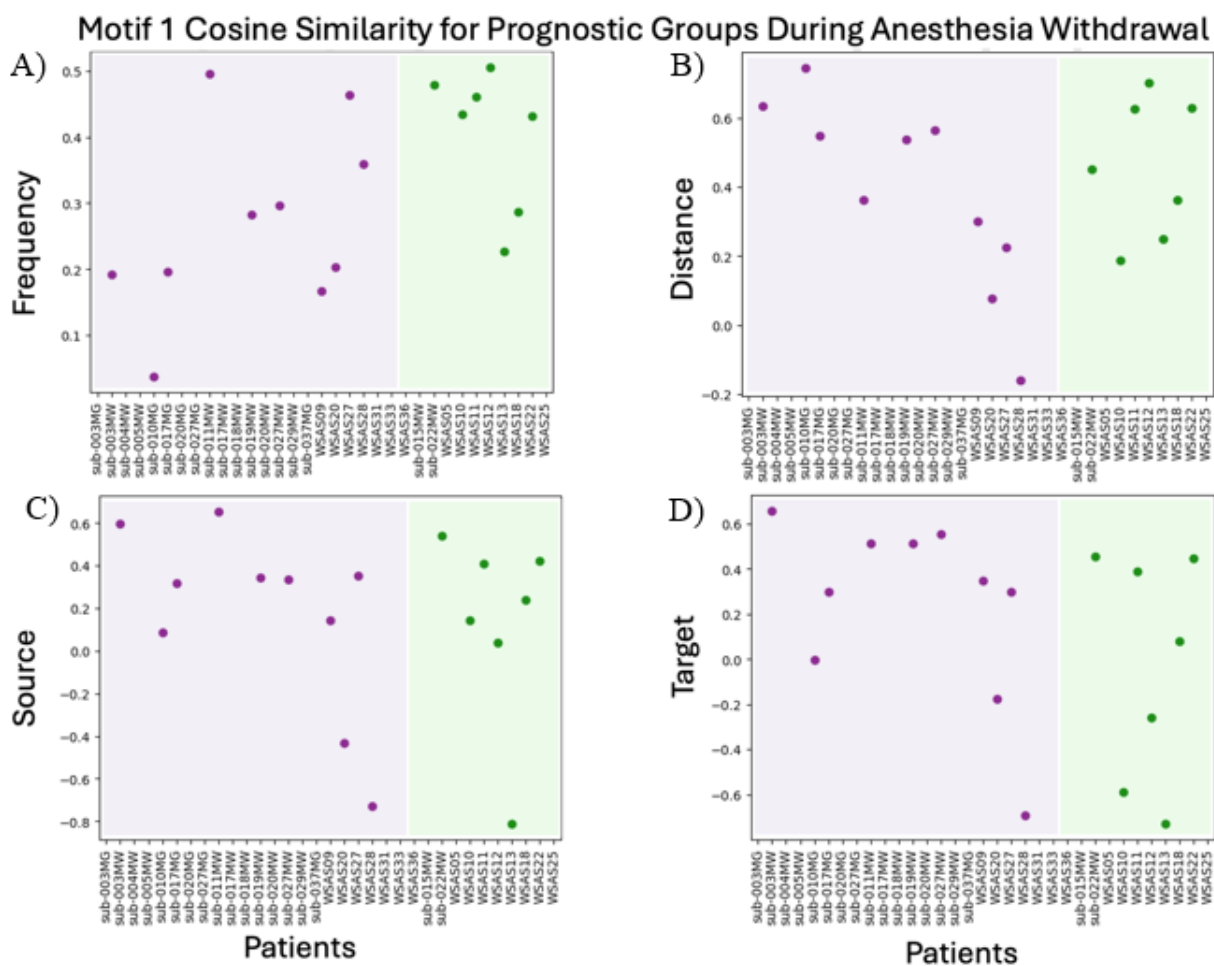


Figure 1.5. Individual cosine similarity values for motif 1 frequency (A), distance (B), source (C), and target (D) properties during propofol withdrawal. Purple = recovered, green = not recovered.

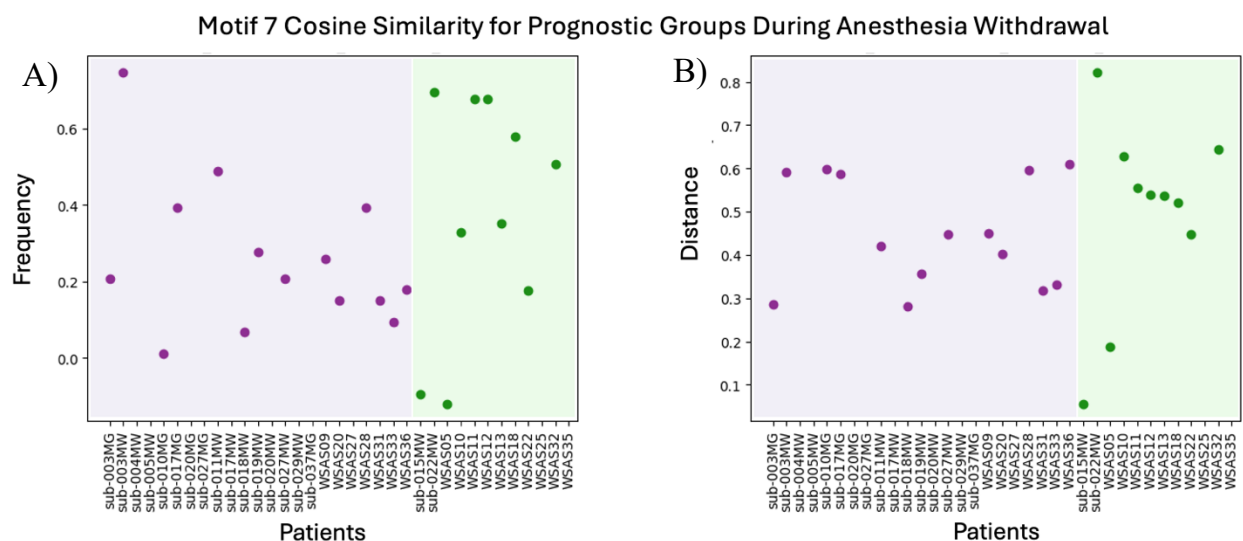


Figure 1.6. Individual cosine similarity values for motif 7 frequency (A) and distance (B) properties during propofol withdrawal. Purple = recovered, green = not recovered.

Diagnostic Analyses

Similarly, neither M1 nor M7 showed a significant difference in topological reconfiguration for frequency (M1: $U = 41.0$, $p = 1.00$; M7: $U = 71.0$, $p = .799$), distance (M1: $U = 25.0$, $p = .567$; M7: $U = 70.0$, $p = .799$), source (M1: $U = 42.0$, $p = 1.00$), or target (M1: $U = 38.0$, $p = 1.00$) properties across diagnostic categories [favorable GCS (M1: $n = 5$, M7: $n = 7$); unfavorable GCS (M1: $n = 17$, M7: $n = 23$)]. These results were corroborated by group average topographic maps/cosine similarity values (see Supplementary Figure 2 for M1 and Supplementary Figure 3 for M7) and cosine similarity scatterplots (M1: Supplementary Figure 4, M7: Supplementary Figure 5).

Motif Topological Reconfiguration During Propofol Administration

Prognostic Analyses

During propofol administration, neither motif showed a significant difference in topological reconfiguration for frequency (M1: $U = 17.0, p = .621$; M7: $U = 41.0, p = .780$), distance (M1: $U = 13.0, p = .434$; M7: $U = 34.0, p = .600$), source (M1: $U = 19.0, p = .764$), or target (M1: $U = 23.0, p = .962$) properties across prognostic categories [recovered (M1: $n = 8$, M7: $n = 10$); not recovered (M1: $n = 6$, M7: $n = 9$)]. These results were corroborated by group average topographic maps/cosine similarity values (e.g., Figure 1.7) and cosine similarity scatterplots (e.g., Figure 1.8).

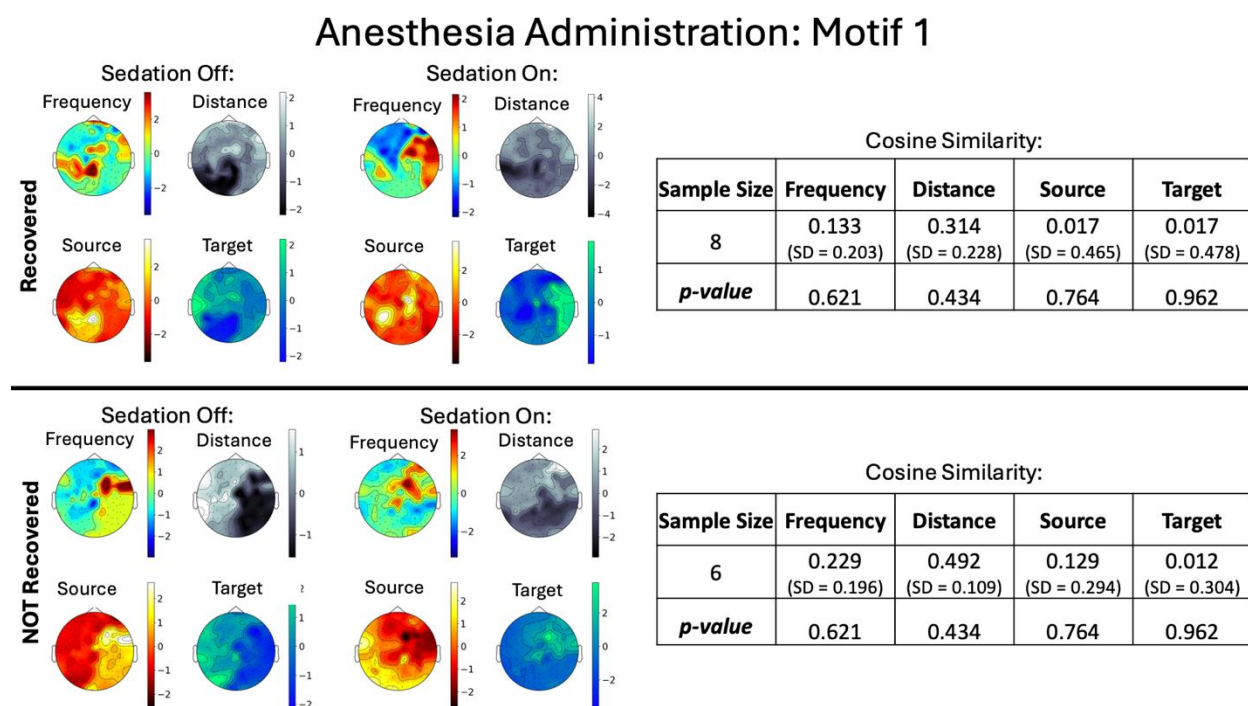


Figure 1.7. Topological plots between prognostic groups for motif 1 frequency, distance, source, and target properties during anesthesia administration. Motif properties were plotted using nodal Z-scores during sedation off (pre-anesthesia administration) and sedation on (post-anesthesia

administration) states. Cosine similarity mean and standard deviation (SD) values between sedation off and on states are displayed in the tables. Group data for recovered patients are displayed on top and not recovered patients on the bottom.

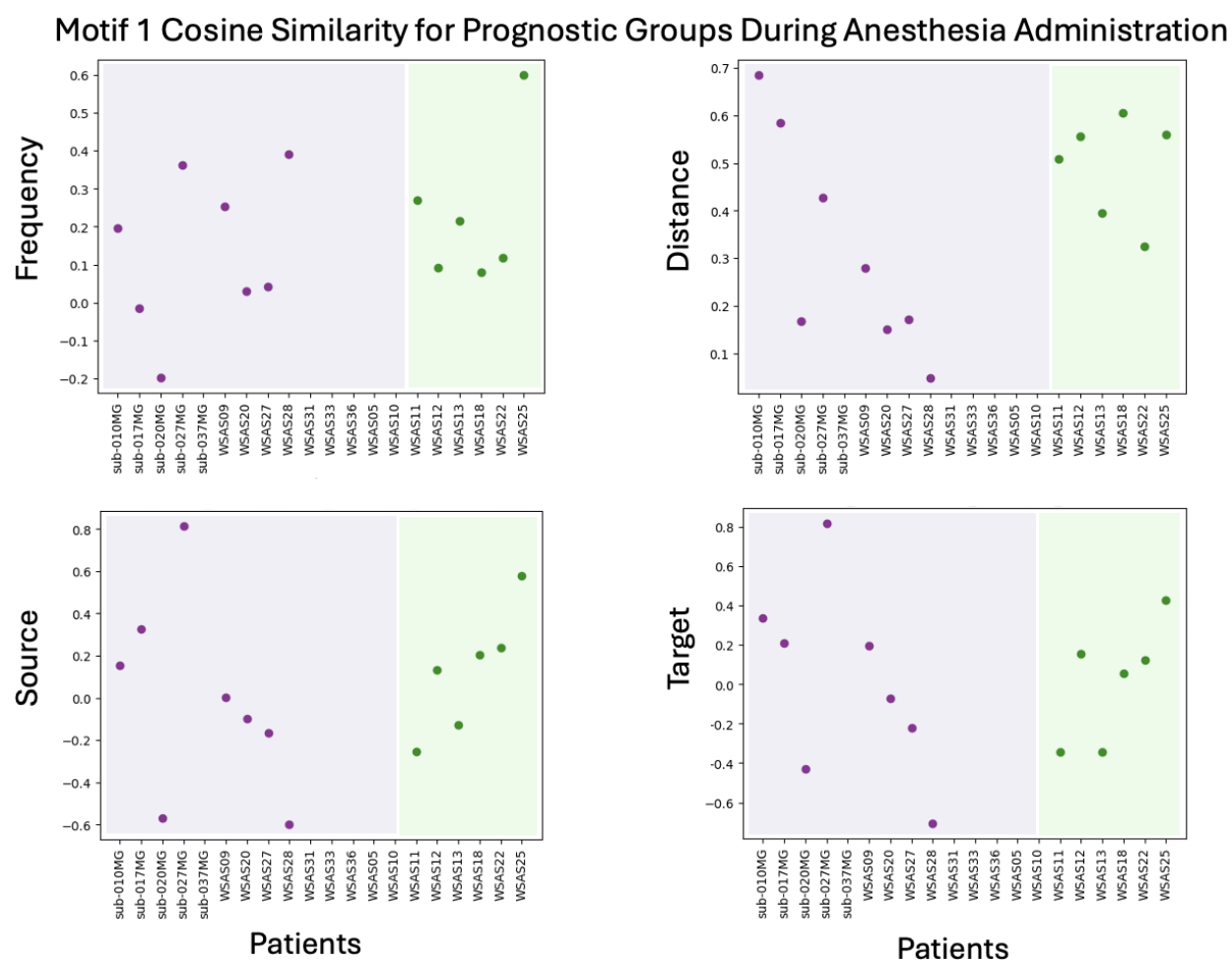


Figure 1.8. Individual cosine similarity values for motif 1 frequency (A), distance (B), source (C), and target (D) properties during propofol administration. Purple = recovered, green = not recovered.

Diagnostic Analyses

Similarly, neither motif showed a significant difference in topological reconfiguration for frequency (M1: $U = 30.0, p = 1.00$; M7: $U = 42.0, p = .857$), distance (M1: $U = 25.0, p = .862$; M7: $U = 34.0, p = .799$), source (M1: $U = 25.0, p = .862$), or target (M1: $U = 30.0, p = 1.00$) properties across diagnostic categories [favorable GCS (M1: $n = 5, M7: n = 5$); unfavorable GCS (M1: $n = 13, M7: n = 18$)]. These null results were corroborated by group average topographic maps/cosine similarity values (e.g., Supplementary Figure 6) and cosine similarity scatterplots (e.g., Supplementary Figure 7).

Return of Motif Topology to Baseline Patterns

Prognostic Analyses

When comparing baseline states, neither motif showed a significant difference in topological reconfiguration for frequency (M1: $U = 10.0, p = .434$; M7: $U = 23.0, p = .600$), distance (M1: $U = 13.0, p = .506$; M7: $U = 25.0, p = .606$), source (M1: $U = 11.0, p = .434$), or target (M1: $U = 10.0, p = .434$) properties across prognostic groups [recovered (M1: $n = 7, M7: n = 8$); not recovered (M1: $n = 6, M7: n = 8$)]. Both groups had motif topologies return to baseline patterns after anesthetic perturbation (M1: Figure 1.9, M7: Figure 1.10). These results were corroborated by cosine similarity scatterplots (M1: Figure 1.11, M7: Figure 1.12).

Baseline States: Motif 1

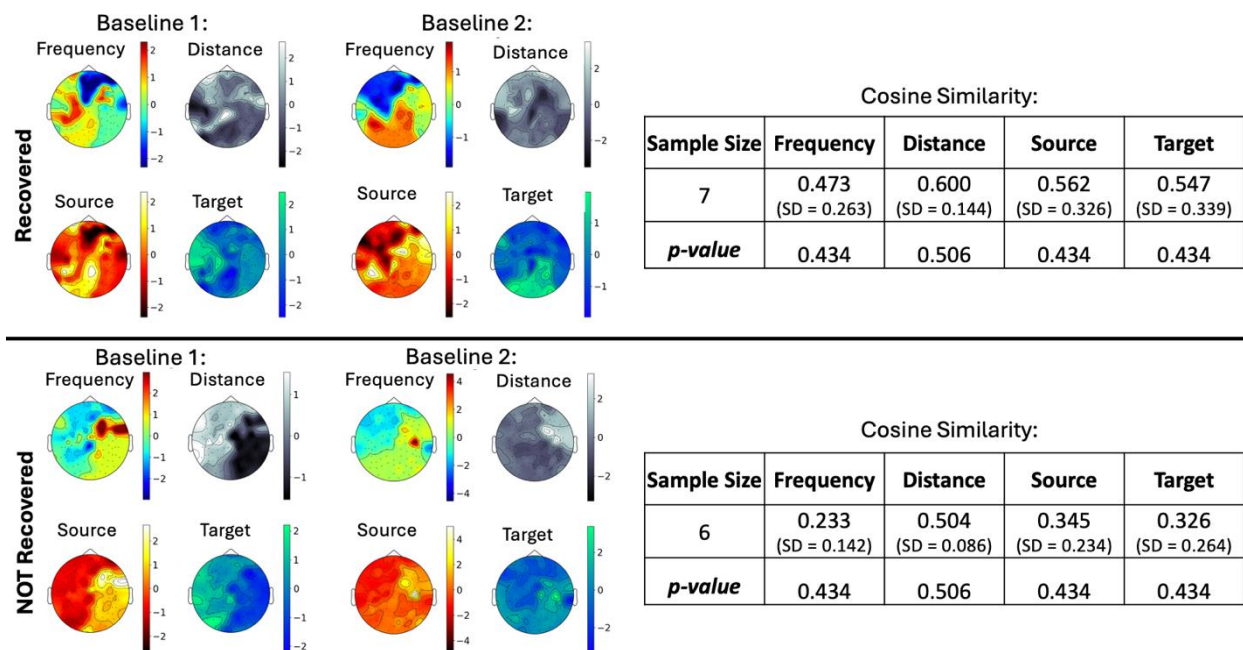


Figure 1.9. Topological plots between prognostic groups for motif 1 frequency, distance, and target properties during baseline states. Motif properties were plotted using nodal Z-scores during baseline 1 and baseline 2 states. Cosine similarity mean and standard deviation (SD) values between baseline states are displayed in the tables. Group data for recovered patients are displayed on top and not recovered patients on the bottom.

Baseline States: Motif 7

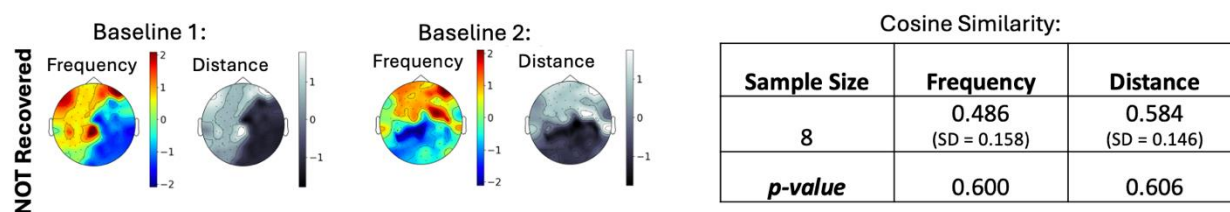
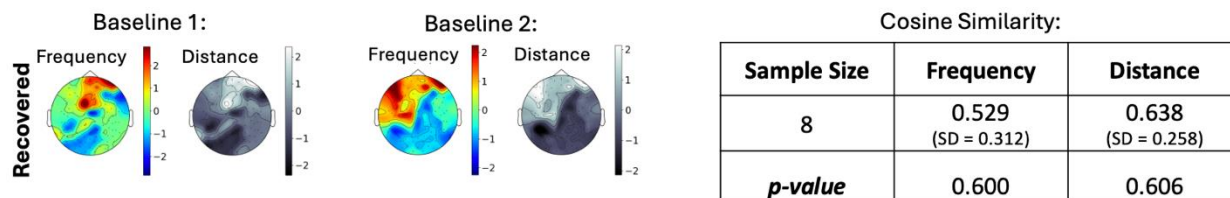


Figure 1.10. Topological plots between prognostic groups for motif 7 frequency and distance properties during baseline states. Motif properties were plotted using nodal Z-scores during baseline 1 and baseline 2 states. Cosine similarity mean and standard deviation (SD) values between baseline states are displayed in the tables. Group data for recovered patients are displayed on top and not recovered patients on the bottom.

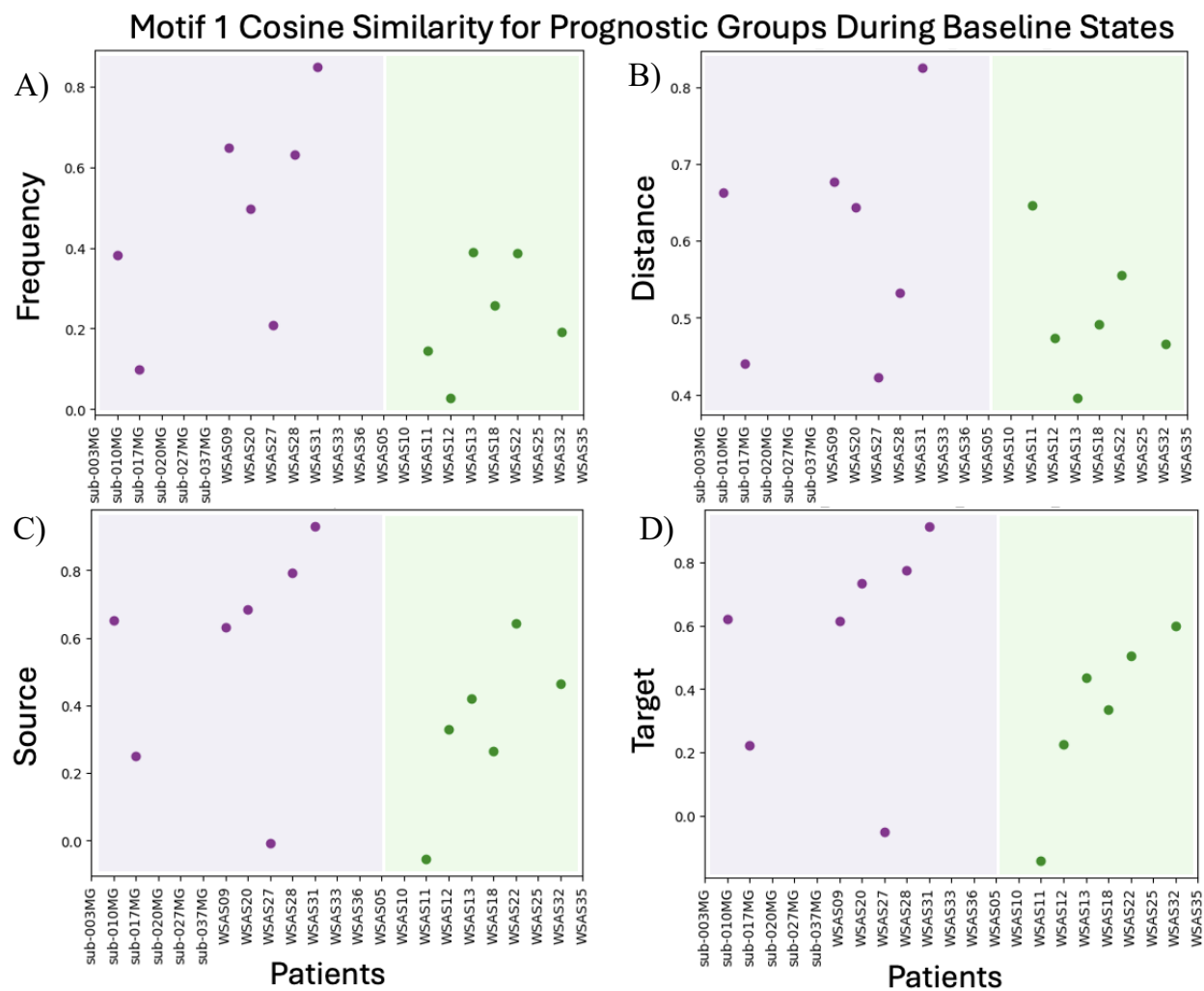


Figure 1.11. Individual cosine similarity values for motif 1 frequency (A), distance (B), source (C), and target (D) properties during baseline states. Purple = recovered, green = not recovered.

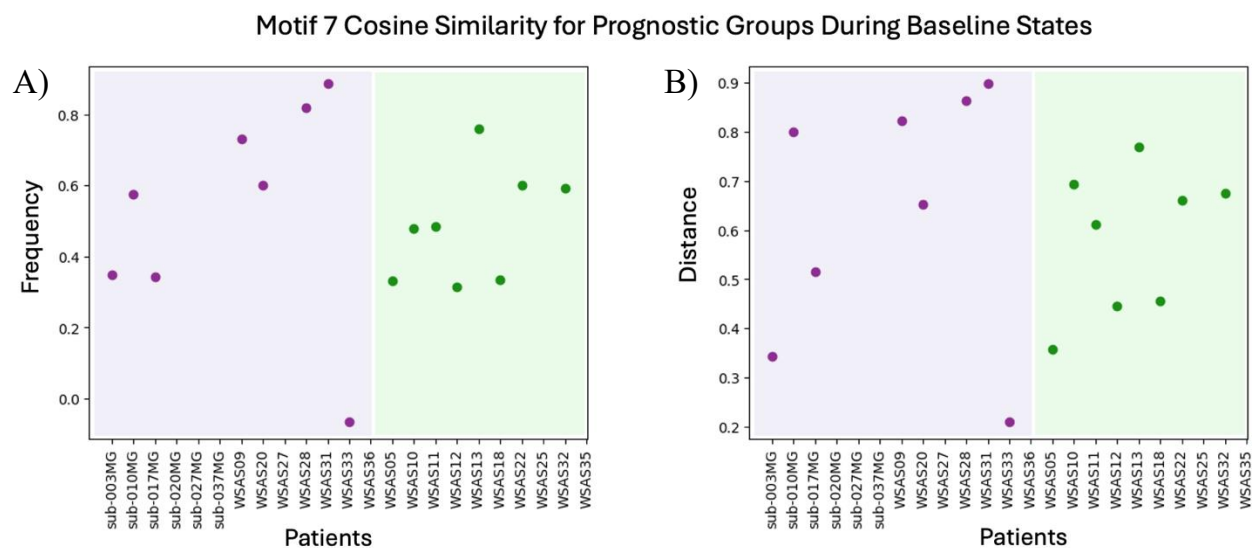


Figure 1.12. Individual cosine similarity values for motif 7 frequency (A) and distance (B) properties during baseline states. Purple = recovered, green = not recovered.

Diagnostic Analyses

Similarly, neither motif showed a significant difference in topological reconfiguration for frequency (M1: $U = 6.0$, $p = .156$; M7: $U = 15.0$, $p = .294$), distance (M1: $U = 20.0$, $p = .862$; M7: $U = 18.0$, $p = .294$), source (M1: $U = 11.0$, $p = .276$), or target (M1: $U = 10.0$, $p = .276$) properties across diagnostic categories [favorable GCS (M1: $n = 5$, M7: $n = 5$); unfavorable GCS (M1: $n = 11$, M7: $n = 15$)]. These null results were corroborated by group average topographic maps/cosine similarity values (M1: Supplementary Figure 8, M7: Supplementary Figure 9) and cosine similarity scatterplots (M1: Supplementary Figure 10, M7: Supplementary Figure 11).

Changes in Motif Scalar Counts Across Anesthesia States

Prognostic Analyses

As for non-topological scalar counts of motif frequency, distance, source, and target values, there were no meaningful changes in motif counts between anesthesia states. It followed that motif scalar counts did not meaningfully differ between the recovered and non-recovered groups. This was true for all anesthesia state comparisons; thus, a representative example of prognostic group motif scalar counts during anesthesia withdrawal is shown in Table 1.1. These results were further corroborated by looking at the plots of individual patient counts. For example, after plotting M1 frequency counts during anesthesia withdrawal (Figure 1.13), the number of times M1 occurred does not distinguish prognostic groups in either sedation state.

Motif 1 Frequency Counts

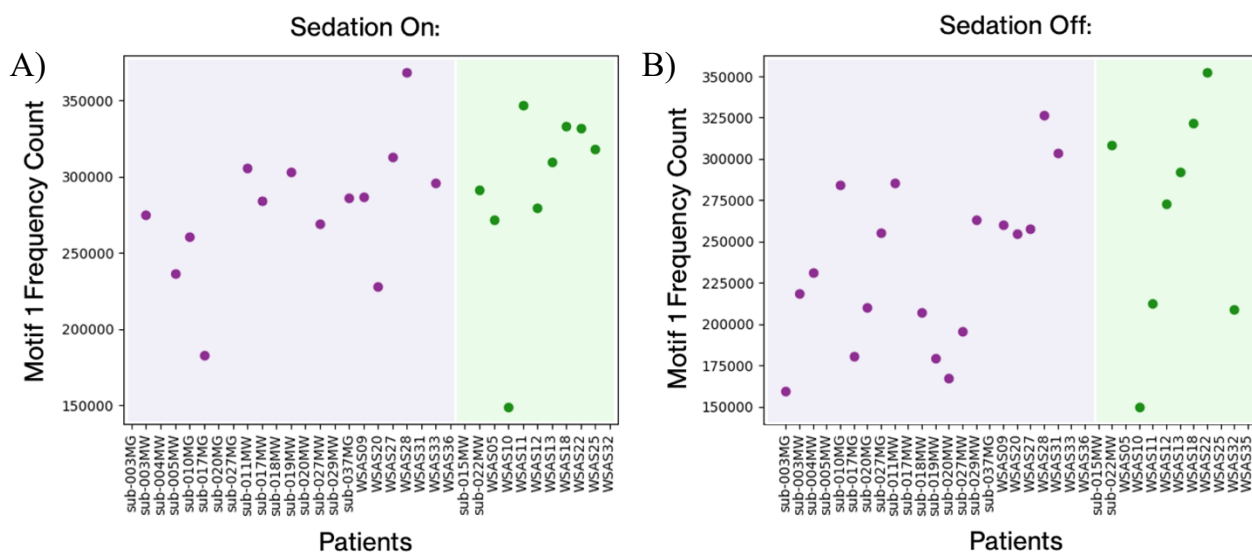


Figure 1.13. Non-topological scalar counts of motif 1 frequency during anesthesia withdrawal. Plotted are individual frequency counts for each patient while sedation was on (pre-anesthesia withdrawal) in A and while sedation was off (post-anesthesia withdrawal) in B. Purple = recovered, green = not recovered.

Diagnostic Analyses

Given that motif scalar counts did not meaningfully change between anesthesia states, these counts were also unable to distinguish diagnostic patient groups. This was true for all anesthesia state comparisons, and a representative example of diagnostic group motif scalar counts during anesthesia withdrawal is shown in Supplementary Table 1. These null results were also corroborated by plotting individual patient counts. For example, after plotting M1 frequency counts during anesthesia withdrawal (Supplementary Figure 12), the frequency of M1 fails to distinguish between diagnostic groups in both the sedation on and off states.

Whole-Network Controls

Graph Theory Properties

There were no meaningful differences in any of the graph theory metrics between prognostic or diagnostic groups. Results were very similar across prognostic/diagnostic group and anesthesia state comparisons; thus, a representative example of recovered versus not recovered patients during anesthesia withdrawal is shown in Figure 1.14. Small-worldness, clustering coefficient, and modularity were marginally lower in patients when they were on, versus off, sedation. However, global efficiency was virtually unaffected by changes in anesthesia. These findings replicate that of past literature (Liang et al., 2023; Nadin et al., 2020).

Anesthesia Withdrawal Control Analyses: Graph Theory

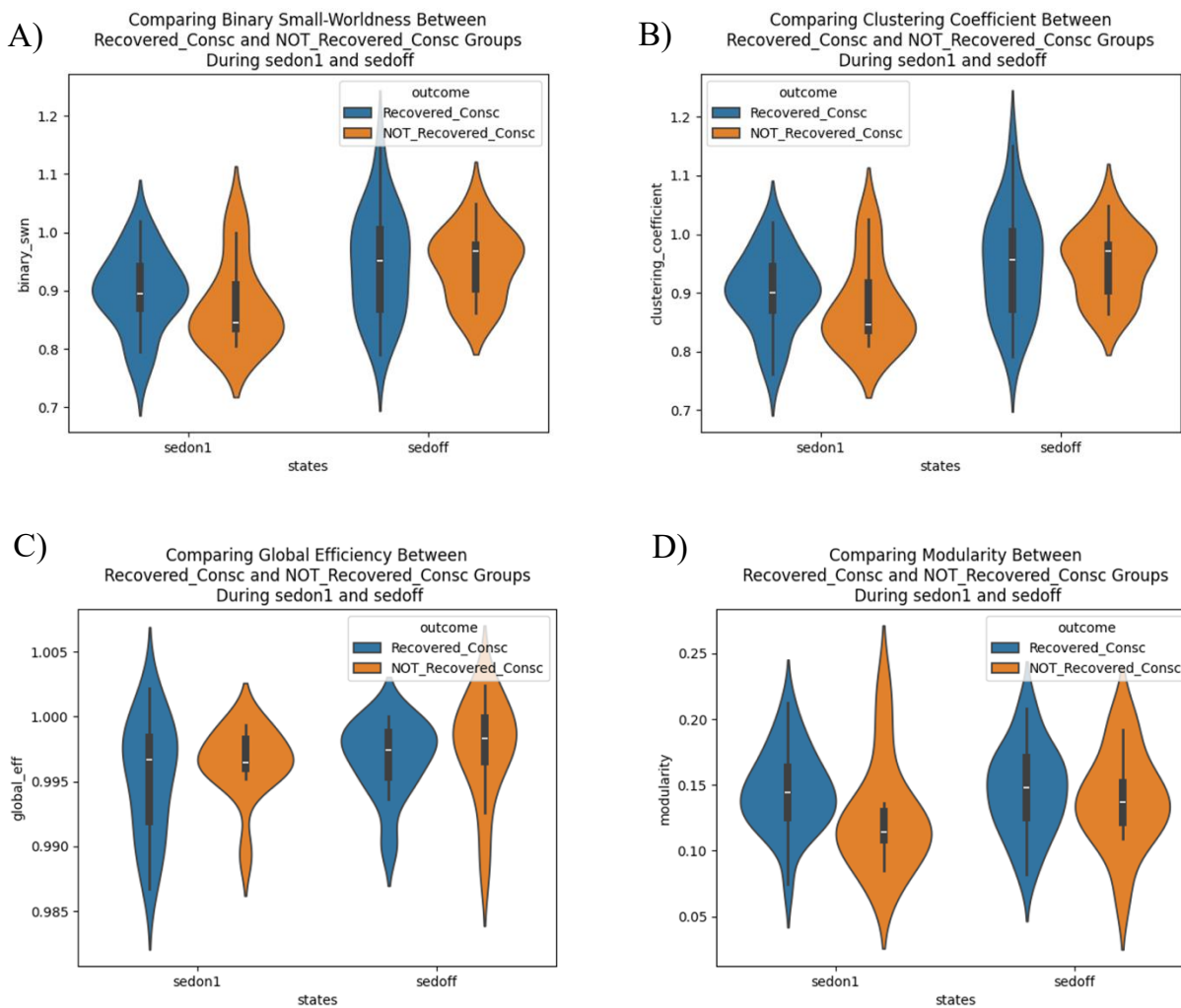


Figure 1.14. Whole-network small-worldness (A), clustering coefficient (B), global efficiency (C), and modularity (D) between prognostic groups during anesthesia withdrawal. Within each plot, network scores while sedation was on (pre-anesthesia withdrawal) and sedation was off (post-anesthesia withdrawal) are shown for recovered (blue) and not recovered (orange) patients.

Topological Controls

Alpha Power Topologies

Power topology was virtually unchanged across anesthesia states, and thus, there was no meaningful difference in power reconfiguration between prognostic or diagnostic groups. Results were consistent across group and anesthesia state comparisons: A representative example of recovered versus not recovered patients during anesthesia withdrawal is shown in Figure 1.15. Given that alpha power was topologically static across sedation states, while motifs reconfigured, our data suggests that power and motif topologies are relatively independent of one another.

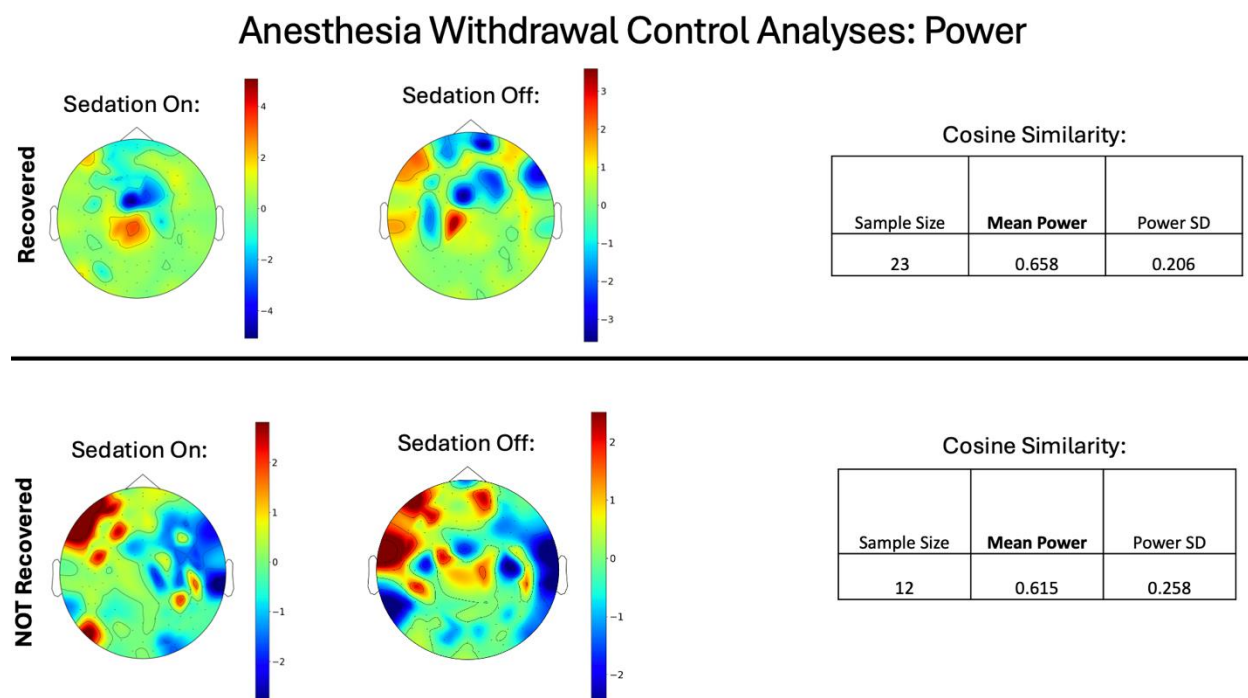


Figure 1.15. Topological plots between prognostic groups for alpha power during anesthesia withdrawal. Alpha power was plotted using nodal Z-scores while sedation was on (pre-anesthesia withdrawal) and sedation was off (post-anesthesia withdrawal). Cosine similarity mean and standard deviation (SD) values between sedation on and off states are displayed in the tables. Group data for recovered patients are displayed on top and not recovered patients on the bottom.

Network Hub Topologies

Network hub topology reconfigured across anesthesia states, but no meaningful difference in the degree of reconfiguration was observed between prognostic or diagnostic groups. Results were similar across prognostic/diagnostic group and anesthesia state comparisons – with a representative example of recovered versus not recovered patients during anesthesia withdrawal being shown in Figure 1.16. Network hubs underwent different topological changes than M1 or M7 (e.g., see Figure 1.16 versus Figures 1.3 and 1.4, respectively). Thus, our data suggests that node degree and motif topologies are also relatively independent of one another.

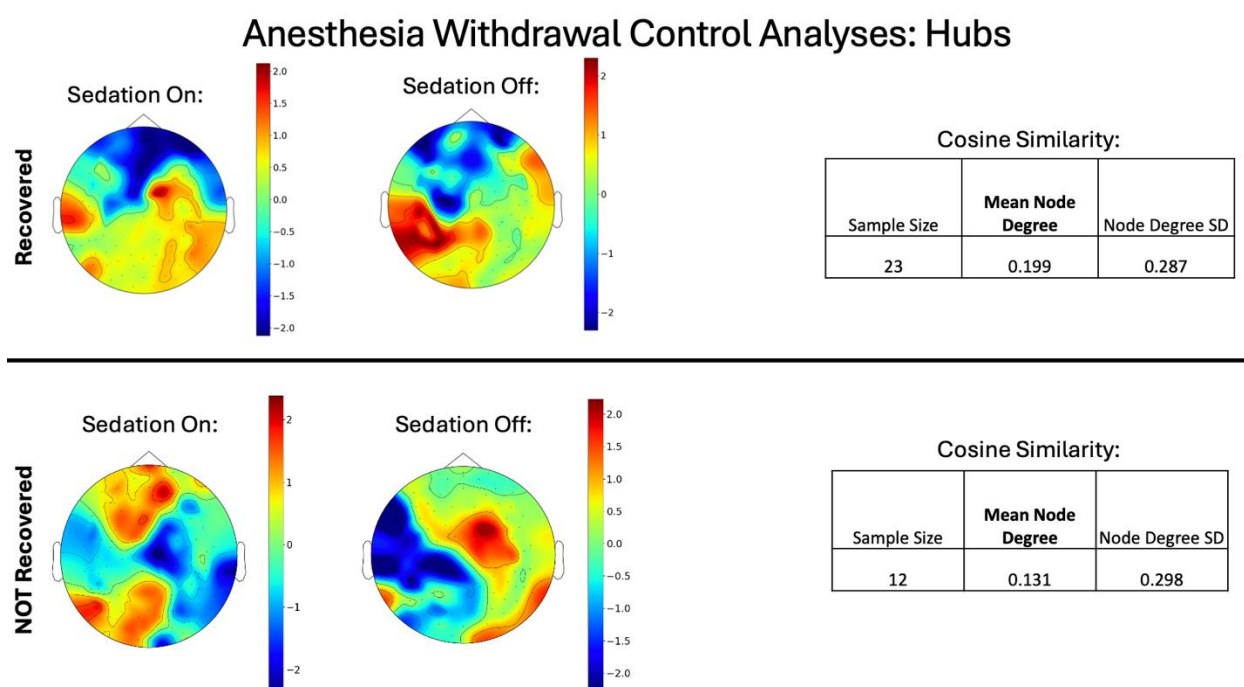


Figure 1.16. Topological plots between prognostic groups for network hubs during anesthesia withdrawal. Node degree was plotted using nodal Z-scores while sedation was on (pre-anesthesia withdrawal) and sedation was off (post-anesthesia withdrawal). Cosine similarity mean and

standard deviation (SD) values between sedation on and off states are displayed in the tables. Group data for recovered patients are displayed on top and not recovered patients on the bottom.

Alpha Peak Identification

Given the null results found when testing the clinical utility of network motifs, we followed-up our analyses with an investigation into the number of patients who had an alpha peak in their power spectra. Very few patients had a periodic EEG peak in the alpha frequency band, as only 7 out of 42 patients had an identified alpha peak during anesthesia withdrawal, and 2 out of 27 patients for anesthesia administration and baseline state analyses.

Discussion

The specific aim of this study was to test whether 3-node motifs derived from alpha band functional connectivity had prognostic or diagnostic utility for a cohort of coma and DOC patients in the ICU. To this end, we identified significant motifs in unresponsive brain-injured patients and analyzed how they reconfigured across varying levels of propofol anesthesia. For our prognostic analyses, we examined whether the topological reconfiguration of these motifs could be used to differentiate patients who recovered command-follow abilities from those who did not. Then, for our diagnostic analyses, we tested the ability of motifs to differentiate patients with severe brain injury ($GCS \leq 8$) from those with moderate to mild injury. Beyond the aforementioned tests of clinical utility, we also explored descriptive and scalar motif properties to test whether the significant connection patterns identified in our cohort of patients was in agreement with those identified by past literature. Strengths of our study included the use of a

within-subject design, as patient topological changes were quantified as an individual was exposed to varying levels of propofol anesthesia. This within-subject design helped control for, though it did not eliminate, the influence of our patient cohort's mixed etiologies. Furthermore, it was a strength that we utilized resting-state EEG recordings, which are not dependent upon factors such as patient task-compliance and task-specific cognitive abilities. Our project also served as a robust replication study, testing the reproducibility of the results found by Nadin et al. (2020). We used the same software pipelines for data analysis and similar anesthetic protocols as the original study, but with a larger sample size.

As for what we found, motifs 1 and 7 (depicted in Figure 1.1) recurred at significant frequencies in our cohort of patients and reconfigured between sedation states. Notably, Duclos et al. (2021) identified these same two motifs as significantly altering topology between states in which healthy controls were being administered general anesthesia (first with propofol, then isoflurane) and when they were free from sedation. Furthermore, M1 and M7 were the motifs found to significantly reoccur and undergo propofol-induced reconfiguration in the three DOC patients analyzed in the case series by Nadin et al. (2020).

Not only did we replicate the identity of the motifs expected to reoccur and topologically reconfigure between sedation states in unresponsive brain-injured patients, but we also replicated their descriptive characteristics. For example, we found that M1 spanned approximately five-fold further across the scalp than M7. Thus, we replicated past findings that M1 consists of long-range chain-like connections and M7 of short-range loop-like connections (Duclos et al., 2021). These complementary forms of information processing fit nicely into many current theories of

consciousness and, more generally, dynamical systems which argue that proper neural functioning is achieved through a balance of local and global integration (Arvin et al., 2022; Tononi, 2004; R. Wang et al., 2021). These theories are backed by robust experimental evidence showing that coma/DOC patients display a lack of long-range FC, relative to healthy controls (Coulborn et al., 2021; Maki-Marttunen et al., 2013; Panda et al., 2022). Rather, the FC of unresponsive patients are biased towards segregation and local integration (López-González et al., 2021; Martínez et al., 2020), providing a potential explanation as to why M1 (supporting long-range global integration) emerged as a significant motif in fewer patients than M7 (supporting short-range local integration). For example, during anesthesia withdrawal, M1 was significant in 22 out of 43 patients, while M7 was significant in 30 out of 43 patients.

Although M1 was present in a smaller proportion of patients, when M1 did significantly recur, it did so approximately two-fold more often than M7. The more frequent recurrence of M1 relative to M7 has been found in studies of DOC patients (Guo et al., 2023), healthy controls (Duclos et al., 2021), and the *Caenorhabditis elegans* nervous system (Prill et al., 2005). The relative abundance of a given motif is hypothesized to be influenced by factors such as its utility in modular goal shifting (Kashtan & Alon, 2005) and robustness to perturbations (Prill et al., 2005). Of particular relevance to our experimental paradigm, Prill et al. (2005) found that the relative abundance of a given motif in various biological systems (ranging from yeast transcription networks to the *C. elegans* nervous system) is positively correlated with the relative stability of the motif to network perturbations. Thus, our finding that M1 has a greater frequency than M7 may, in part, be explained by M1 being more robust against anesthetic perturbations.

Furthermore, null findings in motif scalar properties were replicated. Using hd-EEG, Duclos et al. (2021) found that motif scalar frequency (i.e., the total number of times a given motif occurred, irrespective of topology) did not significantly change as healthy controls were administered, then recovered from, general anesthesia. Further, using magnetic resonance imaging, Guo et al. (2023) found that whole-brain motif frequency does not distinguish healthy controls from DOC patients. In alignment with this past literature, we found motif scalar frequency was unable to distinguish coma and DOC patient prognostic or diagnostic groups. Further, we expanded upon the existing body of literature by including motif distance, source, and target occurrences in our scalar control analyses – yielding similar null results. Additionally, in analyzing whole-brain graph theory metrics, we replicated patterns in clustering coefficient, small-worldness, global efficiency, and modularity observed previously. That is, when tracking the brain of DOC patients during anesthesia admission and withdrawal, there is a marginal decrease in small-worldness, clustering coefficient, and modularity when patients are on sedation (Liang et al., 2023; Nadin et al., 2020), while global efficiency remained virtually unchanged (Nadin et al., 2020). Finally, our finding that motif topologies are independent from that of alpha hubs and power is also consistent with past literature (Duclos et al., 2021; Nadin et al., 2020).

Despite replicating previously discovered motif properties and control analyses, 3-node motifs in the alpha band showed neither diagnostic nor prognostic value for our cohort of coma and DOC patients – in contrast to what has been suggested by previous literature. As for potential explanations for our observations, it could be that our null results accurately reflect the “ground truth” and that, for our cohort of patients, 3-node motifs derived from 8-13 Hz EEG do

not reflect diagnosis or prognostic potential. Indeed, the only study which has used EEG to investigate motifs in unresponsive brain-injured patients was the case series by Nadin et al. (2020) – from which only two patients had EEG collected during propofol administration and withdrawal. Alternatively, it could be that 3-node alpha motifs have clinical value, but because of analytical limitations, it is difficult to utilize motifs. For example, the nature of our motif analyses resulted in high patient data attrition rates.

In order to conduct motif topological analyses between states, not only did patients have to show significant motifs, but they needed to be present in both anesthesia states. For example, for anesthesia withdrawal analyses, motifs needed to be present in sedation on to off states. This condition was met a fraction of the time for both M1 (22/43 patients) and M7 (30/43 patients). Then, these sample sizes were further divided up according to patient diagnostic and prognostic labels. However, despite the attrition that occurred when analyzing motifs on a group level, we do not believe that our results were simply due to modest sample sizes, since no emerging trend could be identified between diagnostic or prognostic groups in any of our scatter plots.

As a post-hoc analysis, we investigated how often EEG alpha peaks were present in our patient cohort. Our rationale being that this analysis may help explain our null results: if most of our patients lack an alpha peak, then connectivity analyses on this frequency band – from which all motif and control metrics were derived – would not be very informative about clinical outcomes. As suspected, alpha peaks were identified in an overwhelming minority of patients across all three anesthesia state transitions. Indeed, past literature has found that it is common for periodic EEG peaks to be absent in coma/DOC patients (Bai et al., 2023; Edlow et al., 2021;

Maschke et al., 2022). This periodic EEG suppression is particularly noticeable in alpha and beta (14–40 Hz) frequency bands, where non-brain-injured adults often display visually identifiable peaks in their EEG spectra (Forgacs et al., 2017). It is hypothesized that this suppression of periodic oscillations is due to the severity of brain damage – specifically thalamocortical deafferentation (Edlow et al., 2021; Timofeev et al., 2000). Given that we screened for patients with severe brain injury (GCS \leq 8 while on sedation), a “self-selection” process may have occurred in that we recruited patients who were less likely to have alpha peaks in virtue of their degree of injury. If so, this may be regarded as an inherent limitation of conducting FC analyses on coma/DOC patients: the analyses may not be appropriate for all patients – particularly those with severe and diffuse brain injury.

Given that alpha connectivity has been found to be the most promising conical frequency band for using motifs to track levels of consciousness (Duclos et al., 2021; Nadin et al., 2020), and the propensity for coma/DOC patients to have broadband periodic EEG suppression (Edlow et al., 2021; Maschke et al., 2022), we do not believe that more fruitful results would have been obtained by focusing on a different frequency band. Rather, in the future, if one chooses to conduct FC analyses on severe brain-injured patients, we recommend that the approach be more personalized. For example, by first confirming the presence of periodic peaks in the patient’s EEG power spectral density, then running connectivity analyses on the individual patient’s most dominant peak.

Conclusion

This study investigated the descriptive properties and clinical utility of 3-node network motifs for coma and DOC patients of mixed etiologies as they underwent transitions in propofol anesthesia exposure. We successfully replicated past findings that motifs 1 and 7 reconfigure with changes in propofol anesthesia. Further, we replicated the properties of motifs 1 and 7 in alignment with past literature. However, motifs failed to show prognostic or diagnostic value for any of our anesthesia state transitions. Our data suggests that the lack of prognostic and diagnostic potential of motifs was likely the result of absent alpha peaks in our cohort of coma and DOC patients. In the future, studies employing FC analyses should opt for a more personalized approach to diagnosis and prognostication – such as focusing on an individual’s dominant periodic EEG peak, rather than applying one conical frequency band to all patients.

Chapter 2: Using Anesthetic-Induced Brain Network Reconfiguration to Prognosticate Recovery from Coma After Cardiac Arrest

Kira Dolhan^{1,2}, Mypinder Sekhon^{3,4}, & Stefanie Blain-Moraes^{2,5}

1. Integrated Program in Neuroscience, McGill University, Montreal, Canada
2. Montreal General Hospital, McGill University Health Centre, Montreal, Canada
3. Vancouver General Hospital, University of British Columbia, Vancouver, British Columbia, Canada
4. Vancouver Coastal Health Research Institute, University of British Columbia, Vancouver, British Columbia, Canada
5. School of Physical and Occupational Therapy, McGill University, Montreal, Canada

Introduction

Leveraging anesthetic-induced signatures of brain network reconfiguration has emerged as a promising avenue for improving prognostication in coma and DOC patients. Past literature has shown that general anesthetics such as propofol, isoflurane, and sevoflurane induce a reversible EEG power anteriorization in healthy controls (Blain-Moraes et al., 2017), surgical patients (John et al., 2001), and primates (Tinker et al., 1977). Power anteriorization has been observed in various frequency ranges, however, anteriorization in the alpha band is particularly salient and occurs under a variety of anesthetics (Akeju et al., 2014; Li et al., 2019; Purdon et al., 2013). This anteriorization of alpha power is reflected in graph theoretical network hubs, as

power and node degree are related (H. Lee et al., 2013). Furthermore, anesthetic-induced reconfiguration in hubs have been linked to that of directed FC (Moon et al., 2015). More specifically, phase-lead alpha connectivity of frontal to parietal regions associated with wakefulness is reversed during propofol anesthesia (and returns to feedback dominance after anesthetic withdrawal; H. Lee et al., 2013; U. Lee et al., 2009, 2013). This effect also appears to be anesthetic-agnostic (U. Lee et al., 2013). Thus, reversible anesthetic-induced changes in alpha FC – specifically power/hubs and directed frontoparietal connectivity – serve as promising candidates for tracking levels of consciousness under general anesthesia.

Inspired by these promising lines of research, many novel tools are being developed to help treat and prognosticate unresponsive brain-injured patients (e.g., Guo et al., 2023; Liang et al., 2023; B. Liu et al., 2021). However, even the more validated metrics – such as the perturbational complexity index – suffer from issues surrounding clinical translatability (Casali et al., 2013). For example, many of these metrics are designed for hd-EEG comprised of upwards of 128 electrodes (Hermann et al., 2021; Sitt et al., 2014; Stefan et al., 2018). In contrast, the devices which are typically available and routinely used in the clinic are comprised of a mere 16 to 20 electrodes (Acharya et al., 2016). Differences in these systems with respect to factors such as spatial resolution and sampling rate will have an influence on tool efficacy. Furthermore, many of these novel tools are designed within the framework of a controlled experimental paradigm – ranging from anesthesia administration to evoking event-related potentials (Duclos et al., 2022; Hermann et al., 2021). In clinical reality, however, circumstances are far less controlled. It is often pragmatically unrealistic to expose severely brain-injured patients who are

receiving life-sustaining treatment to experimental paradigms, nor are families often open to the idea of their loved one going through additional testing above and beyond what is standard of care (Young et al., 2022).

This study aimed to test the clinical translatability of a previously developed prognostic tool for coma and DOC patients, known as the Adaptive Reconfiguration Index (ARI). This metric is a sum composite score of changes in whole-network hubs and directed FC as patients are exposed to varying levels of general anesthesia (Duclos et al., 2022). Much like our hypotheses regarding motifs, the theory behind the ARI is that patients with favorable outcomes will show greater anesthetic-induced changes in their brain networks relative to those who do not recover. In a preliminary study, coma and DOC patients ($n = 12$) were previously weaned off sedation, had propofol administered, then had propofol subsequently withdrawn while 128- or 64- channel EEG was recorded (Duclos et al., 2022). Using this hd-EEG, the ARI was calculated from hub topology and directed FC changes in the alpha frequency band, which categorized all 12 patients with 100% accuracy based on whether or not they recovered command-following abilities three months after the EEG recording session (Duclos et al., 2022). The group of patients who recovered were found to have greater ARI scores (i.e., larger changes in hub topology and directed FC between anesthesia states), relative to those who did not recover.

Given the potential promise of the ARI as a prognostic tool using hd-EEG, we expanded upon the preliminary study by Duclos et al. (2022) and tested the ARI on clinical-grade 19-channel EEG recorded from post-cardiac arrest coma patients. The purpose of this extension was to test the ARI's translatability to a more realistic clinical environment and practice. This was

addressed through several means. First, 19-channel EEG was used, which is far more prevalent in the clinic than hd-EEG (Chu, 2015; Kondziella et al., 2020). Second, instead of using three anesthesia states (sedation off, on, then off) to calculate the ARI (Duclos et al., 2022), we took EEG recordings from only two states (sedation on and off). Anesthesia administration in the clinic does not occur according to predefined anesthetic protocols. Thus, we did not use EEG recordings from an experimental paradigm with a controlled target effect site concentration (Duclos et al., 2022). Rather, we used secondary data taken from clinical assessments. Finally, we tested the ARI using an automated preprocessing pipeline to try and address the limitations to clinical translatability that come with using EEG data which was manually preprocessed by a trained professional. We hypothesized that: 1) the ARI would successfully categorize recovered and non-recovered coma patients using 19-channel EEG recorded from two anesthesia states, and 2) recovered patients would have greater ARI scores than non-recovered patients. Patient recovery was quantified using Cerebral Performance Category (CPC) scores.

Methods

Anesthetic Protocol

Coma patients ($n = 16$) with severe brain injury due to cardiac arrest had 19-channel EEG recorded during two anesthesia states: while receiving propofol anesthesia, and while not receiving sedation. This was a secondary data analysis of clinical EEG data that was originally collected as part of standard of care at Vancouver General Hospital. Enrollment in the study occurred within 72 hours of the cardiac arrest incident. Inclusion criteria was as follows: cardiac

arrest which lasted over 10 minutes and required cardiopulmonary resuscitation; GCS ≤ 8 and motor score ≤ 5 after return of spontaneous circulation. Patients were excluded from the study if they had withdrawal of life-sustaining treatment (WOLST) planned within the next 24-hours; a history of traumatic brain injury, intracranial hemorrhage, or stroke; concurrent coagulopathy; concurrent anti-platelet or anticoagulant medications; or cardiac catheterization planned within the next 7 days. The patient cohort had an age range of 31 to 73 years-old (mean = 51.4 years-old) and was comprised of 4 females.

Behavioural Assessments

To quantify functional outcome, CPC (Jennett & Bond, 1975; Perkins et al., 2015) scores were measured after return of spontaneous circulation. Outcomes were defined as favorable for CPC scores ≤ 3 . This cut-off was selected because a CPC = 4 is defined as a patient in a coma or DOC, while a CPC = 5 indicates death.

EEG Recording and Preprocessing

EEG was recorded at a sampling rate of 512 Hz using a 19-channel Natus system (Natus Medical, Inc., USA). Continuous resting-state recordings were conducted as part of clinical monitoring; thus, we extracted two segments of EEG from each patient: one in which they were receiving propofol anesthesia, and another when they were free from general anesthesia. All anesthesia states were approximately 5 minutes in length. EEG was preprocessed by bandpass filtering between 0.5 and 45 Hz, notch filtering at 60 and 120 Hz, re-referencing to the average of the mastoids, segmenting recordings into 10-second epochs, subsampling the data to 250 Hz, and removing non-brain electrodes. Then, Python's *AutoReject* (Jas et al., 2016, 2017) was

applied to automatically interpolate bad channels and reject noisy epochs. The following *AutoReject* parameters were used: number interpolates = [3,4], consensus = [0.4, 0.5, 0.6, 0.7, 0.8, 0.9, 1.0], threshold method = random search, random state = 42. Various signal thresholds were tested for identifying bad epochs by comparing *AutoReject* performance on a subset of patients with manual identification of bad epochs by a trained EEG analyst. A threshold of 5 μV was found to perform best on our recordings. For the follow data analyses, recordings were bandpass filtered at 8-13 Hz to isolate the alpha frequency band.

Functional Network Construction

Weighted FC was quantified using wPLI (Vinck et al., 2011) and directed FC using dPLI (Stam & van Straaten, 2012). These FC metrics were calculated as outlined previously (see *Chapter 1* under *Methods: Functional Network Construction*) with two exceptions: w/dPLI were calculated using 20 random surrogate networks and only two anesthesia states were analyzed (sedation on and off). All w/dPLI matrices were calculated using custom Python scripts adapted from Duclos et al. (2022).

Network Hub Topologies

Node degree was calculated as outlined previously in *Chapter 1* (see *Methods: Network Hub Topologies*) for anesthesia on and off states. Hub analyses were conducted using custom Python scripts adapted from Duclos et al. (2022).

Calculating the Adaptive Reconfiguration Index

To calculate the ARI, node degree topology and dPLI across the scalp were subtracted between anesthesia on and off states. Both measures were translated into Z-scores and normalized changes in node degree and dPLI across the two anesthesia states were then summed together into a single number, creating the ARI score. Thus, the ARI is calculated as follows:

$$\Delta Hub = \left| \sum_i (A_i - B_i) \right|, \quad \Delta dPLI = \left| \sum_i \sum_j (A_{ij} - B_{ij}) \right|$$

$$\Delta Hub_z, \Delta dPLI_z = \frac{x - \mu}{SD}$$

$$ARI = \Delta Hub_z + \Delta dPLI_z$$

Where $A_i - B_i$ indicates degree for node i during sedation states A and B , $A_{ij} - B_{ij}$ indicates dPLI between nodes i and j during sedation states A and B , and $\frac{x - \mu}{SD}$ indicates a given hub or dPLI score (x) subtracted by the average score (μ) over the standard deviation (SD) (Duclos et al., 2022). ARI scores were then fed into a logistic regression model to classify recovered versus not recovered patients. The logistic regression model was employed using Python's Scikit-learn (Pedregosa et al., 2011) and various parameter values were tested. Ultimately, an optimal fit for our data was found using the following parameters: random state = 42, penalty = L1, C = 1, solver = liblinear.

Results

Hub Reconfiguration

The recovered group showed large variation in patient hub values, while the non-recovered group showed a relatively small range in patient variation (Figure 2.1). However, hubs were able to discriminate between prognostic groups since, on average, non-recovered patients had greater hub reconfiguration between sedation states than recovered patients (Figure 2.1).

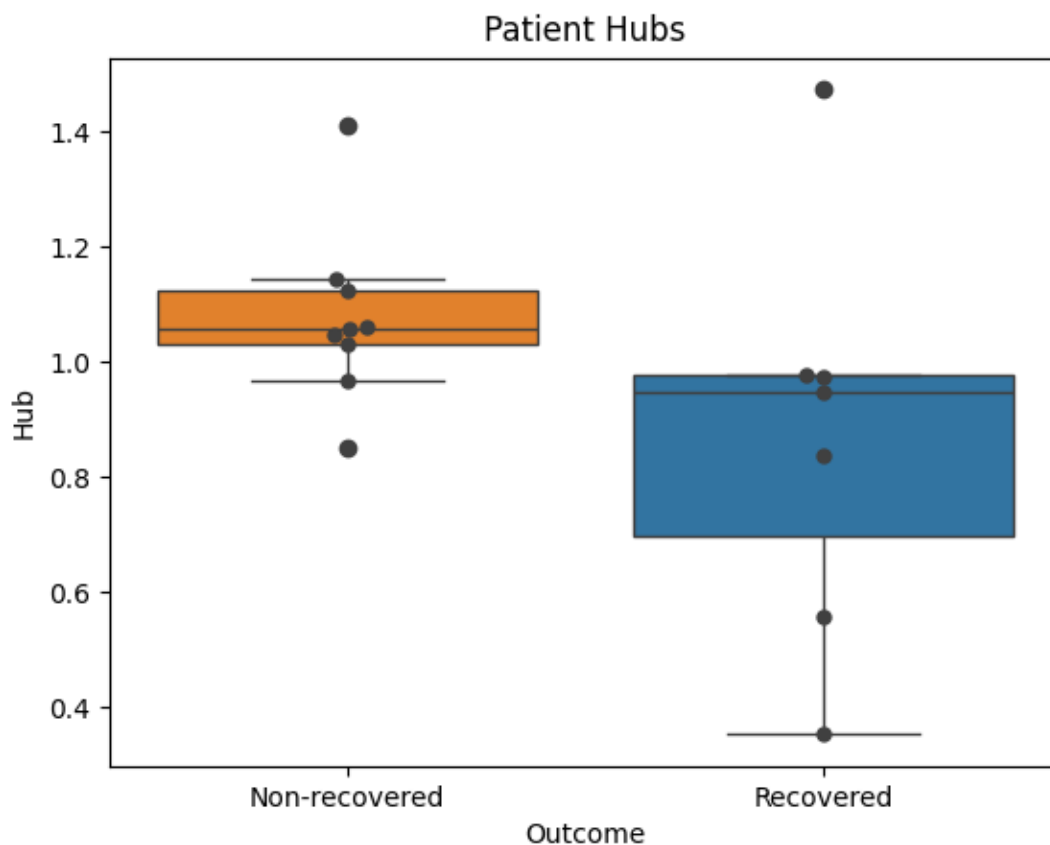


Figure 2.1. Box plots depicting the degree of topological hub (node degree) reconfiguration between sedation on and off states for coma patients who did not recover consciousness (orange) and for patients who recovered consciousness (blue) 6-months post-cardiac arrest. The degree of

hub reconfiguration was quantified by subtracting average hub topologies while patients were on versus off propofol sedation.

Directed Functional Connectivity Reconfiguration

In contrast to network hubs, the non-recovered group showed greater variation in their dPLI values compared to the recovered group (Figure 2.2). Furthermore, dPLI was relatively ineffective at discriminating between prognostic groups – as both groups showed comparable degrees of dPLI reconfiguration between sedation states (Figure 2.2).

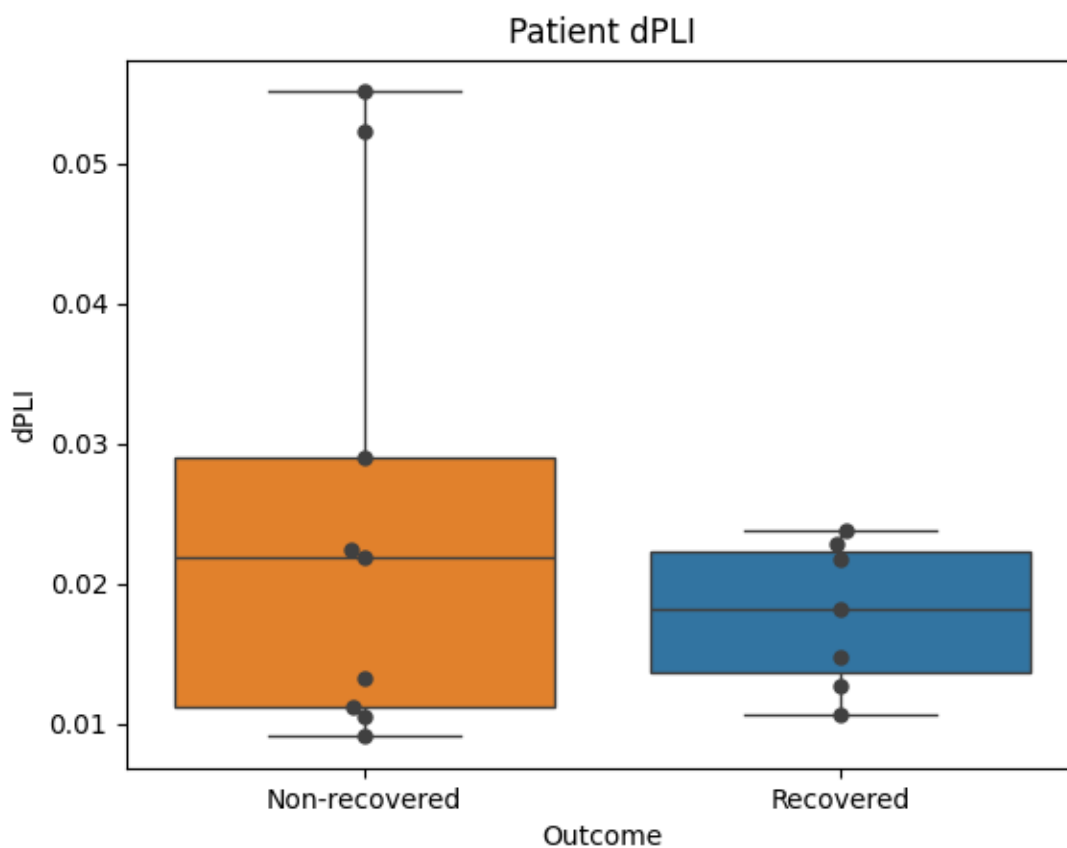


Figure 2.2. Box plots depicting the degree of reconfiguration in the directed phase-lag index (dPLI) between sedation on and off states for coma patients who did not recover consciousness

(orange) and for patients who recovered consciousness (blue) 6-months post-cardiac arrest. The degree of dPLI reconfiguration was quantified by subtracting average dPLI matrices while patients were on versus off propofol sedation.

Logistic Regression Model Performance

The model was able to discriminate between prognostic groups with an accuracy which exceeded chance levels for a range of classification thresholds – as indicated by the receiver operating characteristic (ROC) curve of the logistic regression model fitted to the Vancouver General Hospital data (Figure 2.3). More specifically, the model achieved an area under the ROC curve of 0.76 (Figure 2.3). The model correctly labeled 6 non-recovered and 6 recovered patients, while incorrectly labeling 1 recovered patient and 3 non-recovered patients (Figure 2.4), resulting in an accuracy score of 0.75, sensitivity of 0.67, and specificity of 0.86.

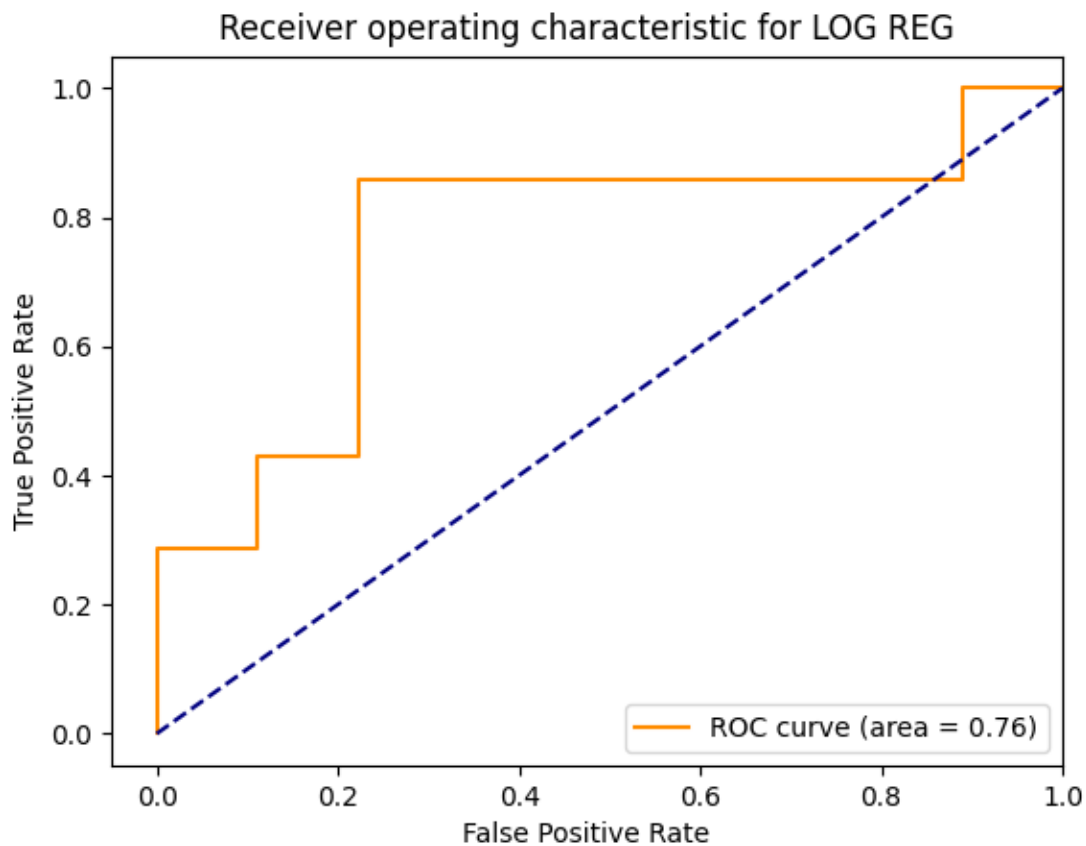


Figure 2.3. The receiver operating characteristic (ROC) curve for the logistic regression (log reg) model categorizing recovered versus non-recovered post-cardiac arrest comatose patients. Model performance for different classification thresholds is plotted with the orange line and chance classification is represented by the blue dotted line. The area under the ROC curve is 0.76.

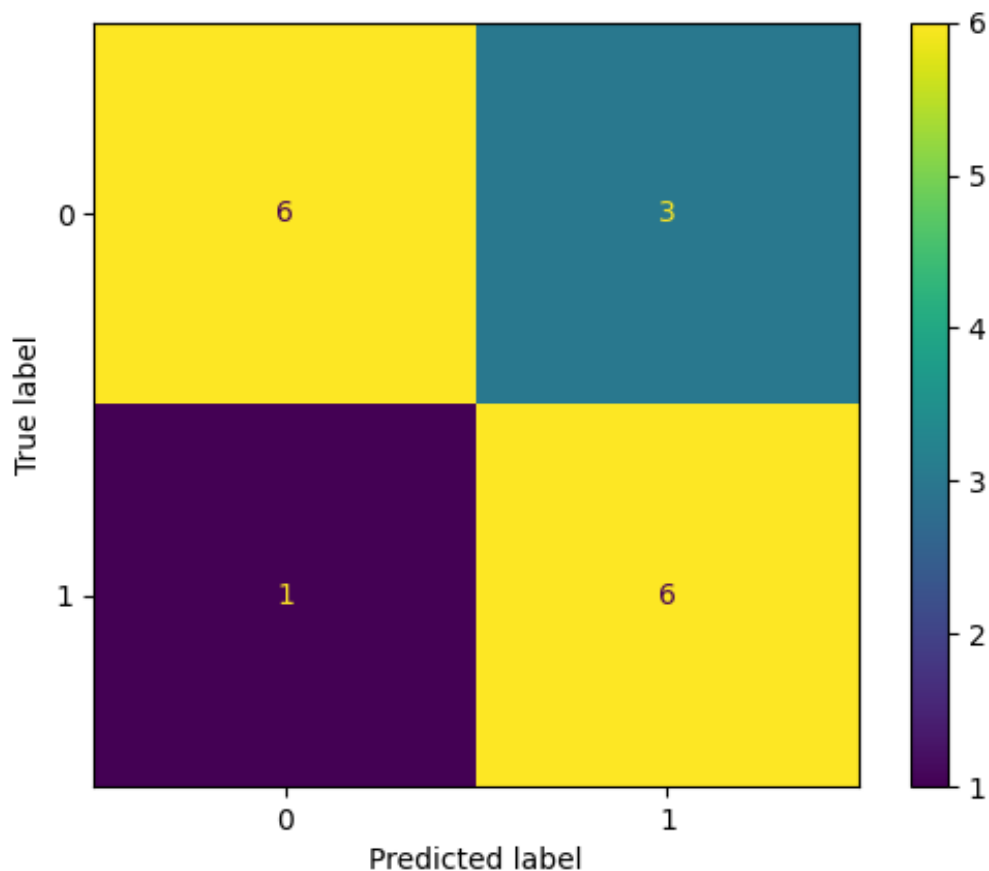


Figure 2.4. Confusion matrix for the logistic regression model categorizing recovered versus non-recovered post-cardiac arrest comatose patients. 0 = non-recovered, 1 = recovered. The color bar depicts the number of patients who belong to a given cell of the 2 x 2 matrix, ranging from 1 (purple) to 6 (yellow).

The decision boundary of the logistic regression model is plotted in Figure 2.5, with normalized dPLI and hub values plotted on the x and y axes, respectively. The section of the plot shaded in blue represents the feature space in which the logistic regression model would predict a patient to recover, and the area shaded in orange the feature space in which the model would

predict an absence of recovery. Individual patient plots with patient labels are overlaid so that we can compare model performance with clinical reality. It is visually evident from Figure 2.5 that the model incorrectly classified recovered patient 9 (P9) – a clear outlier in our dataset – as well as non-recovered patients 6 (P6), 10-C (P10-C) and 22 (P22). It can also be seen that, counter to our second hypothesis, recovered patients showed a trend for smaller network reconfiguration between sedation states relative to non-recovered patients. To analyze this further, we took case studies from our cohort of patients, and investigated network reconfiguration on an individual level.

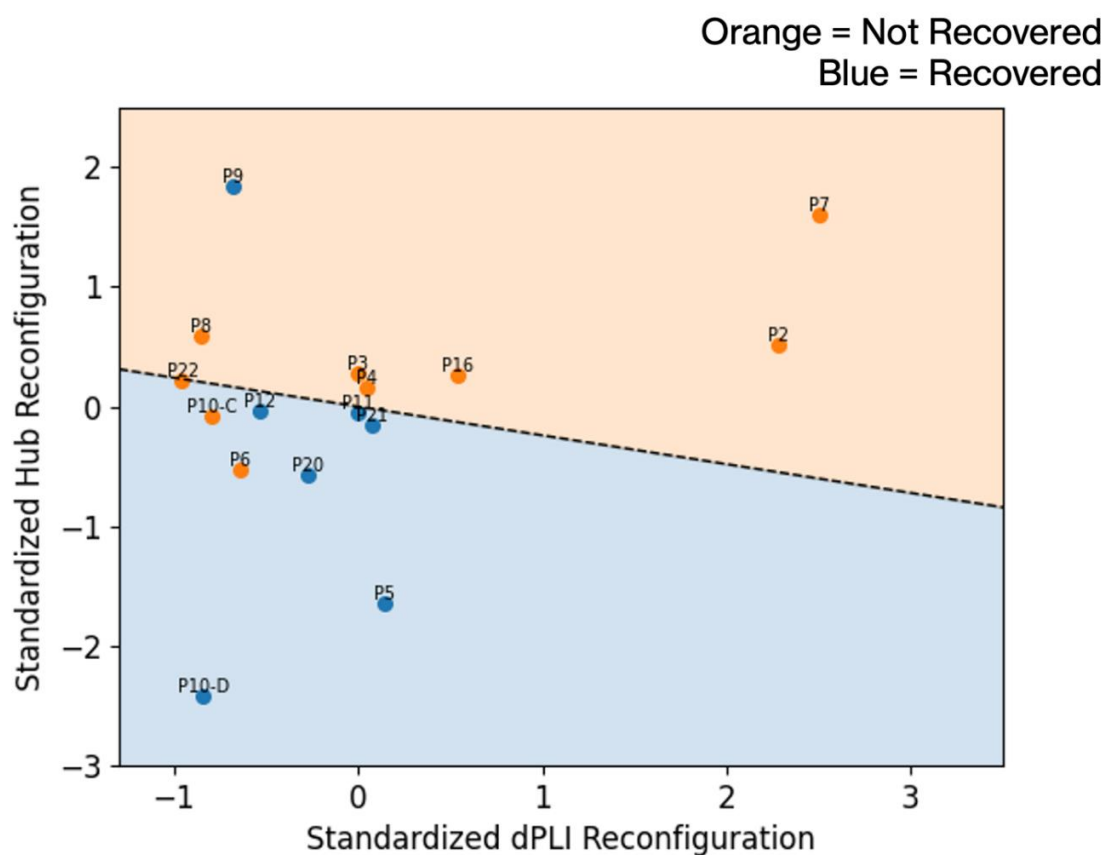


Figure 2.5. The logistic regression decision boundary (indicated by the dotted black line) plotted in the feature space of the Adaptive Reconfiguration Index. Normalized dPLI and hub values are plotted on the x and y axes, respectively. Blue shading represents the feature space in which the

model would predict patient recovery, and orange shading the feature space in which the model would predict an absence of recovery. Individual patient plots with patient labels are overlaid overtop, with recovered patients indicated by blue dots and non-recovered patients by orange dots.

Case Studies

Recovered Patients

In analyzing recovered patients who were correctly classified by the logistic regression model, we observed that network reconfiguration for individual patients reflected group results: recovered patients showed minimal network reconfiguration between sedation states. As two examples, we have plotted wPLI, dPLI, and normalized hub values both on and off propofol sedation for patients 5 (P5; Figure 2.6) and 20 (P20; Figure 2.7) who were correctly classified by the logistic regression model. P5 had a 6-month CPC score of 1, indicating mild or minimal disability, while P20 had a CPC score of 2, indicating moderate disability. Both patients recovered from a coma/DOC status, yet their networks were relatively static between sedation on and off states.

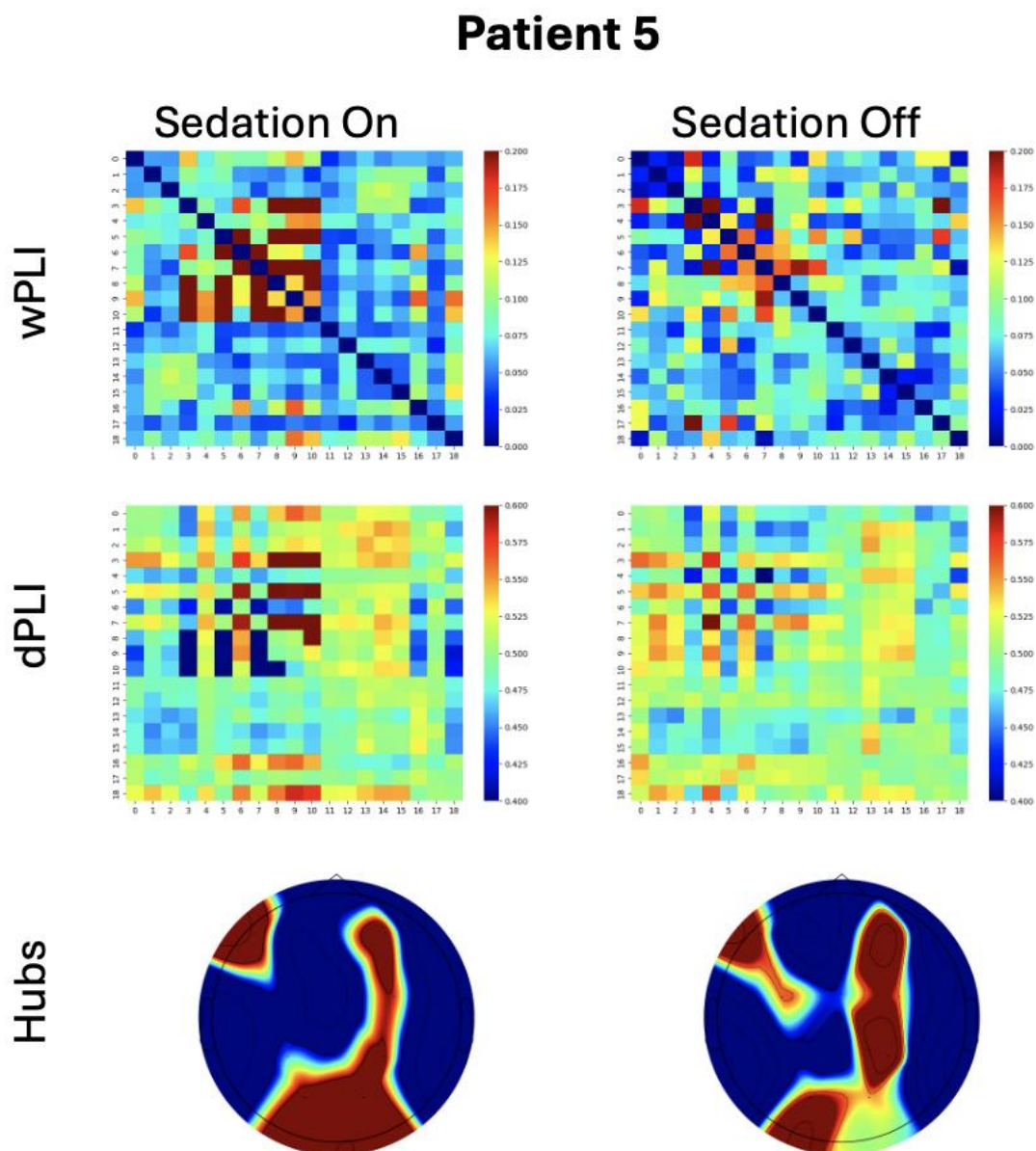


Figure 2.6. Weighted phase-lag index (wPLI), directed phase-lag index (dPLI), and normalized hubs for recovered patient 5. Average network measures while propofol sedation was being administered are depicted in the left column, and measures while propofol was off are depicted in the right column. The x and y axes for the wPLI and dPLI plots depict electroencephalography channel numbers, with the w/dPLI values between all pairwise combinations of electrodes indexed by the color bar.

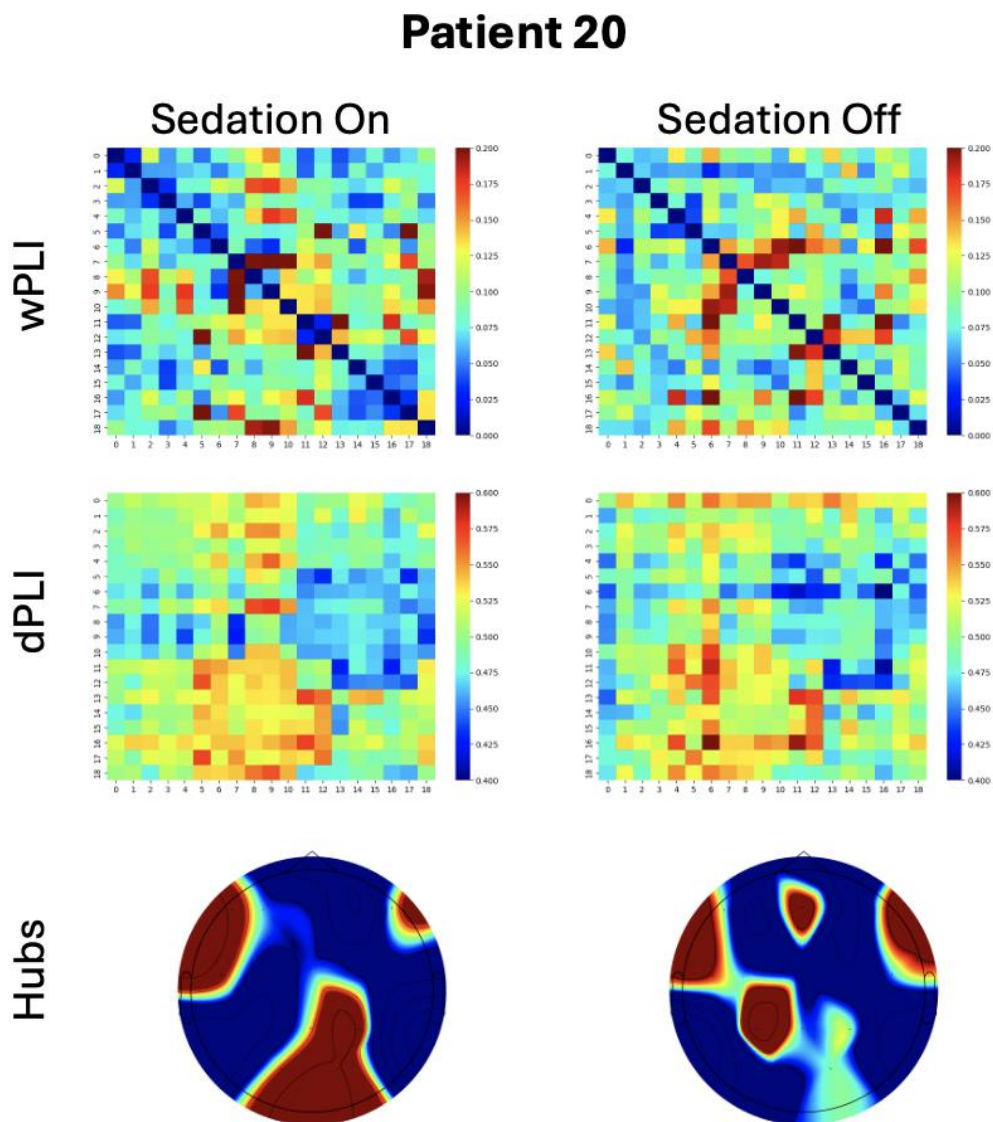


Figure 2.7. Weighted phase-lag index (wPLI), directed phase-lag index (dPLI), and normalized hubs for recovered patient 20. Average network measures while propofol sedation was being administered are depicted in the left column, and measures while propofol was off are depicted in the right column. The x and y axes for the wPLI and dPLI plots depict electroencephalography channel numbers, with the w/dPLI values between all pairwise combinations of electrodes indexed by the color bar.

Non-Recovered Patients

Individual patients who did not recover consciousness were found to show relatively high wPLI, dPLI, and hub reconfiguration between sedation states. Two examples are plotted: patients 2 (P2; Figure 2.8) and 16 (P16; Figure 2.9), who were correctly classified by the logistic regression model. Both patients had a 6-month CPC score of 5 (indicating death), but despite their unfavorable outcomes, they show dramatic network changes between sedation states – counter to our second hypothesis. For P2, in moving from sedation on the off columns (Figure 2.8), weighted connectivity became weaker, directional connectivity was neutralized, and we observe changes in hub topology. For P16 (Figure 2.9), weighted connectivity became stronger, there was an increase in feedback directed connectivity, and there were also changes in hub topology.

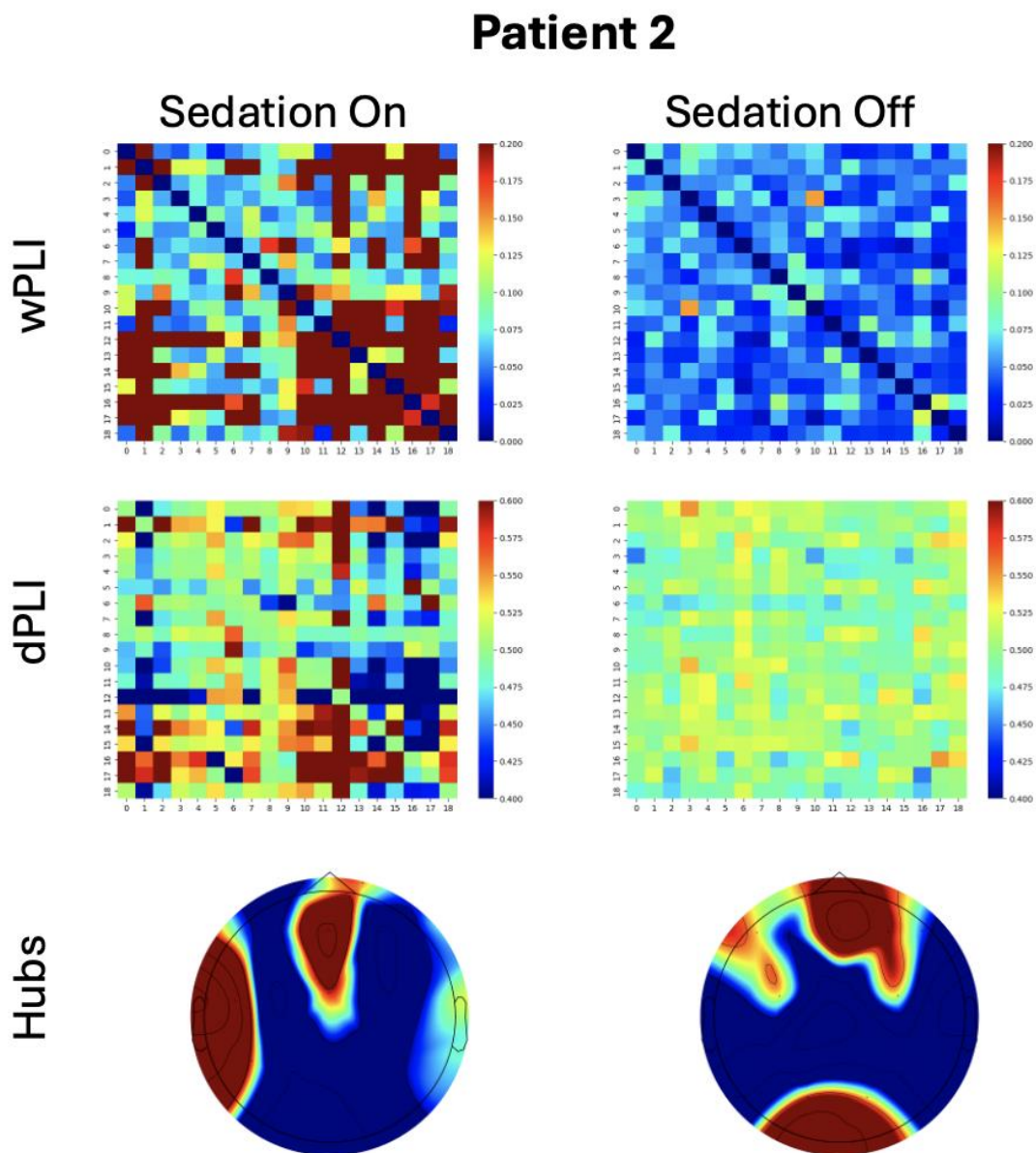


Figure 2.8. Weighted phase-lag index (wPLI), directed phase-lag index (dPLI), and normalized hubs for non-recovered patient 2. Average network measures while propofol sedation was being administered are depicted in the left column, and measures while propofol was off are depicted in the right column. The x and y axes for the wPLI and dPLI plots depict electroencephalography channel numbers, with the w/dPLI values between all pairwise combinations of electrodes indexed by the color bar.

Patient 16

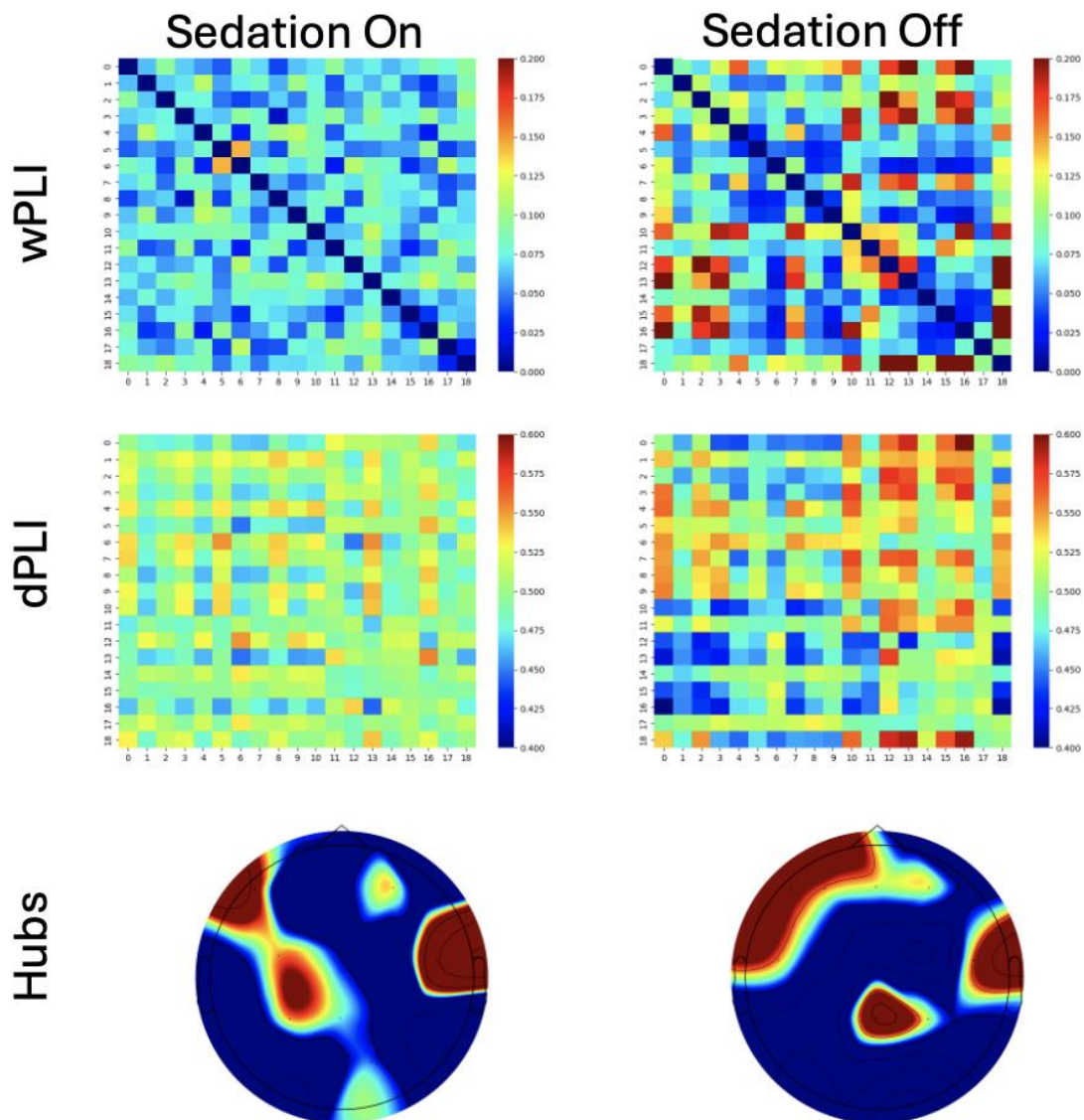


Figure 2.9. Weighted phase-lag index (wPLI), directed phase-lag index (dPLI), and normalized hubs for non-recovered patient 16. Average network measures while propofol sedation was being administered are depicted in the left column, and measures while propofol was off are depicted in the right column. The x and y axes for the wPLI and dPLI plots depict electroencephalography channel numbers, with the w/dPLI values between all pairwise combinations of electrodes indexed by the color bar.

Outlier Patient

Finally, we analyzed the wPLI, dPLI, and normalized hub reconfiguration for our one clear outlier: P9 (Figure 2.10). The logistic regression model predicted that P9 would not recover, however, they scored a CPC of 1 at 6-months post-injury. This patient had minimal reconfiguration in their directed FC and a slight reduction in weighted connectivity when off sedation, but their hub topology underwent great reconfiguration between sedation states (Figure 2.10). Indeed, this large reconfiguration is what we had expected to see in recovered patients, based on the preliminary ARI study by Duclos et al. (2022). Importantly, P9 did not stand out from our patient cohort in terms of their age or sex (47-year-old male).

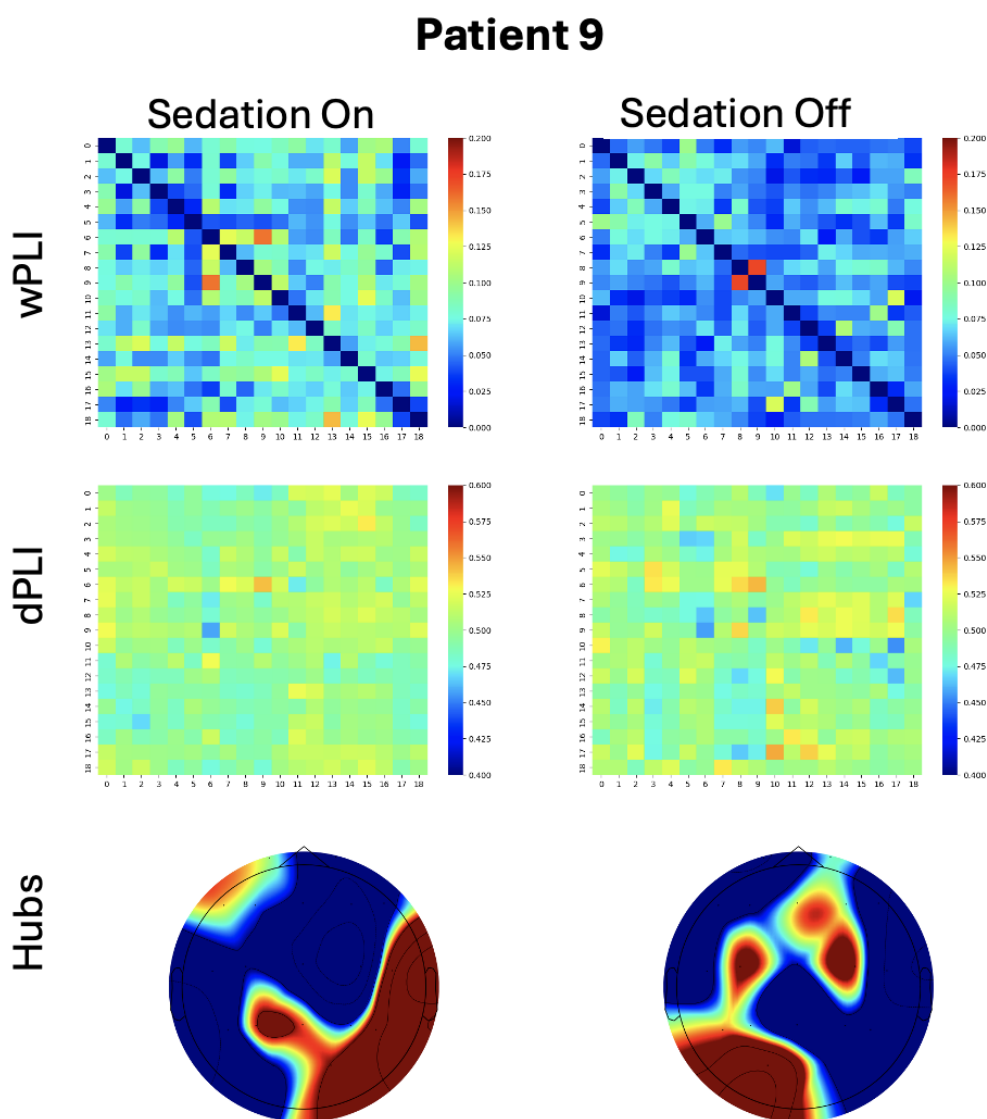


Figure 2.10. Weighted phase-lag index (wPLI), directed phase-lag index (dPLI), and normalized hubs for recovered patient 9 – an outlier in our dataset. Average network measures while propofol sedation was being administered are depicted in the left column, and measures while propofol was off are depicted in the right column. The x and y axes for the wPLI and dPLI plots depict electroencephalography channel numbers, with the w/dPLI values between all pairwise combinations of electrodes indexed by the color bar.

Discussion

In this study, we tested whether the ARI could be used in the ICU for prognostication of comatose patients with hypoxic-ischemic brain injury. Our focus was on testing the clinical utility of the ARI, using anesthetic-induced changes in directed FC and network hub topologies to predict coma/DOC patient recovery. Our project differed from that of Duclos et al. (2022) in that we studied comatose patients with post-cardiac arrest etiology, and our methodology was designed to further emphasize clinical translatability. In contrast to the methods of Duclos et al. (2022), we collected data using 19-channel clinical-grade EEG, sedation epochs were taken from what was available in clinic (rather than conducting a controlled anesthetic paradigm), and data was preprocessed and analyzed using an automated pipeline. We analyzed the prognostic utility of topological changes in dPLI and hub metrics individually, as well as composite ARI scores which were used as input in a logistic regression model. A strength of this project included our methodological design tailored for realistic clinical settings, as we took the ARI pipeline and adapted it for low-density EEG using only two anesthesia states extracted from clinical assessments. Additionally, in focusing on one etiology, we eliminated the potential confounds that come with treating coma and DOC patients of mixed etiologies as one homogenous group. This was further controlled for using our within-subject design, as network reconfiguration was quantified for each individual patient before and after receiving propofol.

The logistic regression model was able to classify recovered versus non-recovered comatose patients with an accuracy of 0.75, sensitivity of 0.67, and specificity of 0.86. Of the 16 patients tested, 6 non-recovered and 6 recovered patients were correctly labeled, while 1

recovered patient and 3 non-recovered patients were incorrectly labeled. Thus, our preliminary results indicate that the ARI may have prognostic value for hypoxic-ischemic brain-injured comatose patients in the ICU. However, our analyses will have to be replicated with a larger sample size, and analytical limitations concerning WOLST will need to be addressed, before any strong conclusions about the prognostic utility of the ARI can be made. Furthermore, a threshold of accuracy defining whether or not the ARI was “successful” in categorizing prognostic groups will need to be determined through future research. A natural starting point would be to try and exceed the accuracy rate of physician predictions for coma and DOC patient outcomes given the tools currently used in the ICU as standard of care. Unfortunately, physician accuracy rates have not been quantified as of the writing of this thesis, so a threshold for “success” was not numerically defined for the ARI. Defining this threshold will be important prerequisite research for moving a given prognostic tool from the lab into clinical practice.

When analyzing the relative importance of ARI’s component metrics, anesthetic-induced topological reconfiguration in hubs was more effective at categorizing prognostic groups than that of dPLI. This replicated the results of Duclos et al. (2022), who also found hubs to be more prognostically valuable for their mixed etiology patient cohort. However, in contrast to Duclos et al. (2022), we found that the recovered group showed a trend for smaller reconfiguration between sedation states relative to non-recovered patients. This trend contradicted our second hypothesis, in which we predicted that recovered patients would show greater topological reconfiguration. Given the relative importance of hubs compared to dPLI, this unexpected group-level trend in ARI scores was largely driven by hub reconfiguration. There are several potential

explanations for this observation. First, it is important to note that we tested a patient cohort with a focused ethology: hypoxic-ischemic brain injury due to cardiac arrest. The original ARI paper by Duclos et al. (2022) included 4 anoxic patients, and only one of the patients was in the acute stage of less than 2 week after acquiring their brain injury, when we could catch them in the ICU. Indeed, past studies have shown that EEG signatures for indexing DOC severity are etiology-dependent (Colombo et al., 2023; Maschke et al., 2024). For example, Colombo et al. (2023) have found that alpha posterior-anterior ratio and the spectral exponent can index DOC severity in non-anoxic patients, but not anoxic patients.

It is also important to consider that patients with anoxic injuries display unique resting-state EEG signatures, distinct from that of other etiologies such as stroke or traumatic brain injury (Colombo et al., 2023). Most notably, anoxic brain injury due to cardiac arrest causes broadband EEG suppression (Forgacs et al., 2017; Park et al., 2023). The mechanism behind this suppression is hypothesized to be structural and/or functional deafferentation of thalamocortical networks, which disrupts the oscillatory EEG activity observed in healthy, intact brains (Edlow et al., 2021; Lemieux et al., 2014). Our counterintuitive observation that non-recovered patients exhibited greater network reconfiguration may also be explained by this robust post-anoxic EEG signature. Broadband EEG suppression scales with the degree of thalamocortical injury, such that patients with worse brain injuries exhibit greater EEG suppression; in fact, broadband EEG suppression and low-amplitude background activity are widely used as markers of poor prognostic outcome in anoxic patients (Beuchat et al., 2018; Forgacs et al., 2017). Thus, non-recovered patients, in virtue of their poor prognosis, are more likely to have greater broadband

EEG suppression relative to recovered patients. Furthermore, as outlined earlier in this chapter (see the *Introduction of Chapter 2*), general anesthesia induces characteristic network signatures such as alpha hub anteriorization and the neutralization of FC feedback dominance (Blain-Moraes et al., 2017; U. Lee et al., 2009; Moon et al., 2015). These two factors, in combination, may have caused greater anesthetic-induced network reconfiguration in the non-recovered group: patients with a poor prognosis are more likely to exhibit suppressed EEG during their baseline state, and thus when anesthesia was administered, propofol's EEG signature resulted in a larger change from baseline. The recovered group, in contrast, was less likely to show such severe EEG suppression during baseline, and in virtue of having greater network activity when off sedation, did not undergo such dramatic network reconfiguration to display these characteristic anesthetic-induced network signatures.

Furthermore, this counterintuitive trend could have been the result of group differences in propofol doses. Since we were using secondary data extracted from clinical assessments, patients were not receiving a standardized propofol dose. Instead, the anesthetic concentration was tailored to each patient's clinical needs as determined by healthcare professionals. Thus, it is plausible that patients in the non-recovered group required greater propofol infusion concentrations to manage factors such as pain and intracranial pressure (Wu et al., 2020). The data which we had access to for the purposes of this project did not include a complete profile of each patient's anesthetic doses. This limits our interpretation of the results, since we were unable to confirm whether systematic group differences in propofol concentrations existed. Our results indicate the importance of collecting this information in the future: if the prognostic groups

systematically differed in their propofol infusion concentrations, the group receiving a larger infusion would undergo greater anesthetic-induced network reconfiguration.

It is also important to note that, in our dataset, all patients with an outcome of death underwent some form of WOLST – either in palliative care or the ICU. This could further explain our observed counterintuitive trend in network reconfiguration, as all but one of our non-recovered patients had died by 6-months post-injury. It is possible that, if this cohort continued to receive treatment, a number of patients may have recovered consciousness. Given this limitation, it would be ideal for future studies to include non-recovered patients who have not undergone WOLST. However, we acknowledge the great difficulty of achieving this in a realistic clinical setting, since decisions regarding WOLST are commonplace in North America and are often made quickly after hospital admission (Kotchoubey & Pavlov, 2018; Sandroni et al., 2021; Turgeon et al., 2011). For example, a study on six Canadian level-one trauma centres have found that WOLST accounted for 70% of deaths and approximately half of these deaths occurred within the first 3 days after hospital admission (Turgeon et al., 2011).

Future research on prognostic tools for coma/DOC patients using general anesthesia should try to address the aforementioned limitations of controlling for group differences in anesthetic dose and the presence of WOLST. Furthermore, it would be beneficial to use a personalized approach to patient prognostication, understanding that a given technique may not effectively predict functional outcome for all patient populations. For example, patients with hypoxic-ischemic brain injury often show resting-state EEG signatures which differ from other etiologies (Colombo et al., 2023). It is also important to be mindful of biological sex, as only 4 of

our 16 patients were female. These patient demographics should be considered when designing novel clinical tools. One approach is to focus on a targeted patient population, or, if the sample size allows, to apply a specific prognostic index to a heterogeneous patient group but analyze the results with patients stratified by factors such as sex and etiology.

Conclusion

In this study, we investigated the prognostic value of propofol-induced topological reconfigurations in alpha network hubs and directed connectivity for comatose patients in the ICU following cardiac arrest. The focus of this study was on testing clinical translatability: we examined whether these metrics could be used as a prognostic tool using EEG epochs taken from clinical electrophysiological assessments – without the use of hd-EEG or controlled anesthetic protocols. Our results suggest that anesthetic-induced changes in alpha connectivity may potentially be able to delineate patients who recover command-following abilities within a year post-injury. Unexpectedly, the non-recovered patient group showed a trend toward greater network reconfiguration between sedation states compared to the recovered patients. This may have been due to our focus on patients with an anoxic etiology, propofol dose-dependent effects, or the inclusion of non-recovered patients who underwent WOLST. In the future, novel prognostication tools should be developed in consideration of these limitations, with a focus on personalized medicine that accounts for patient demographic information such as sex and etiology.

Discussion

Throughout this thesis, we have measured propofol-induced reconfigurations in brain network FC, with the goal of examining whether reactivity to these anesthetic perturbations could be used to help diagnose or prognosticate coma and DOC patients in the ICU. To this end, we conducted two studies focused on different FC metrics and patient subpopulations.

In Chapter 1, we investigated whether brain network motifs had prognostic or diagnostic value for coma and DOC patients of mixed etiologies. In accordance with past literature, we found that M1 and M7 significantly recurred in severely brain-injured patients and reconfigured across propofol anesthesia states. Further, we replicated the descriptive properties of these motifs: M1 consisted of long-range chain-like connections, and M7 short-range loop-like connections. M1 also had a frequency which was approximately two-fold greater than M7. However, despite being able to replicate these descriptive characteristics, and using motif analytical pipelines adopted from past literature, we did not find motif topological reconfiguration to have prognostic or diagnostic value. This finding was robust across anesthesia states, and contrasted preliminary studies looking at the clinical utility of motifs in DOC patients (Guo et al., 2023; Nadin et al., 2020). Thus, our study suggests that motifs exist in coma and DOC patient neural networks, but they fail to discriminate patients into diagnostic or prognostic categories when derived from hd-EEG.

In Chapter 2, we tested the clinical translatability of the ARI – which uses propofol-induced topological changes in directed FC and node degree to categorize coma/DOC patients based on prognostic outcome. We expanded upon the original study by Duclos et al. (2022) by

testing the ARI on 19-channel clinical EEG originally collected as part of standard of care for post-cardiac arrest comatose patients at Vancouver General Hospital. After inputting ARI scores into a logistic regression model, we obtained an accuracy score of 0.75, sensitivity of 0.67, specificity of 0.86, and area under the ROC curve of 0.76. As found by Duclos et al. (2022), we observed that network hubs were better able to discriminate prognostic categories than dPLI reconfiguration. Unexpectedly, the recovered group was found to display a trend for smaller propofol-induced network reconfiguration relative to the non-recovered group. In summary, this study suggests that the ARI may have prognostic utility for comatose patients with cardiac arrest etiology, however, this will need to be tested with a larger sample size and analytical challenges surrounding patient WOLST must be addressed before a confident assertion about the ARI's prognostic value can be made.

Consciousness and its Many Definitions

Throughout this thesis, we have repeatedly referred to candidate metrics which may be able to measure patient “consciousness”. However, it is imperative for researchers to be explicit and specific as to what they are specifically referring to when they purport to be studying “consciousness” – as the term is not inherently well-defined. Rather, “consciousness” can refer to a large range of neural and cognitive phenomena, including the difference between sleep and wakefulness, the focus of attention, qualia (subjective, qualitative experience), higher-order thought, and awareness of stimuli (Block, 1995; Chalmers, 1995; Churchland, 1996). In an effort to evade some of the definitional confusion that comes with consciousness being an umbrella term, or mongrel concept (Block, 1995), we opened this thesis by stating that, in clinical

contexts, “consciousness” is used to refer to patient arousal and awareness. Even then, the issue deserves more nuanced consideration.

In working with coma/DOC patients, we are trying to identify metrics which correlate with neurological and behavioural arousal and reactivity to stimuli in severely brain-injured humans. Research findings derived from this clinical context should not be overextended to other, potentially unrelated, concepts which fall under the umbrella term *consciousness* (Carruthers, 2000; Churchland, 1988; Wilkes, 1984). For example, if in the future an EEG signature is found which correlates with coma/DOC patient diagnosis in an extremely robust and reliable manner, there would still be empirical work to be done before claiming that a neural correlate of consciousness has been identified. Similarly, we should be careful about deriving a general theory of consciousness from this hypothetical EEG signature. The signature may not apply to healthy, non-brain-injured individuals, or non-human animals (Birch et al., 2020; Carls-Diamante, 2022; López-González et al., 2021). Further, it may be entirely unrelated to other definitions of consciousness – such as dreaming, introspection, attention, or qualia (Carruthers, 2000; Churchland, 1988; Wilkes, 1984). Even then, we argue that this outcome would not necessarily be problematic. In accepting consciousness as a mongrel concept, it is plausible that many distinct neural signatures and theories will be required before we can start developing a satisfying mechanistic explanation of consciousness (Carruthers, 2000; Churchland, 1988; Wilkes, 1984). Rather than advocating for a (singular) theory of consciousness, we encourage the field to take a more nuanced approach. Instead of assuming that one theory, or a given set of neural correlates, is correct and can account for the concept of consciousness in its entirety, we

encourage the field to be mindful of the context in which a specific finding has (and has yet to be) empirically tested and to embrace the idea that many empirically supported theories can mutually exist (Hochstein, 2016, 2023). In the context of this thesis, we focused on EEG-based FC correlates for coma and DOC patients which may be able to aid in diagnostic and prognostic categorization. Before further empirical testing, our findings should not be overextended to other contexts; this thesis did not present evidence regarding qualia, kinds of conscious experiences (e.g., across different species), higher-order thought, etc.

Modeling Cognition at Different Spatiotemporal Scales

The concept of explanations at various levels, or scales, has also recurred throughout this thesis. For example, in Chapter 1 we focused on the clinical utility of meso-scale network motifs, while in Chapter 2 we moved to the macro-scale of whole brain FC (Betzel et al., 2018). When working across different spatiotemporal scales, it is important to consider that certain models or mechanistic explanations may only be applicable at certain scales (Dennett, 1969; Hochstein, 2022). We are not speaking about the metaphysics of a given phenomenon, but rather, about epistemology (Drayson, 2014). For instance, when scientifically describing a cognitive phenomenon, concepts which apply at the system level (i.e., the “person level”) may not neatly map onto system sub-systems (i.e., the “sub-person level”; Dennett, 1969). In the context of this thesis, concepts such as “conscious awareness of environmental stimuli” apply to the person level of the patient – including all the integrated sub-systems which comprise the individual. However, when considering any one individual sub-system (e.g., a neural network of alpha connectivity in the patient’s visual cortex), we do not claim that the given network, in isolation,

has the ability to consciously perceive its environment. This is in no way to diminish the explanatory power of breaking down a system into sub-components. Rather, it is simply something to be mindful of: when deciding to model a cognitive phenomenon at a given spatiotemporal scale, we are inherently foregrounding and backgrounding different information (Hochstein, 2022). As a consequence, different (and potentially contradictory) scientific explanations and descriptions of the same phenomena can arise at different scales. Not only is this unproblematic, but it is a natural consequence of modeling, and therefore simplifying, the phenomenon that we wish to explain (Dennett, 1969; Hochstein, 2022, 2023). Thus, it is not necessary that models across different spatial scales – such as network motifs and whole-brain FC – form one uniform, coherent, uncontradictory explanation. Instead, we may find that different/contradictory models or neural signatures have clinical utility at different spatiotemporal levels.

Limitations of this Thesis

With the scope of our project more explicitly defined, there are some limitations to this thesis which should be addressed. Firstly, patients were categorized into diagnostic and prognostic groups according to behavioural assessments – including the CGS, CPC, and overt command-following abilities. However, a large body of literature has shown that assessing patients purely from behavioural examinations is unreliable (Edlow et al., 2021; Giacino et al., 2018; Owen et al., 2006; Schnakers et al., 2007); indeed, this was our motivation for focusing on the development of clinical EEG markers. For example, covert command-following was not examined in our patient cohorts, despite the fact that an estimated 15 to 20% of coma/DOC

patients have cognitive-motor dissociation (Edlow et al., 2021; Naci & Owen, 2022; Owen et al., 2006). It is plausible, in this thesis and more broadly in coma/DOC research, that signs of patient arousal and awareness are unknowingly being overlooked. This is important to consider when researchers categorize patients, for example, into “recovered” and “non-recovered” groups. We are searching for correlations between FC signatures and our best guess as to whether a patient is awake/aware based on behavioural examinations. Not only are we unable to draw causal connections, but we do not have an objective “group truth”: we cannot be sure that our patients were not diagnostically or prognostically mislabeled.

Additionally, both chapters of this thesis focused specifically on FC in the alpha frequency band. Indeed, there is a long history of research suggesting that FC and graph theory metrics derived from the alpha band have clinical utility for coma/DOC patients (Babiloni et al., 2009; Chennu et al., 2014; U. Lee et al., 2009; Sokoliuk & Cruse, 2018). Given that motifs were found to track anesthetic-induced changes in consciousness most effectively in the alpha band (Duclos et al., 2021; Nadin et al., 2020), and the ARI was developed to measure anesthetic-induced changes in alpha-based network markers (Duclos et al., 2022), our focus on alpha connectivity was empirically driven. Having this said, it is important to acknowledge that frequency bands other than alpha, and non-oscillatory EEG signatures, also show clinical relevance and are important to coma/DOC research (Bourdillon et al., 2020; Maschke et al., 2022; Thibaut et al., 2018). Just as we are not proponents for one singular theory of consciousness, we are not under the impression that one canonical frequency band will be the “key” to treating and assessing severely brain-injured patients. Rather, according to previous

literature, alpha connectivity was the most appropriate place to start our investigations into network motifs and the ARI.

It is also important to note that both chapters in this thesis consisted of retrospective prognostic categorization. That is, EEG signatures were used to categorize patients into prognostic groups after their outcome had already been determined. However, in the ICU, clinicians aim to predict future, prospective outcomes – not retrospectively categorize patients based on their functional outcome months after a brain injury (Edlow et al., 2021; Maciel et al., 2020). Thus, future research should include prospective analyses of candidate prognostic tools. Retrospective analyses have value in the early development stages of a given prognostic tool, but prospective studies will need to be conducted before a given tool can be considered truly “predictive” and of clinical utility in the ICU.

Strengths of this Thesis

As for strengths of the overall thesis, both chapters employed propofol anesthesia as a brain perturbation. Relevant to clinical translatability, temporary disruptions in general anesthesia are standard of care for unresponsive brain-injured patients in the ICU, as anesthesia is typically withdrawn for daily behavioural assessments, then re-administered after the examination (Edlow et al., 2021; Gosseries et al., 2011). Thus, our general methodology does not necessitate the use of additional equipment beyond what is already commonplace in the ICU. Furthermore, we utilized within-subject designs: reconfiguration in brain networks were quantified by comparing a given EEG signature across anesthetic transitions. In using a specific

patient as their own “baseline” comparison, we avoid difficulties that come when comparing across patients, or comparing patients to healthy controls. As we have seen, coma and DOC patients are very heterogeneous, and their demographic information has important implications regarding which clinical tools and treatments will be most appropriate (Colombo et al., 2023; Maschke et al., 2024). Our within-subjects designs inherently account for some of this variation. Of note, we also made sure to utilize resting-state EEG across our studies. This has advantages over task-based EEG in that electrophysiological signatures are not dependent on a patient’s willingness or ability to complete a certain task (Bareham et al., 2018; Edlow et al., 2021). This is particularly important, as we are dealing with severely brain-injured patients who show great heterogeneity in their region and extent of injury. Thus, the cognitive capacities which remain intact after injury vary widely across patients (Covington & Duff, 2021; Schnakers, 2024). Furthermore, it is well documented that patient arousal/awareness largely fluctuates over time, meaning that, for task-based paradigms, a given patient may be able (and willing) to complete the task at one time point, but not another (Bareham et al., 2018; Giacino et al., 2018).

Throughout this thesis, we have also contributed to the scientific literature by conducting high-quality replication studies. In both chapters, we sought to test and expand upon diagnostic and prognostic FC markers which were promising in past preliminary studies of coma/DOC patients. To this end, we utilized the original code from Duclos et al. (2021) and Nadin et al. (2020) for our motif and network control analyses in Chapter 1, and the code from Duclos et al. (2022) for our ARI analyses in Chapter 2. Brain networks were constructed, and motifs as well as the ARI were quantified in the same way as the original studies. Furthermore, we maintained the

core methodology used in these original studies: propofol anesthesia was used to perpetuate the brain, within-subject topological network reconfigurations were measured, and EEG was recorded from the patients' bedside. Thus, discrepancies in the findings reported in this thesis and the preliminary studies which inspired our projects cannot be attributed to fundamental differences in code, methodology, or the tools used to collect and analyze data.

It is difficult to build a convincing case for null results, however, through our parallel methodology to Duclos et al. (2021) and Nadin et al. (2020), and the thoroughness with which we analyzed our results, we believe that we have made a strong argument for our null findings in Chapter 1. For example, we made a point of examining and presenting our results through different means, including group-level statistics as well as individual patient scatterplots. These null prognostic and diagnostic results are particularly important, since all of the currently published preliminary studies on motifs suggest that they have diagnostic and prognostic value for DOC patients (Guo et al., 2023; Nadin et al., 2020).

Finally, in testing the clinical translatability for the ARI in Chapter 2, we adapted the entire ARI pipeline from Duclos et al. (2022) to clinical data. This included becoming familiar with, and adjusting the ARI code for, 19-channel EEG in lieu of hd-EEG; using a 2-state rather than a 3-state anesthetic analysis; testing and developing an automated preprocessing pipeline for clinical EEG; and organizing EEG epochs derived from standard of care recordings instead of a controlled anesthetic protocol. Thus, novel and significant expansions to the ARI pipeline were made, which will be of importance for future work that moves this prognostic tool from the lab to the ICU.

Conclusion

The objective of this thesis was to investigate whether propofol-induced reconfigurations in functional brain network topologies could be leveraged as prognostic and/or diagnostic tools for coma/DOC patients in the ICU. In the first chapter, we focused on topological changes in 3-node alpha motifs calculated from hd-EEG. A long-range chain-like motif and a short-range loop-like motif were identified in coma and DOC patients of mixed etiologies. Both motifs topologically reconfigured across sedation states, as well as prognostic and diagnostic patient groups. Thus, 3-node motifs failed to demonstrate prognostic or diagnostic utility for our cohort of coma and DOC patients. In the second chapter, we examined whether directed FC and hub topologies could be used to prognosticate patients in a coma following cardiac arrest using clinical-grade EEG recorded as part of standard of care. Patients were categorized above-chance levels, suggesting that network topological reconfiguration may have prognostic value for post-cardiac arrest patients when clinical-EEG is used. However, these results should be further investigated with a larger sample size and after addressing WOLST patients. Overall, the findings of this thesis suggest that future studies should account for patient demographic information, such as etiology, when developing novel clinical tools for coma and DOC patients.

Bibliography

- Acharya, J. N., Hani, A. J., Thirumala, P. D., & Tsuchida, T. N. (2016). American Clinical Neurophysiology Society Guideline 3: A Proposal for Standard Montages to Be Used in Clinical EEG. *Journal of Clinical Neurophysiology: Official Publication of the American Electroencephalographic Society*, 33(4), 312–316.
<https://doi.org/10.1097/WNP.0000000000000317>
- Akeju, O., Westover, M. B., Pavone, K. J., Sampson, A. L., Hartnack, K. E., Brown, E. N., & Purdon, P. L. (2014). Effects of Sevoflurane and Propofol on Frontal Electroencephalogram Power and Coherence. *Anesthesiology*, 121(5), 990–998.
<https://doi.org/10.1097/ALN.0000000000000436>
- Arvin, S., Glud, A. N., & Yonehara, K. (2022). Short- and Long-Range Connections Differentially Modulate the Dynamics and State of Small-World Networks. *Frontiers in Computational Neuroscience*, 15, 783474. <https://doi.org/10.3389/fncom.2021.783474>
- Babiloni, C., Sarà, M., Vecchio, F., Pistoia, F., Sebastiano, F., Onorati, P., Albertini, G., Pasqualetti, P., Cibelli, G., Buffo, P., & Rossini, P. M. (2009). Cortical sources of resting-state alpha rhythms are abnormal in persistent vegetative state patients. *Clinical Neurophysiology*, 120(4), 719–729. <https://doi.org/10.1016/j.clinph.2009.02.157>
- Bai, Y., Gong, A., Wang, Q., Guo, Y., Zhang, Y., & Feng, Z. (2023). Breakdown of oscillatory effective networks in disorders of consciousness. *CNS Neuroscience & Therapeutics*, 30(3), e14469. <https://doi.org/10.1111/cns.14469>

-
- Bareham, C. A., Allanson, J., Roberts, N., Hutchinson, P. J. A., Pickard, J. D., Menon, D. K., & Chennu, S. (2018). Longitudinal Bedside Assessments of Brain Networks in Disorders of Consciousness: Case Reports From the Field. *Frontiers in Neurology, 9*.
<https://doi.org/10.3389/fneur.2018.00676>
- Benghanem, S., Pruvost-Robieux, E., Bouchereau, E., Gavaret, M., & Cariou, A. (2022). Prognostication after cardiac arrest: How EEG and evoked potentials may improve the challenge. *Annals of Intensive Care, 12*(1), 111. <https://doi.org/10.1186/s13613-022-01083-9>
- Betzal, R. F., Medaglia, J. D., & Bassett, D. S. (2018). Diversity of meso-scale architecture in human and non-human connectomes. *Nature Communications, 9*(1), 346.
<https://doi.org/10.1038/s41467-017-02681-z>
- Beuchat, I., Solari, D., Novy, J., Oddo, M., & Rossetti, A. O. (2018). Standardized EEG interpretation in patients after cardiac arrest: Correlation with other prognostic predictors. *Resuscitation, 126*, 143–146. <https://doi.org/10.1016/j.resuscitation.2018.03.012>
- Birch, J., Schnell, A. K., & Clayton, N. S. (2020). Dimensions of Animal Consciousness. *Trends in Cognitive Sciences, 24*(10), 789–801. <https://doi.org/10.1016/j.tics.2020.07.007>
- Blain-Moraes, S., Tarnal, V., Vanini, G., Bel-Behar, T., Janke, E., Picton, P., Golmirzaie, G., Palanca, B. J. A., Avidan, M. S., Kelz, M. B., & Mashour, G. A. (2017). Network Efficiency and Posterior Alpha Patterns Are Markers of Recovery from General Anesthesia: A High-Density Electroencephalography Study in Healthy Volunteers. *Frontiers in Human Neuroscience, 11*, 328. <https://doi.org/10.3389/fnhum.2017.00328>

-
- Block, N. (1995). On a Confusion About a Function of Consciousness. *Brain and Behavioral Sciences*, 18(2), 227–247. <https://doi.org/10.1017/s0140525x00038188>
- Bourdillon, P., Hermann, B., Guénot, M., Bastuji, H., Isnard, J., King, J.-R., Sitt, J., & Naccache, L. (2020). Brain-scale cortico-cortical functional connectivity in the delta-theta band is a robust signature of conscious states: An intracranial and scalp EEG study. *Scientific Reports*, 10(1), 14037. <https://doi.org/10.1038/s41598-020-70447-7>
- Bullmore, E., & Sporns, O. (2009). Complex brain networks: Graph theoretical analysis of structural and functional systems. *Nature Reviews Neuroscience*, 10(3), 186–198. <https://doi.org/10.1038/nrn2575>
- Carls-Diamante, S. (2022). Where Is It Like to Be an Octopus? *Frontiers in Systems Neuroscience*, 16. <https://doi.org/10.3389/fnsys.2022.840022>
- Carruthers, P. (2000). *Phenomenal Consciousness: A Naturalistic Theory*. Cambridge University Press.
- Casali, A. G., Gosseries, O., Rosanova, M., Boly, M., Sarasso, S., Casali, K. R., Casarotto, S., Bruno, M.-A., Laureys, S., Tononi, G., & Massimini, M. (2013). A theoretically based index of consciousness independent of sensory processing and behavior. *Science Translational Medicine*, 5(198), 198ra105. <https://doi.org/10.1126/scitranslmed.3006294>
- Chalmers, D. J. (1995). Facing up to the problem of consciousness. *Journal of Consciousness Studies*, 2(3), 200–219.
- Chennu, S., Annen, J., Wannez, S., Thibaut, A., Chatelle, C., Cassol, H., Martens, G., Schnakers, C., Gosseries, O., Menon, D., & Laureys, S. (2017). Brain networks predict metabolism,

- diagnosis and prognosis at the bedside in disorders of consciousness. *Brain*, 140(8), 2120–2132. <https://doi.org/10.1093/brain/awx163>
- Chennu, S., Finoia, P., Kamau, E., Allanson, J., Williams, G. B., Monti, M. M., Noreika, V., Arnatkeviciute, A., Canales-Johnson, A., Olivares, F., Cabezas-Soto, D., Menon, D. K., Pickard, J. D., Owen, A. M., & Bekinschtein, T. A. (2014). Spectral Signatures of Reorganised Brain Networks in Disorders of Consciousness. *PLOS Computational Biology*, 10(10), e1003887. <https://doi.org/10.1371/journal.pcbi.1003887>
- Chu, C. J. (2015). High density EEG—What do we have to lose? *Clinical Neurophysiology : Official Journal of the International Federation of Clinical Neurophysiology*, 126(3), 433–434. <https://doi.org/10.1016/j.clinph.2014.07.003>
- Churchland, P. S. (1988). Reduction and the Neurobiological Basis of Consciousness. In A. J. Marcel & E. Bisiach (Eds.), *Consciousness in Contemporary Science*. Oxford University Press.
- Churchland, P. S. (1996). The Hornswoggle Problem. *Journal of Consciousness Studies*, 3(5–6), 402–408.
- Claassen, J., Doyle, K., Matory, A., Couch, C., Burger, K. M., Velazquez, A., Okonkwo, J. U., King, J.-R., Park, S., Agarwal, S., Roh, D., Megjhani, M., Eliseyev, A., Connolly, E. S., & Rohaut, B. (2019). Detection of Brain Activation in Unresponsive Patients with Acute Brain Injury. *The New England Journal of Medicine*, 380(26), 2497–2505. <https://doi.org/10.1056/NEJMoa1812757>
- Colombo, M. A., Comanducci, A., Casarotto, S., Derchi, C.-C., Annen, J., Viganò, A., Mazza, A., Trimarchi, P. D., Boly, M., Fecchio, M., Bodart, O., Navarro, J., Laureys, S., Gosseries,

-
- O., Massimini, M., Sarasso, S., & Rosanova, M. (2023). Beyond alpha power: EEG spatial and spectral gradients robustly stratify disorders of consciousness. *Cerebral Cortex (New York, NY)*, 33(11), 7193–7210. <https://doi.org/10.1093/cercor/bhad031>
- Coulborn, S., Taylor, C., Naci, L., Owen, A. M., & Fernández-Espejo, D. (2021). Disruptions in Effective Connectivity within and between Default Mode Network and Anterior Forebrain Mesocircuit in Prolonged Disorders of Consciousness. *Brain Sciences*, 11(6), Article 6. <https://doi.org/10.3390/brainsci11060749>
- Covington, N. V., & Duff, M. C. (2021). Heterogeneity Is a Hallmark of Traumatic Brain Injury, Not a Limitation: A New Perspective on Study Design in Rehabilitation Research. *American Journal of Speech-Language Pathology*, 30(2S), 974–985. https://doi.org/10.1044/2020_AJSLP-20-00081
- Demertzi, A., Antonopoulos, G., Heine, L., Voss, H. U., Crone, J. S., de Los Angeles, C., Bahri, M. A., Di Perri, C., Vanhaudenhuyse, A., Charland-Verville, V., Kronbichler, M., Trinka, E., Phillips, C., Gomez, F., Tshibanda, L., Soddu, A., Schiff, N. D., Whitfield-Gabrieli, S., & Laureys, S. (2015). Intrinsic functional connectivity differentiates minimally conscious from unresponsive patients. *Brain*, 138(9), 2619–2631. <https://doi.org/10.1093/brain/awv169>
- Dennett, D. C. (1969). *Content and consciousness* (pp. xii, 198). Humanities Press.
- Di Gregorio, F., La Porta, F., Petrone, V., Battaglia, S., Orlandi, S., Ippolito, G., Romei, V., Piperno, R., & Lullini, G. (2022). Accuracy of EEG Biomarkers in the Detection of Clinical Outcome in Disorders of Consciousness after Severe Acquired Brain Injury:

-
- Preliminary Results of a Pilot Study Using a Machine Learning Approach. *Biomedicines*, 10(8), Article 8. <https://doi.org/10.3390/biomedicines10081897>
- Donoghue, T., Haller, M., Peterson, E. J., Varma, P., Sebastian, P., Gao, R., Noto, T., Lara, A. H., Wallis, J. D., Knight, R. T., Shestyuk, A., & Voytek, B. (2020). Parameterizing neural power spectra into periodic and aperiodic components. *Nature Neuroscience*, 23(12), Article 12. <https://doi.org/10.1038/s41593-020-00744-x>
- Drayson, Z. (2014). The Personal/Subpersonal Distinction. *Philosophy Compass*, 9(5), 338–346. <https://doi.org/10.1111/phc3.12124>
- Duclos, C., Maschke, C., Mahdid, Y., Nadin, D., Rokos, A., Arbour, C., Badawy, M., Létourneau, J., Owen, A. M., Plourde, G., & Blain-Moraes, S. (2022). Brain Responses to Propofol in Advance of Recovery from Coma and Disorders of Consciousness: A Preliminary Study. *American Journal of Respiratory and Critical Care Medicine*, 205(2), 171–182. <https://doi.org/10.1164/rccm.202105-1223OC>
- Duclos, C., Nadin, D., Mahdid, Y., Tarnal, V., Picton, P., Vanini, G., Golmirzaie, G., Janke, E., Avidan, M. S., Kelz, M. B., Mashour, G. A., & Blain-Moraes, S. (2021). Brain network motifs are markers of loss and recovery of consciousness. *Scientific Reports*, 11(1), Article 1. <https://doi.org/10.1038/s41598-021-83482-9>
- Edlow, B. L., Claassen, J., Schiff, N. D., & Greer, D. M. (2021). Recovery from disorders of consciousness: Mechanisms, prognosis and emerging therapies. *Nature Reviews Neurology*, 17(3), Article 3. <https://doi.org/10.1038/s41582-020-00428-x>

-
- Estraneo, A., & Trojano, L. (2018). Prognosis in Disorders of Consciousness. In C. Schnakers & S. Laureys (Eds.), *Coma and Disorders of Consciousness* (pp. 17–36). Springer International Publishing. https://doi.org/10.1007/978-3-319-55964-3_2
- Forgacs, P. B., Frey, H., Velazquez, A., Thompson, S., Brodie, D., Moitra, V., Rabani, L., Park, S., Agarwal, S., Falo, M. C., Schiff, N. D., & Claassen, J. (2017). Dynamic regimes of neocortical activity linked to corticothalamic integrity correlate with outcomes in acute anoxic brain injury after cardiac arrest. *Annals of Clinical and Translational Neurology*, 4(2), 119–129. <https://doi.org/10.1002/acn3.385>
- Giacino, J. T., Kalmar, K., & Whyte, J. (2004). The JFK Coma Recovery Scale-Revised: Measurement characteristics and diagnostic utility. *Archives of Physical Medicine and Rehabilitation*, 85(12), 2020–2029. <https://doi.org/10.1016/j.apmr.2004.02.033>
- Giacino, J. T., Katz, D. I., Schiff, N. D., Whyte, J., Ashman, E. J., Ashwal, S., Barbano, R., Hammond, F. M., Laureys, S., Ling, G. S. F., Nakase-Richardson, R., Seel, R. T., Yablon, S., Getchius, T. S. D., Gronseth, G. S., & Armstrong, M. J. (2018). Practice guideline update recommendations summary: Disorders of consciousness. *Neurology*, 91(10), 450–460. <https://doi.org/10.1212/WNL.0000000000005926>
- Gosseries, O., Bruno, M.-A., Chatelle, C., Vanhaudenhuyse, A., Schnakers, C., Soddu, A., & Laureys, S. (2011). Disorders of consciousness: What's in a name? *NeuroRehabilitation*, 28(1), Article 1. <https://doi.org/10.3233/NRE-2011-0625>
- Gosseries, O., & Laureys, S. (2022). Severe Brain Damage: Coma and Related Disorders of Consciousness. In D. W. Pfaff, N. D. Volkow, & J. L. Rubenstein (Eds.), *Neuroscience in*

-
- the 21st Century: From Basic to Clinical* (pp. 3757–3790). Springer International Publishing. https://doi.org/10.1007/978-3-030-88832-9_95
- Guo, Y., Cao, B., He, Y., Xie, Q., Liang, Q., Lan, Y., Zhang, M., Qiu, Y., Yu, R., & Huang, R. (2023). Disrupted multi-scale topological organization of directed functional brain networks in patients with disorders of consciousness. *Brain Communications*, *5*(2), fcad069. <https://doi.org/10.1093/braincomms/fcad069>
- Hermann, B., Stender, J., Habert, M.-O., Kas, A., Denis-Valente, M., Raimondo, F., Pérez, P., Rohaut, B., Sitt, J. D., & Naccache, L. (2021). Multimodal FDG-PET and EEG assessment improves diagnosis and prognostication of disorders of consciousness. *NeuroImage: Clinical*, *30*, 102601. <https://doi.org/10.1016/j.nicl.2021.102601>
- Hochstein, E. (2016). One mechanism, many models: A distributed theory of mechanistic explanation. *Synthese*, *193*(5), 1387–1407. <https://doi.org/10.1007/s11229-015-0844-8>
- Hochstein, E. (2022). Foregrounding and backgrounding: A new interpretation of “levels” in science. *European Journal for Philosophy of Science*, *12*(2), 23. <https://doi.org/10.1007/s13194-022-00457-x>
- Hochstein, E. (2023). Integration Without Integrated Models or Theories. *Synthese*, *202*(3), 1–25. <https://doi.org/10.1007/s11229-023-04298-w>
- Jas, M., Engemann, D. A., Bekhti, Y., Raimondo, F., & Gramfort, A. (2017). Autoreject: Automated artifact rejection for MEG and EEG data. *NeuroImage*, *159*, 417–429. <https://doi.org/10.1016/j.neuroimage.2017.06.030>

-
- Jas, M., Engemann, D., Raimondo, F., Bekhti, Y., & Gramfort, A. (2016). Automated rejection and repair of bad trials in MEG/EEG. *2016 International Workshop on Pattern Recognition in Neuroimaging (PRNI)*, 1–4. <https://doi.org/10.1109/PRNI.2016.7552336>
- Jennett, B., & Bond, M. (1975). ASSESSMENT OF OUTCOME AFTER SEVERE BRAIN DAMAGE: A Practical Scale. *The Lancet*, *305*(7905), 480–484. [https://doi.org/10.1016/S0140-6736\(75\)92830-5](https://doi.org/10.1016/S0140-6736(75)92830-5)
- John, E. R., Prichep, L. S., Kox, W., Valdés-Sosa, P., Bosch-Bayard, J., Aubert, E., Tom, M., diMichele, F., & Gugino, L. D. (2001). Invariant Reversible QEEG Effects of Anesthetics. *Consciousness and Cognition*, *10*(2), 165–183. <https://doi.org/10.1006/ccog.2001.0507>
- Kafashan, M., Ching, S., & Palanca, B. J. A. (2016). Sevoflurane Alters Spatiotemporal Functional Connectivity Motifs That Link Resting-State Networks during Wakefulness. *Frontiers in Neural Circuits*, *10*. <https://www.frontiersin.org/articles/10.3389/fncir.2016.00107>
- Kashtan, N., & Alon, U. (2005). Spontaneous evolution of modularity and network motifs. *Proceedings of the National Academy of Sciences of the United States of America*, *102*(39), 13773–13778. <https://doi.org/10.1073/pnas.0503610102>
- Kondziella, D., Bender, A., Diserens, K., van Erp, W., Estraneo, A., Formisano, R., Laureys, S., Naccache, L., Ozturk, S., Rohaut, B., Sitt, J. D., Stender, J., Tiainen, M., Rossetti, A. O., Gosseries, O., Chatelle, C., & EAN Panel on Coma, Disorders of Consciousness. (2020). European Academy of Neurology guideline on the diagnosis of coma and other disorders

-
- of consciousness. *European Journal of Neurology*, 27(5), 741–756.
<https://doi.org/10.1111/ene.14151>
- Kotchoubey, B., & Pavlov, Y. G. (2018). A Systematic Review and Meta-Analysis of the Relationship Between Brain Data and the Outcome in Disorders of Consciousness. *Frontiers in Neurology*, 9, 315. <https://doi.org/10.3389/fneur.2018.00315>
- Latora, V., & Marchiori, M. (2001). Efficient Behavior of Small-World Networks. *Physical Review Letters*, 87(19), 198701. <https://doi.org/10.1103/PhysRevLett.87.198701>
- Lee, H., Mashour, G. A., Noh, G.-J., Kim, S., & Lee, U. (2013). Reconfiguration of Network Hub Structure after Propofol-induced Unconsciousness. *Anesthesiology*, 119(6), 1347–1359. <https://doi.org/10.1097/ALN.0b013e3182a8ec8c>
- Lee, U., Kim, S., Noh, G.-J., Choi, B.-M., Hwang, E., & Mashour, G. A. (2009). The directionality and functional organization of frontoparietal connectivity during consciousness and anesthesia in humans. *Consciousness and Cognition*, 18(4), 1069–1078. <https://doi.org/10.1016/j.concog.2009.04.004>
- Lee, U., Ku, S., Noh, G., Baek, S., Choi, B., & Mashour, G. A. (2013). Disruption of Frontal–Parietal Communication by Ketamine, Propofol, and Sevoflurane. *Anesthesiology*, 118(6), 1264–1275. <https://doi.org/10.1097/ALN.0b013e31829103f5>
- Lemieux, M., Chen, J.-Y., Lonjers, P., Bazhenov, M., & Timofeev, I. (2014). The impact of cortical deafferentation on the neocortical slow oscillation. *The Journal of Neuroscience: The Official Journal of the Society for Neuroscience*, 34(16), 5689–5703.
<https://doi.org/10.1523/JNEUROSCI.1156-13.2014>

-
- Li, D., Vlisides, P. E., Kelz, M. B., Avidan, M. S., Mashour, G. A., & for the ReCCognition Study Group. (2019). Dynamic Cortical Connectivity during General Anesthesia in Healthy Volunteers. *Anesthesiology*, *130*(6), 870–884.
<https://doi.org/10.1097/ALN.0000000000002656>
- Liang, Z., Lan, Z., Wang, Y., Bai, Y., He, J., Wang, J., & Li, X. (2023). The EEG complexity, information integration and brain network changes in minimally conscious state patients during general anesthesia. *Journal of Neural Engineering*, *20*(6).
<https://doi.org/10.1088/1741-2552/ad12dc>
- Liu, B., Zhang, X., Wang, L., Li, Y., Hou, J., Duan, G., Guo, T., & Wu, D. (2021). Outcome Prediction in Unresponsive Wakefulness Syndrome and Minimally Conscious State by Non-linear Dynamic Analysis of the EEG. *Frontiers in Neurology*, *12*, 510424.
<https://doi.org/10.3389/fneur.2021.510424>
- Liu, Z., Zhang, X., Yu, B., Wang, J., & Lu, X. (2023). Effectiveness on level of consciousness of non-invasive neuromodulation therapy in patients with disorders of consciousness: A systematic review and meta-analysis. *Frontiers in Human Neuroscience*, *17*.
<https://www.frontiersin.org/articles/10.3389/fnhum.2023.1129254>
- López-González, A., Panda, R., Ponce-Alvarez, A., Zamora-López, G., Escrichs, A., Martial, C., Thibaut, A., Gosseries, O., Kringelbach, M. L., Annen, J., Laureys, S., & Deco, G. (2021). Loss of consciousness reduces the stability of brain hubs and the heterogeneity of brain dynamics. *Communications Biology*, *4*(1), 1–15. <https://doi.org/10.1038/s42003-021-02537-9>

-
- Maciel, C. B., Barden, M. M., Youn, T. S., Dhakar, M. B., & Greer, D. M. (2020). Neuroprognostication Practices in Postcardiac Arrest Patients: An International Survey of Critical Care Providers. *Critical Care Medicine*, *48*(2), e107–e114. <https://doi.org/10.1097/CCM.0000000000004107>
- Maki-Marttunen, V., Diez, I., Cortes, J. M., Chialvo, D. R., & Villarreal, M. (2013). Disruption of transfer entropy and inter-hemispheric brain functional connectivity in patients with disorder of consciousness. *Frontiers in Neuroinformatics*, *7*. <https://doi.org/10.3389/fninf.2013.00024>
- Marsh, B., White, M., Morton, N., & Kenny, G. N. (1991). Pharmacokinetic model driven infusion of propofol in children. *British Journal of Anaesthesia*, *67*(1), 41–48. <https://doi.org/10.1093/bja/67.1.41>
- Martínez, D. E., Rudas, J., Demertzi, A., Charland-Verville, V., Soddu, A., Laureys, S., & Gómez, F. (2020). Reconfiguration of large-scale functional connectivity in patients with disorders of consciousness. *Brain and Behavior*, *10*(1), e1476. <https://doi.org/10.1002/brb3.1476>
- Maschke, C., Belloli, L., Manasova, D., Sitt, J. D., & Blain-Moraes, S. (2024). *The role of etiology in the identification of clinical markers of consciousness: Comparing EEG alpha power, complexity, and spectral exponent* (p. 2024.03.20.24304639). medRxiv. <https://doi.org/10.1101/2024.03.20.24304639>
- Maschke, C., Duclos, C., Owen, A. M., Jerbi, K., & Blain-Moraes, S. (2022). *Aperiodic brain activity and response to anesthesia vary in disorders of consciousness* (p. 2022.04.22.489199). bioRxiv. <https://doi.org/10.1101/2022.04.22.489199>

-
- Milo, R., Shen-Orr, S., Itzkovitz, S., Kashtan, N., Chklovskii, D., & Alon, U. (2002). Network motifs: Simple building blocks of complex networks. *Science (New York, N.Y.)*, 298(5594), 824–827. <https://doi.org/10.1126/science.298.5594.824>
- Moon, J.-Y., Lee, U., Blain-Moraes, S., & Mashour, G. A. (2015). General Relationship of Global Topology, Local Dynamics, and Directionality in Large-Scale Brain Networks. *PLOS Computational Biology*, 11(4), e1004225. <https://doi.org/10.1371/journal.pcbi.1004225>
- Mursa, B.-E.-M., Dioşan, L., & Andreica, A. (2021). Network motifs: A key variable in the equation of dynamic flow between macro and micro layers in Complex Networks. *Knowledge-Based Systems*, 213, 106648. <https://doi.org/10.1016/j.knosys.2020.106648>
- Naci, L., & Owen, A. M. (2022). Uncovering Consciousness and Revealing the Preservation of Mental Life in Unresponsive Brain-Injured Patients. *Seminars in Neurology*, 42, 299–308. <https://doi.org/10.1055/a-1892-1715>
- Nadin, D., Duclos, C., Mahdid, Y., Rokos, A., Badawy, M., Létourneau, J., Arbour, C., Plourde, G., & Blain-Moraes, S. (2020). Brain network motif topography may predict emergence from disorders of consciousness: A case series. *Neuroscience of Consciousness*, 2020(1), niaa017. <https://doi.org/10.1093/nc/niaa017>
- Newman, M. E. J. (2006). Modularity and community structure in networks. *Proceedings of the National Academy of Sciences*, 103(23), 8577–8582. <https://doi.org/10.1073/pnas.0601602103>

- Norton, L., Hutchison, R. M., Young, G. B., Lee, D. H., Sharpe, M. D., & Mirsattari, S. M. (2012). Disruptions of functional connectivity in the default mode network of comatose patients. *Neurology*, *78*(3), 175–181. <https://doi.org/10.1212/WNL.0b013e31823fcd61>
- Owen, A. M., Coleman, M. R., Boly, M., Davis, M. H., Laureys, S., & Pickard, J. D. (2006). Detecting Awareness in the Vegetative State. *Science*, *313*(5792), 1402–1402. <https://doi.org/10.1126/science.1130197>
- Panda, R., Thibaut, A., Lopez-Gonzalez, A., Escrichs, A., Bahri, M. A., Hillebrand, A., Deco, G., Laureys, S., Gosseries, O., Annen, J., & Tewarie, P. (2022). Disruption in structural–functional network repertoire and time-resolved subcortical fronto-temporoparietal connectivity in disorders of consciousness. *eLife*, *11*, e77462. <https://doi.org/10.7554/eLife.77462>
- Papadimitriou, C., Weaver, J. A., Guernon, A., Walsh, E., Mallinson, T., & Pape, T. L. B. (2022). “Fluctuation is the norm”: Rehabilitation practitioner perspectives on ambiguity and uncertainty in their work with persons in disordered states of consciousness after traumatic brain injury. *PLoS ONE*, *17*(4), e0267194. <https://doi.org/10.1371/journal.pone.0267194>
- Park, J. S., Kim, E. Y., You, Y., Min, J. H., Jeong, W., Ahn, H. J., In, Y. N., Lee, I. H., Kim, J. M., & Kang, C. (2023). Combination strategy for prognostication in patients undergoing post-resuscitation care after cardiac arrest. *Scientific Reports*, *13*(1), 21880. <https://doi.org/10.1038/s41598-023-49345-1>
- Pedregosa, F., Varoquaux, G., Gramfort, A., Michel, V., Thirion, B., Grisel, O., Blondel, M., Prettenhofer, P., Weiss, R., Dubourg, V., Vanderplas, J., Passos, A., Cournapeau, D.,

-
- Brucher, M., Perrot, M., & Duchesnay, É. (2011). Scikit-learn: Machine Learning in Python. *Journal of Machine Learning Research*, 12(85), 2825–2830.
- Perkins, G. D., Jacobs, I. G., Nadkarni, V. M., Berg, R. A., Bhanji, F., Biarent, D., Bossaert, L. L., Brett, S. J., Chamberlain, D., de Caen, A. R., Deakin, C. D., Finn, J. C., Gräsner, J.-T., Hazinski, M. F., Iwami, T., Koster, R. W., Lim, S. H., Ma, M. H.-M., McNally, B. F., ... Utstein Collaborators. (2015). Cardiac Arrest and Cardiopulmonary Resuscitation Outcome Reports: Update of the Utstein Resuscitation Registry Templates for Out-of-Hospital Cardiac Arrest: A Statement for Healthcare Professionals From a Task Force of the International Liaison Committee on Resuscitation (American Heart Association, European Resuscitation Council, Australian and New Zealand Council on Resuscitation, Heart and Stroke Foundation of Canada, InterAmerican Heart Foundation, Resuscitation Council of Southern Africa, Resuscitation Council of Asia); and the American Heart Association Emergency Cardiovascular Care Committee and the Council on Cardiopulmonary, Critical Care, Perioperative and Resuscitation. *Resuscitation*, 96, 328–340. <https://doi.org/10.1016/j.resuscitation.2014.11.002>
- Perl, Y. S., Pallavicini, C., Ipiña, I. P., Demertzi, A., Bonhomme, V., Martial, C., Panda, R., Annen, J., Ibañez, A., Kringelbach, M., Deco, G., Laufs, H., Sitt, J., Laureys, S., & Tagliazucchi, E. (2021). Perturbations in dynamical models of whole-brain activity dissociate between the level and stability of consciousness. *PLOS Computational Biology*, 17(7), e1009139. <https://doi.org/10.1371/journal.pcbi.1009139>
- Porcaro, C., Nemirovsky, I. E., Riganello, F., Mansour, Z., Cerasa, A., Tonin, P., Stojanoski, B., & Soddu, A. (2022). Diagnostic Developments in Differentiating Unresponsive

-
- Wakefulness Syndrome and the Minimally Conscious State. *Frontiers in Neurology*, 12, 778951. <https://doi.org/10.3389/fneur.2021.778951>
- Prill, R. J., Iglesias, P. A., & Levchenko, A. (2005). Dynamic Properties of Network Motifs Contribute to Biological Network Organization. *PLOS Biology*, 3(11), e343. <https://doi.org/10.1371/journal.pbio.0030343>
- Purdon, P. L., Pierce, E. T., Mukamel, E. A., Prerau, M. J., Walsh, J. L., Wong, K. F. K., Salazar-Gomez, A. F., Harrell, P. G., Sampson, A. L., Cimenser, A., Ching, S., Kopell, N. J., Tavares-Stoeckel, C., Habeeb, K., Merhar, R., & Brown, E. N. (2013). Electroencephalogram signatures of loss and recovery of consciousness from propofol. *Proceedings of the National Academy of Sciences*, 110(12), E1142–E1151. <https://doi.org/10.1073/pnas.1221180110>
- Robertsen, A., Helseth, E., Laake, J. H., & Førde, R. (2019). Neurocritical care physicians' doubt about whether to withdraw life-sustaining treatment the first days after devastating brain injury: An interview study. *Scandinavian Journal of Trauma, Resuscitation and Emergency Medicine*, 27, 81. <https://doi.org/10.1186/s13049-019-0648-9>
- Rubinov, M., & Sporns, O. (2010). Complex network measures of brain connectivity: Uses and interpretations. *NeuroImage*, 52(3), 1059–1069. <https://doi.org/10.1016/j.neuroimage.2009.10.003>
- Sandroni, C., Cronberg, T., & Sekhon, M. (2021). Brain injury after cardiac arrest: Pathophysiology, treatment, and prognosis. *Intensive Care Medicine*, 47(12), 1393–1414. <https://doi.org/10.1007/s00134-021-06548-2>

-
- Schnakers, C. (2020). Update on diagnosis in disorders of consciousness. *Expert Review of Neurotherapeutics*, 20(10), 997–1004. <https://doi.org/10.1080/14737175.2020.1796641>
- Schnakers, C. (2024). Assessing consciousness and cognition in disorders of consciousness. *NeuroRehabilitation*, 54(1), 11–21. <https://doi.org/10.3233/NRE-230140>
- Schnakers, C., Giacino, J., Kalmar, K., Piret, S., Lopez, E., Boly, M., Malone, R., & Laureys, S. (2007). Does the Glasgow Coma Scale correctly diagnose the vegetative and minimally conscious states? *Critical Care*, 11(2), Article 2. <https://doi.org/10.1186/cc5648>
- Schnakers, C., & Laureys, S. (Eds.). (2018). *Coma and Disorders of Consciousness*. Springer International Publishing. <https://doi.org/10.1007/978-3-319-55964-3>
- Schnakers, C., Vanhaudenhuyse, A., Giacino, J., Ventura, M., Boly, M., Majerus, S., Moonen, G., & Laureys, S. (2009). Diagnostic accuracy of the vegetative and minimally conscious state: Clinical consensus versus standardized neurobehavioral assessment. *BMC Neurology*, 9(1), 35. <https://doi.org/10.1186/1471-2377-9-35>
- Shin, J., Mashour, G. A., Ku, S., Kim, S., & Lee, U. (2013). Subgraph “Backbone” Analysis of Dynamic Brain Networks during Consciousness and Anesthesia. *PLOS ONE*, 8(8), e70899. <https://doi.org/10.1371/journal.pone.0070899>
- Sitt, J. D., King, J.-R., El Karoui, I., Rohaut, B., Faugeras, F., Gramfort, A., Cohen, L., Sigman, M., Dehaene, S., & Naccache, L. (2014). Large scale screening of neural signatures of consciousness in patients in a vegetative or minimally conscious state. *Brain*, 137(8), 2258–2270. <https://doi.org/10.1093/brain/awu141>
- Sokoliuk, R., & Cruse, D. (2018). Listening for the rhythm of a conscious brain. *Brain*, 141(11), 3095–3097. <https://doi.org/10.1093/brain/awy267>

-
- Sporns, O., & Betzel, R. F. (2016). Modular Brain Networks. *Annual Review of Psychology*, 67, 613–640. <https://doi.org/10.1146/annurev-psych-122414-033634>
- Sporns, O., & Kötter, R. (2004). Motifs in Brain Networks. *PLOS Biology*, 2(11), e369. <https://doi.org/10.1371/journal.pbio.0020369>
- Stam, C. J., & van Straaten, E. C. W. (2012). Go with the flow: Use of a directed phase lag index (dPLI) to characterize patterns of phase relations in a large-scale model of brain dynamics. *NeuroImage*, 62(3), 1415–1428. <https://doi.org/10.1016/j.neuroimage.2012.05.050>
- Stefan, S., Schorr, B., Lopez-Rolon, A., Kolassa, I.-T., Shock, J. P., Rosenfelder, M., Heck, S., & Bender, A. (2018). Consciousness Indexing and Outcome Prediction with Resting-State EEG in Severe Disorders of Consciousness. *Brain Topography*, 31(5), 848–862. <https://doi.org/10.1007/s10548-018-0643-x>
- Teasdale, G., & Jennett, B. (1974). Assessment of coma and impaired consciousness. A practical scale. *Lancet (London, England)*, 2(7872), 81–84. [https://doi.org/10.1016/s0140-6736\(74\)91639-0](https://doi.org/10.1016/s0140-6736(74)91639-0)
- Thibaut, A., Chennu, S., Chatelle, C., Martens, G., Annen, J., Cassol, H., & Laureys, S. (2018). Theta network centrality correlates with tDCS response in disorders of consciousness. *Brain Stimulation*, 11(6), Article 6.
- Timofeev, I., Grenier, F., Bazhenov, M., Sejnowski, T. J., & Steriade, M. (2000). Origin of Slow Cortical Oscillations in Deafferented Cortical Slabs. *Cerebral Cortex*, 10(12), 1185–1199. <https://doi.org/10.1093/cercor/10.12.1185>

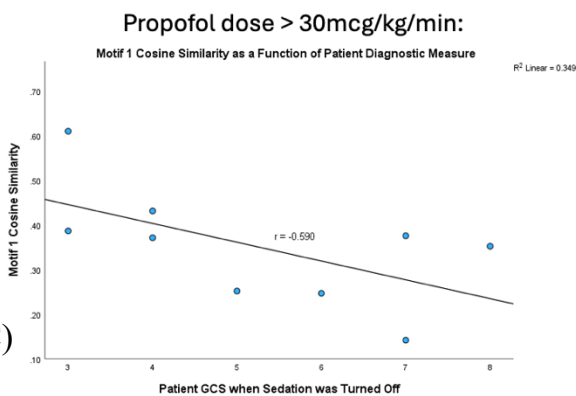
- Tinker, J. H., Sharbrough, F. W., & Michenfelder, J. D. (1977). Anterior shift of the dominant EEG rhythm during anesthesia in the Java monkey: Correlation with anesthetic potency. *Anesthesiology*, *46*(4), 252–259. <https://doi.org/10.1097/00000542-197704000-00005>
- Tononi, G. (2004). An information integration theory of consciousness. *BMC Neuroscience*, *5*(1), 42. <https://doi.org/10.1186/1471-2202-5-42>
- Turgeon, A. F., Lauzier, F., Simard, J.-F., Scales, D. C., Burns, K. E. A., Moore, L., Zygun, D. A., Bernard, F., Meade, M. O., Dung, T. C., Ratnapalan, M., Todd, S., Harlock, J., Fergusson, D. A., & Canadian Critical Care Trials Group. (2011). Mortality associated with withdrawal of life-sustaining therapy for patients with severe traumatic brain injury: A Canadian multicentre cohort study. *CMAJ: Canadian Medical Association Journal = Journal de l'Association Medicale Canadienne*, *183*(14), 1581–1588. <https://doi.org/10.1503/cmaj.101786>
- Turner-Stokes, L., Thakur, V., Dungca, C., Clare, C., & Alfonso, E. (2022). End-of-life care for patients with prolonged disorders of consciousness following withdrawal of life-sustaining treatment: Experience and lessons from an 8-year cohort. *Clinical Medicine*, *22*(6), 559–565. <https://doi.org/10.7861/clinmed.2022-0255>
- Vinck, M., Oostenveld, R., van Wingerden, M., Battaglia, F., & Pennartz, C. M. A. (2011). An improved index of phase-synchronization for electrophysiological data in the presence of volume-conduction, noise and sample-size bias. *NeuroImage*, *55*(4), 1548–1565. <https://doi.org/10.1016/j.neuroimage.2011.01.055>
- Wang, J., Hu, X., Hu, Z., Sun, Z., Laureys, S., & Di, H. (2020). The misdiagnosis of prolonged disorders of consciousness by a clinical consensus compared with repeated coma-

-
- recovery scale-revised assessment. *BMC Neurology*, 20(1), 343.
<https://doi.org/10.1186/s12883-020-01924-9>
- Wang, R., Liu, M., Cheng, X., Wu, Y., Hildebrandt, A., & Zhou, C. (2021). Segregation, integration, and balance of large-scale resting brain networks configure different cognitive abilities. *Proceedings of the National Academy of Sciences*, 118(23), e2022288118. <https://doi.org/10.1073/pnas.2022288118>
- Watts, D. J., & Strogatz, S. H. (1998). Collective dynamics of ‘small-world’ networks. *Nature*, 393(6684), 440–442. <https://doi.org/10.1038/30918>
- Wilkes, K. V. (1984). Is Consciousness Important? *British Journal for the Philosophy of Science*, 35(September), 223–243. <https://doi.org/10.1093/bjps/35.3.223>
- Wu, M., Yin, X., Chen, M., Liu, Y., Zhang, X., Li, T., Long, Y., Wu, X., Pu, L., Zhang, M., Hu, Z., & Ye, L. (2020). Effects of propofol on intracranial pressure and prognosis in patients with severe brain diseases undergoing endotracheal suctioning. *BMC Neurology*, 20(1), 394. <https://doi.org/10.1186/s12883-020-01972-1>
- Young, M. J., Bodien, Y. G., & Edlow, B. L. (2022). Ethical Considerations in Clinical Trials for Disorders of Consciousness. *Brain Sciences*, 12(2), 211.
<https://doi.org/10.3390/brainsci12020211>

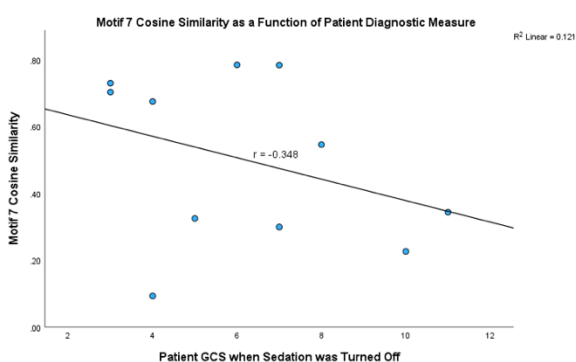
Appendix

Supplementary Material for Chapter 1

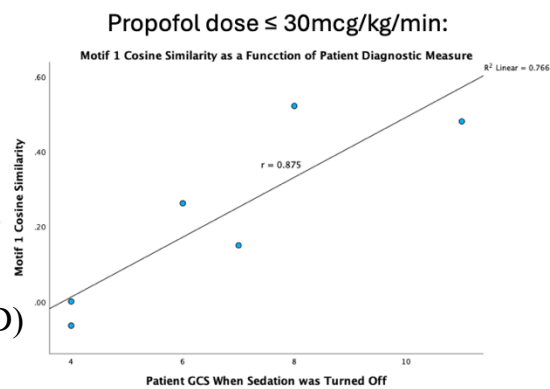
A)



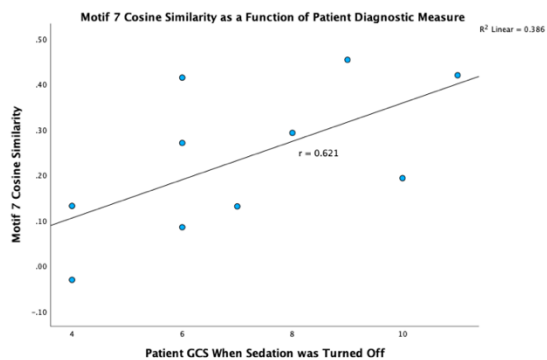
C)



B)

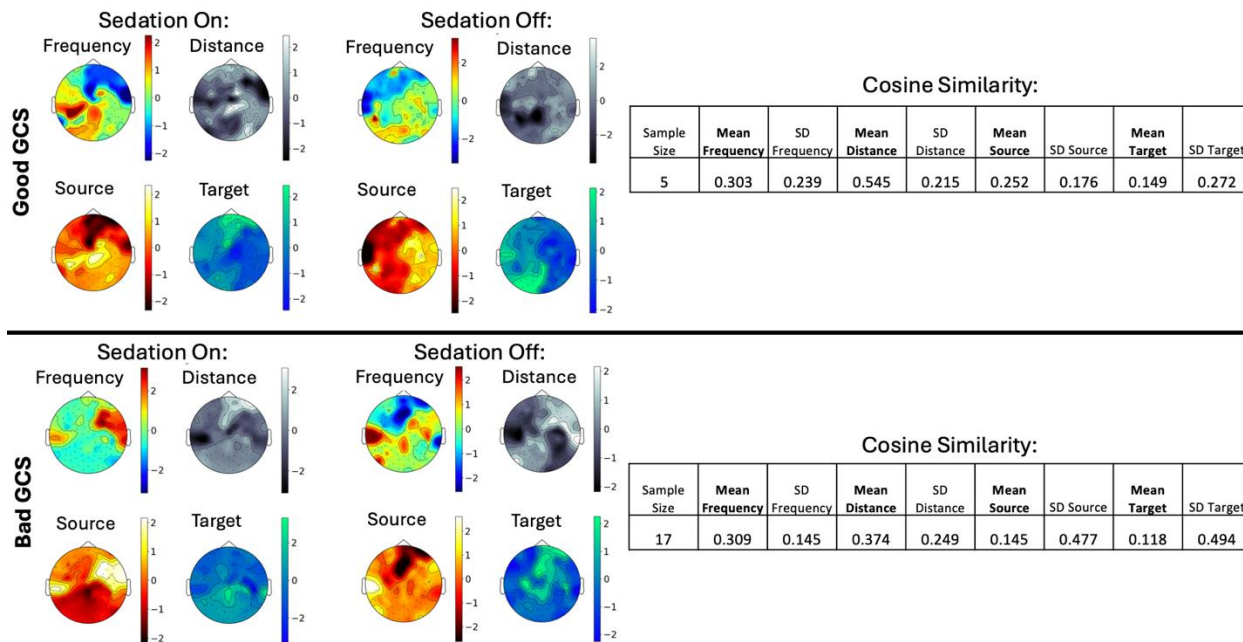


D)



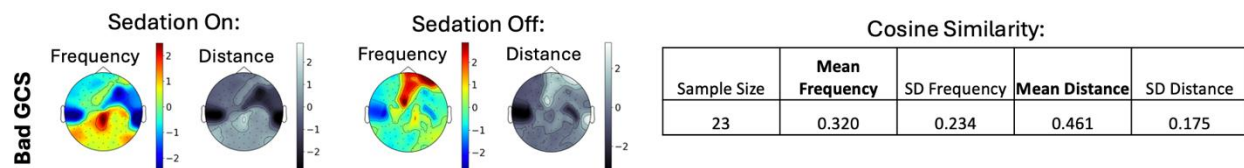
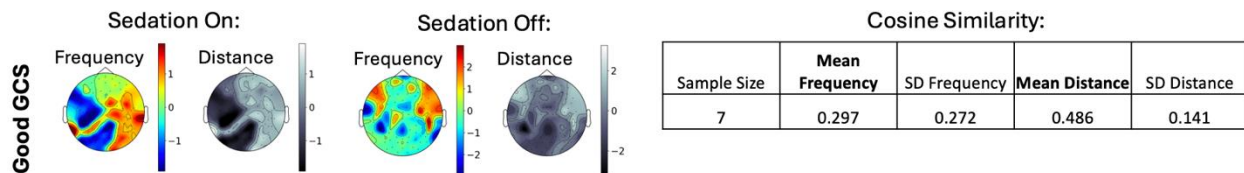
Supplementary Figure 1. Correlations between patient Glasgow Coma Scale (GCS) scores when off sedation and motif frequency cosine similarity during sedation withdrawal. Correlations between patient GCS scores and cosine similarity values for motifs 1 and 7 are displayed for patients who received a propofol dose > 30 mcg/kg/min (A and C, respectively) and a propofol dose ≤ 30 mcg/kg/min (B and D, respectively).

Anesthesia Withdrawal: Motif 1



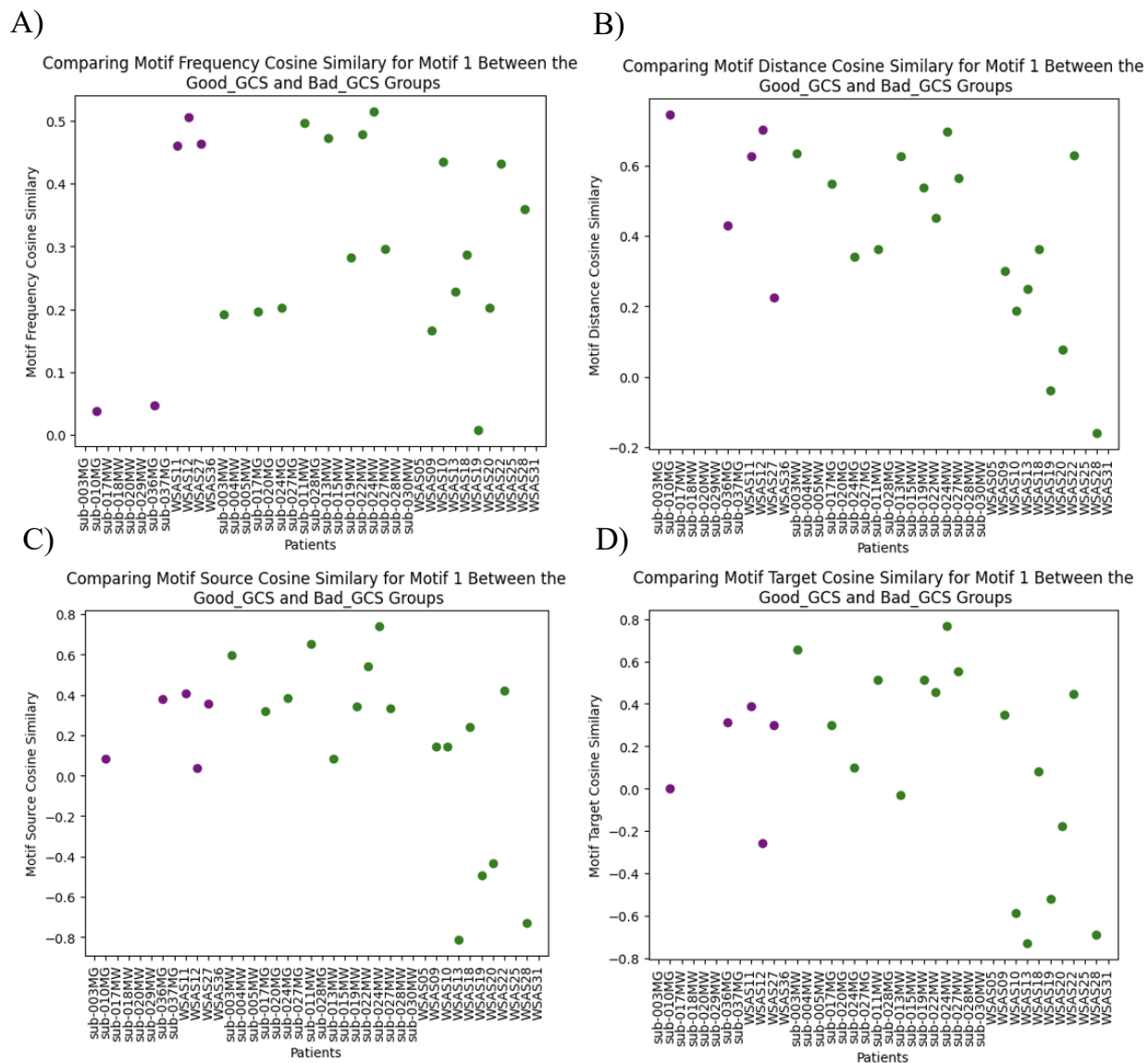
Supplementary Figure 2. Topological plots between diagnostic groups for motif 1 frequency, distance, source, and target properties during anesthesia withdrawal. Motif properties were plotted using nodal Z-scores during sedation off (pre-anesthesia withdrawal) and sedation on (post-anesthesia withdrawal) states. Cosine similarity mean and standard deviation (SD) values between sedation on and off states are displayed in the tables. Group data for patients with favorable Glasgow Coma Scale (GCS) score are displayed on top and patients with an unfavorable GCS on the bottom.

Anesthesia Withdrawal: Motif 7



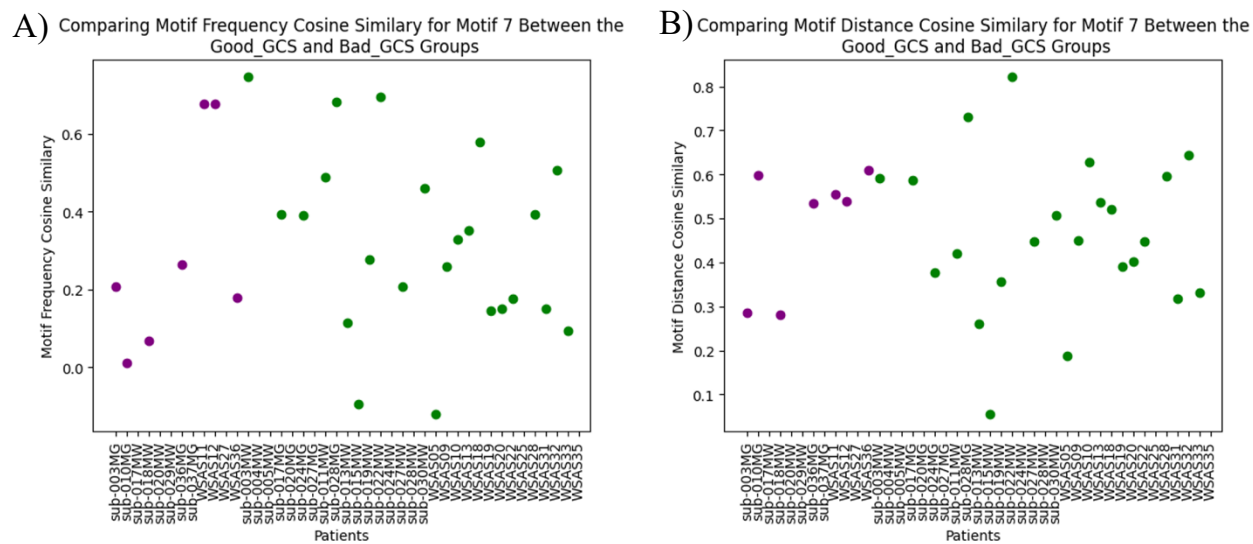
Supplementary Figure 3. Topological plots between diagnostic groups for motif 7 frequency and distance properties during anesthesia withdrawal. Motif properties were plotted using nodal Z-scores during sedation on (pre-anesthesia withdrawal) and sedation off (post-anesthesia withdrawal) states. Cosine similarity mean and standard deviation (SD) values between sedation on and off states are displayed in the tables. Group data for patients with favorable Glasgow Coma Scale (GCS) score are displayed on top and patients with an unfavorable GCS on the bottom.

Anesthesia Withdrawal: Motif 1



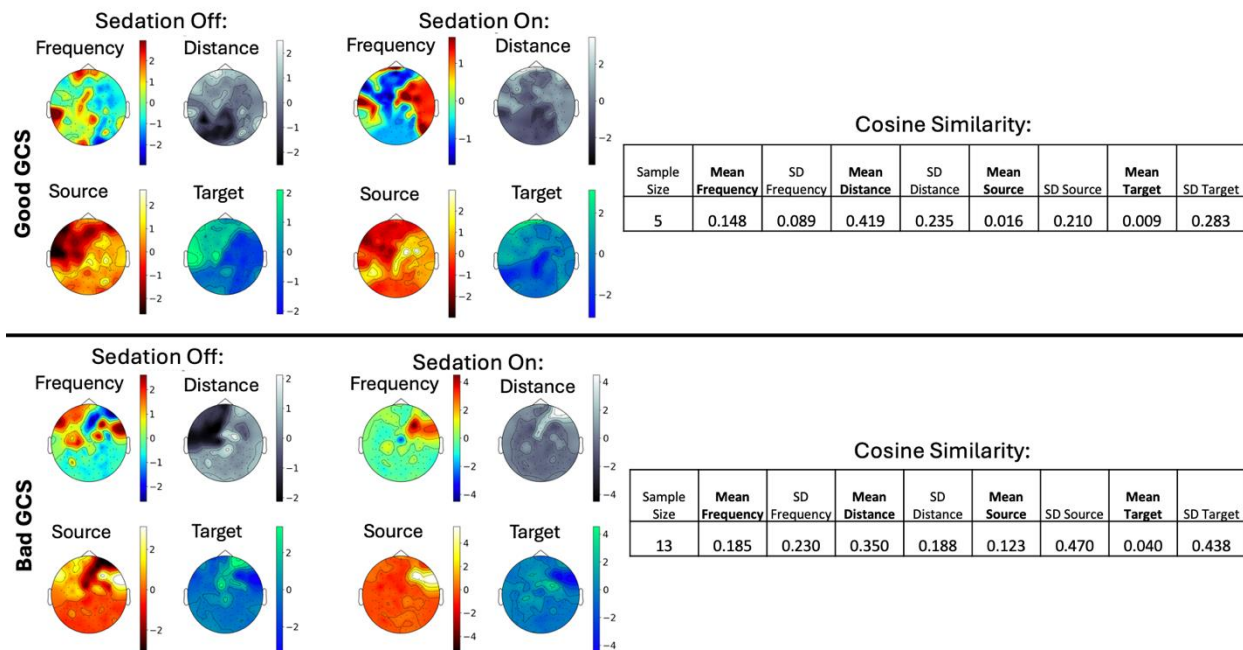
Supplementary Figure 4. Individual cosine similarity values for motif 1 frequency (A), distance (B), source (C), and target (D) properties during propofol withdrawal. Purple = good Glasgow Coma Scale (GCS), green = bad GCS.

Anesthesia Withdrawal: Motif 7



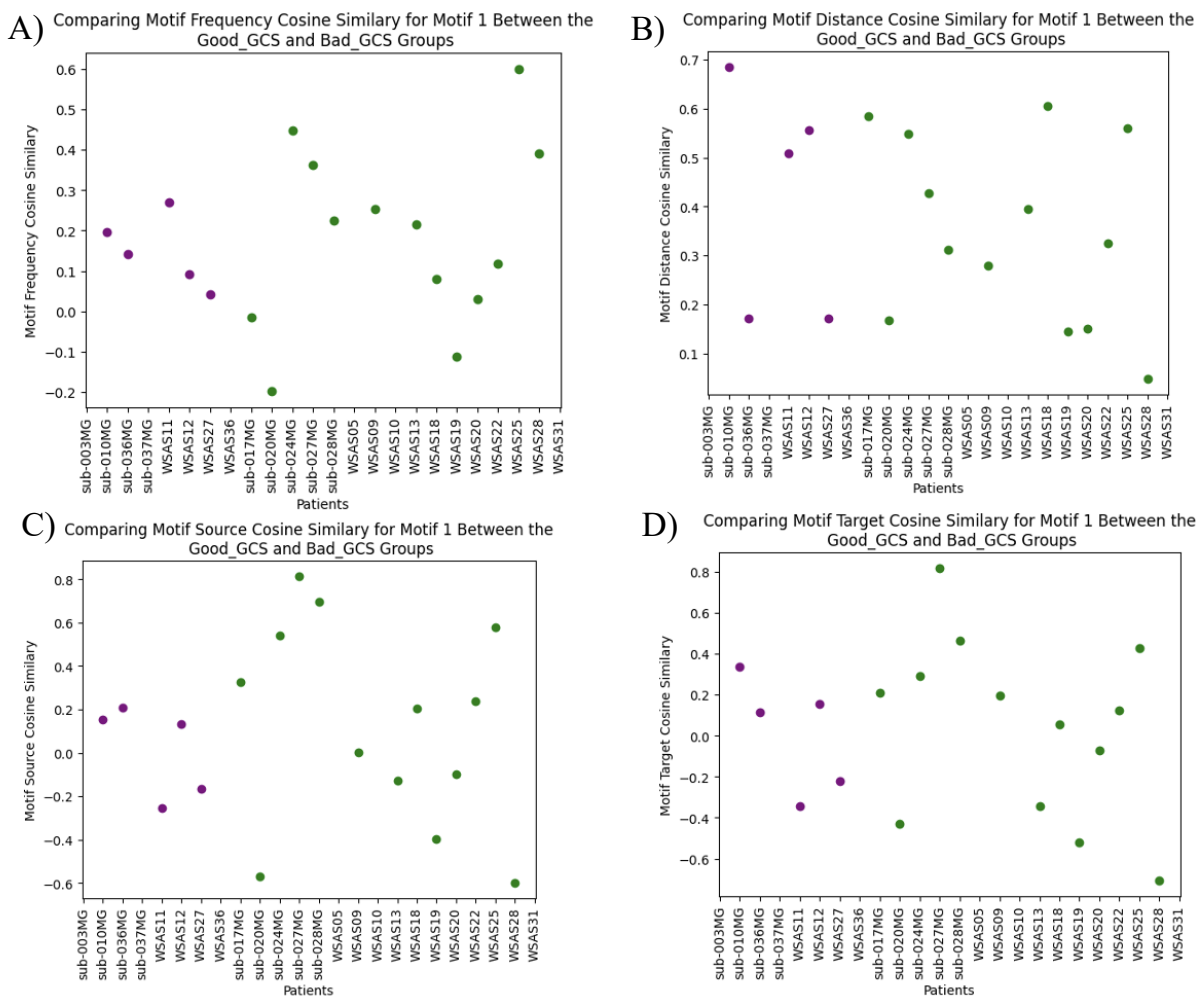
Supplementary Figure 5. Individual cosine similarity values for motif 7 frequency (A) and distance (B) properties during propofol withdrawal. Purple = good Glasgow Coma Scale (GCS), green = bad GCS.

Anesthesia Administration: Motif 1



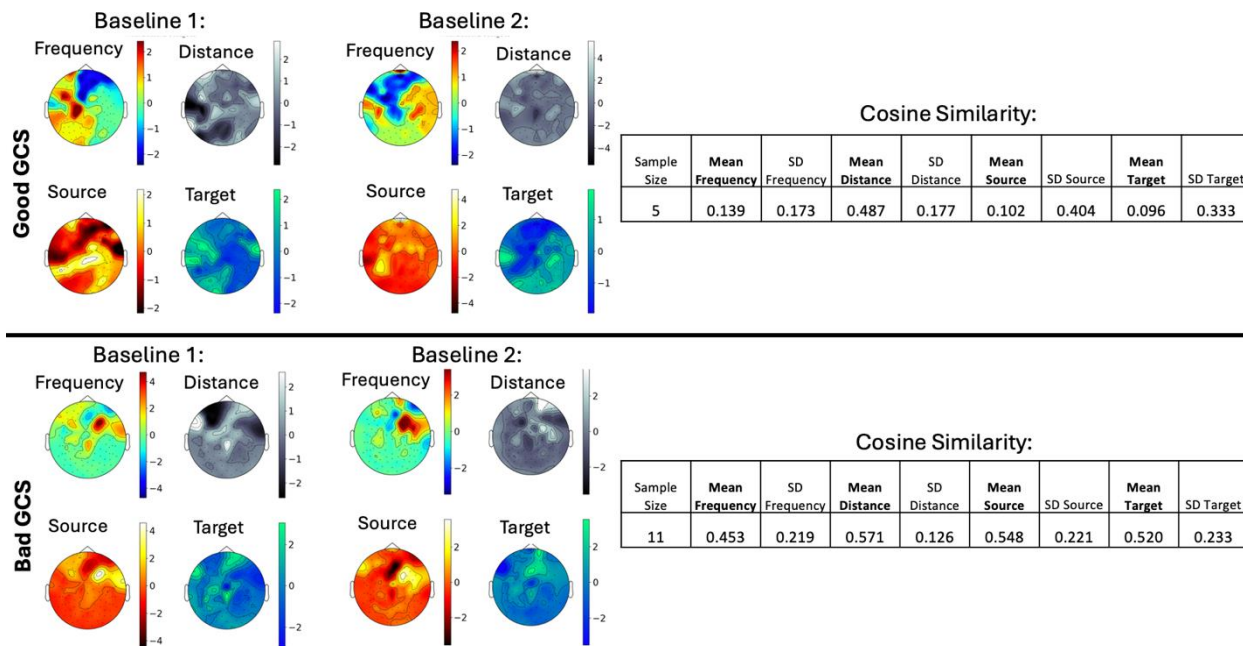
Supplementary Figure 6. Topological plots between diagnostic groups for motif 1 frequency, distance, source, and target properties during anesthesia administration. Motif properties were plotted using nodal Z-scores during sedation off (pre-anesthesia administration) and sedation on (post-anesthesia administration) states. Cosine similarity mean and standard deviation (SD) values between sedation off and on states are displayed in the tables. Group data for patients with favorable Glasgow Coma Scale (GCS) score are displayed on top and patients with an unfavorable GCS on the bottom.

Anesthesia Administration: Motif 1



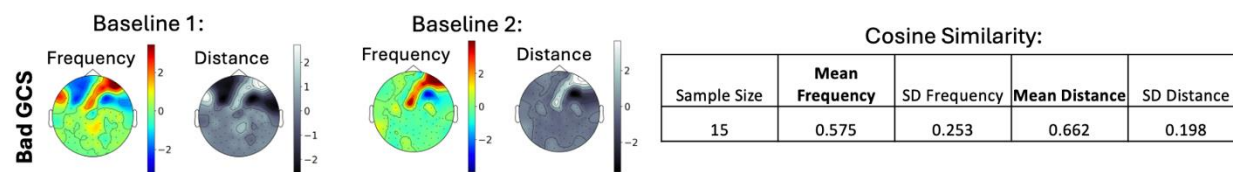
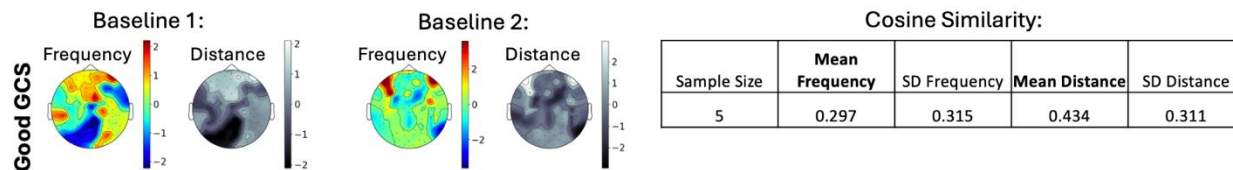
Supplementary Figure 7. Individual cosine similarity values for motif 1 frequency (A), distance (B), source (C), and target (D) properties during propofol administration. Purple = good Glasgow Coma Scale (GCS), green = bad GCS.

Baseline States: Motif 1



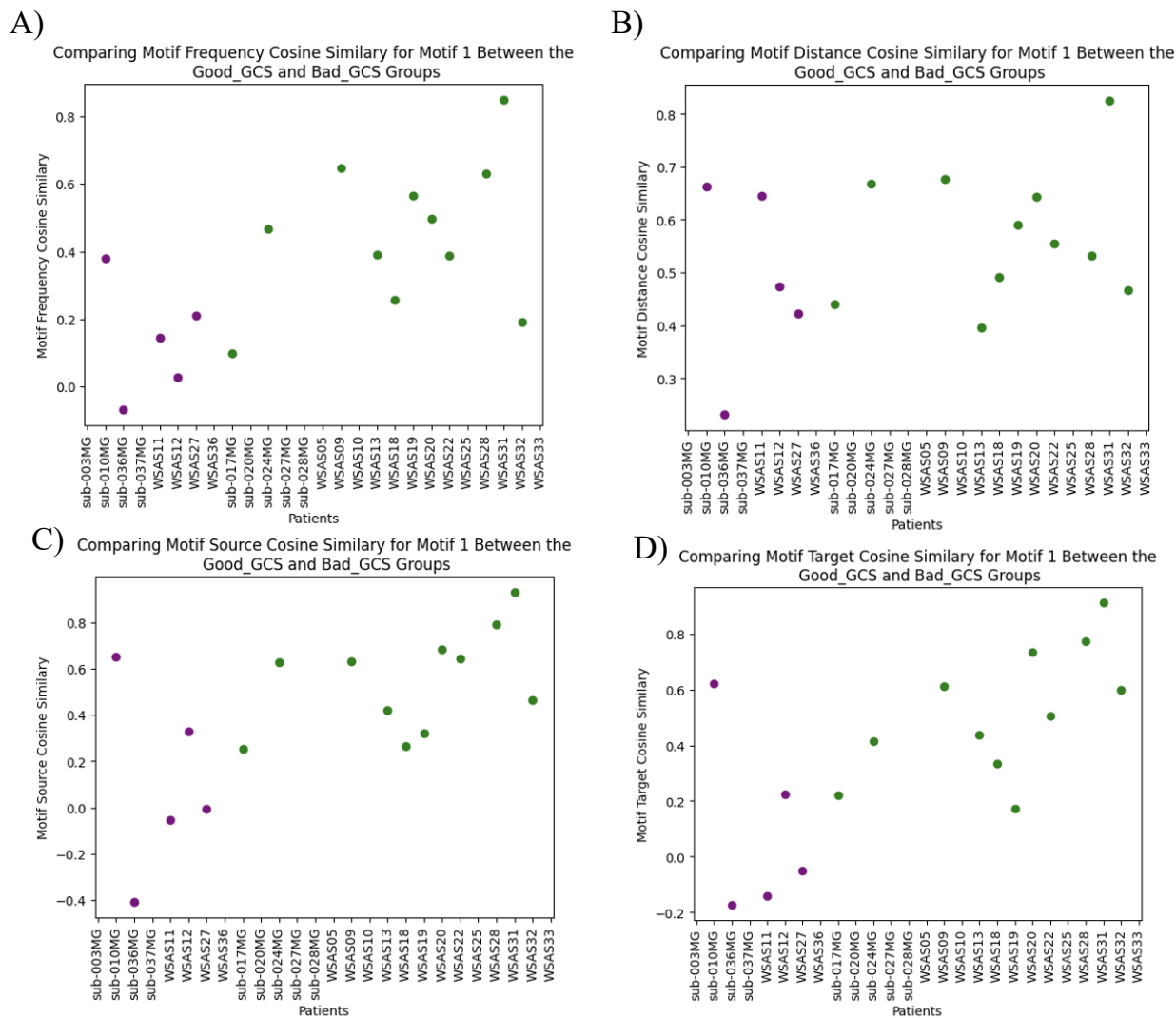
Supplementary Figure 8. Topological plots between diagnostic groups for motif 1 frequency, distance, source, and target properties during baseline states. Motif properties were plotted using nodal Z-scores during baseline 1 and baseline 2 states. Cosine similarity mean and standard deviation (SD) values between baseline states are displayed in the tables. Group data for patients with good Glasgow Coma Scale (GCS) score are displayed on top and patients with a bad GCS on the bottom.

Baseline States: Motif 7



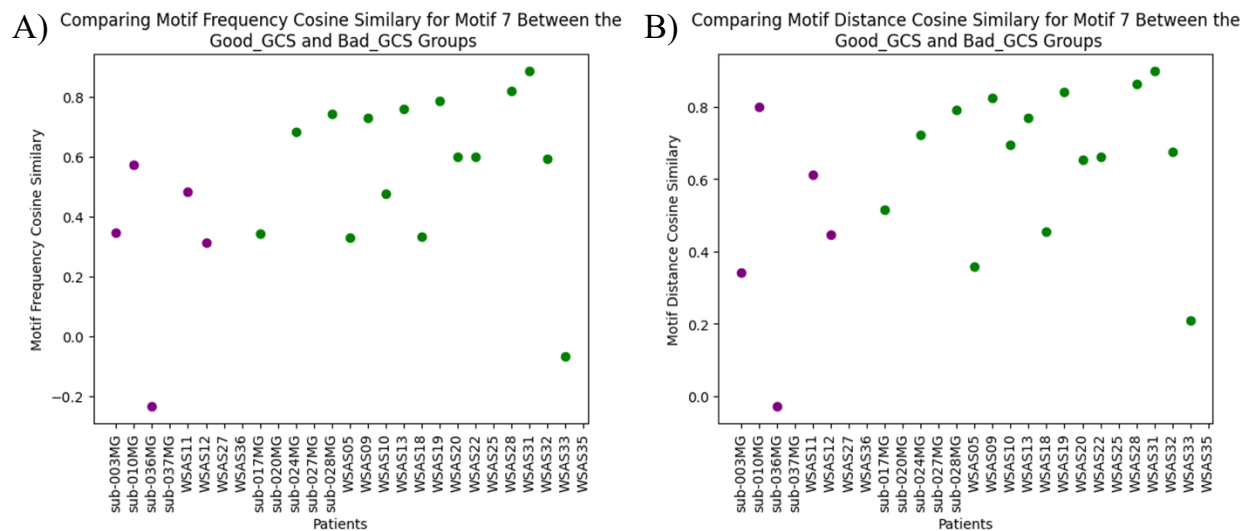
Supplementary Figure 9. Topological plots between diagnostic groups for motif 7 frequency and distance properties during baseline states. Motif properties were plotted using nodal Z-scores during baseline 1 and baseline 2 states. Cosine similarity mean and standard deviation (SD) values between baseline states are displayed in the tables. Group data for patients with good Glasgow Coma Scale (GCS) score are displayed on top and patients with a bad GCS on the bottom.

Baseline States: Motif 1



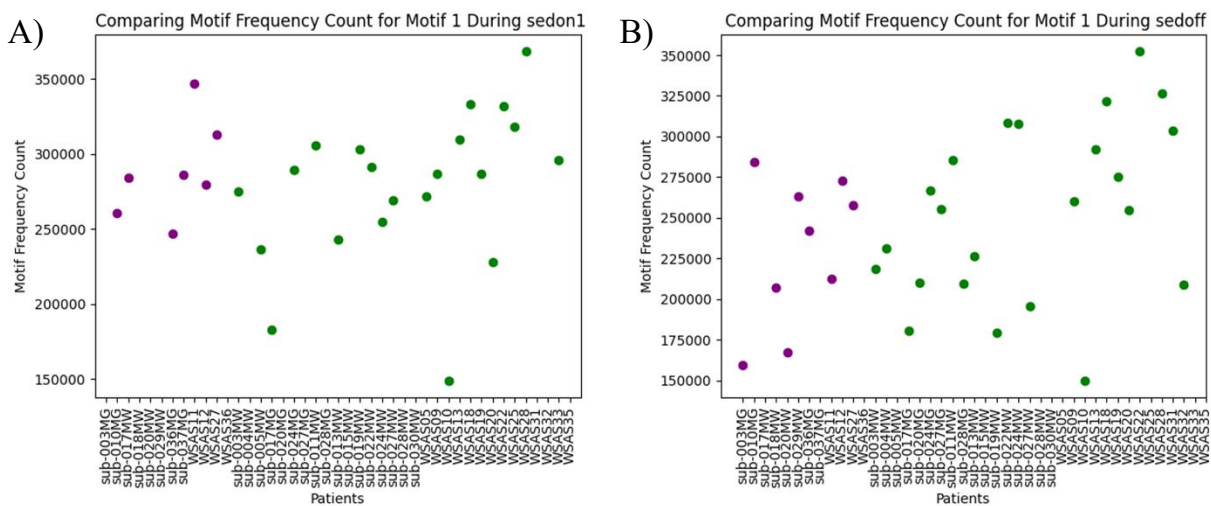
Supplementary Figure 10. Individual cosine similarity values for motif 1 frequency (A), distance (B), source (C), and target (D) properties during baseline states. Purple = good Glasgow Coma Scale (GCS), green = bad GCS.

Baseline States: Motif 7



Supplementary Figure 11. Individual cosine similarity values for motif 7 frequency (A) and distance (B) properties during baseline states. Purple = good Glasgow Coma Scale (GCS), green = bad GCS.

Motif 1 Frequency Counts



Supplementary Figure 12. Non-topological scalar counts of motif 1 frequency during anesthesia withdrawal. Plotted are individual frequency counts for each patient while sedation was on (pre-anesthesia withdrawal) in A and while sedation was off (post-anesthesia withdrawal) in B. Purple = good Glasgow Coma Scale (GCS), green = bad GCS.

Supplementary Table 1. Mean and standard deviation (SD) of motif scalar counts for diagnostic groups during anesthesia withdrawal. For significant motifs 1 and 7, scalar counts for motif frequency, distance, source, and target properties are shown during sedation on (pre-anesthesia withdrawal) and sedation off (post-anesthesia withdrawal) states. Motif counts for patients with a good Glasgow Coma Scale (GCS) score are displayed in the top table and counts for patients with a bad GCS are displayed in the bottom table.

Group: Good GCS										
Motif	State	Sample Size	Mean Frequency	SD Frequency	Mean Distance	SD Distance	Mean Source	SD Source	Mean Target	SD Target
1	Sedation On	7	2.88E+05	3.32E+04	5.70E+06	7.40E+05	1.92E+05	2.22E+04	1.92E+05	2.22E+04
1	Sedation Off	9	2.30E+05	4.55E+04	4.51E+06	8.88E+05	1.53E+05	3.03E+04	1.53E+05	3.03E+04
7	Sedation On	8	1.78E+05	6.04E+04	1.45E+06	5.04E+05	---	---	---	---
7	Sedation Off	9	1.70E+05	6.52E+04	1.40E+06	5.24E+05	---	---	---	---
Group: Bad GCS										
Motif	State	Sample Size	Mean Frequency	SD Frequency	Mean Distance	SD Distance	Mean Source	SD Source	Mean Target	SD Target
1	Sedation On	21	2.78E+05	5.05E+04	5.52E+06	1.06E+06	1.85E+05	3.37E+04	1.85E+05	3.37E+04
1	Sedation Off	23	2.53E+05	5.42E+04	4.99E+06	1.12E+06	1.69E+05	3.61E+04	1.69E+05	3.61E+04
7	Sedation On	26	1.92E+05	4.84E+04	1.56E+06	3.93E+05	---	---	---	---
7	Sedation Off	27	1.88E+05	4.97E+04	1.54E+06	4.19E+05	---	---	---	---